

DETERMINATION OF STRESSES IN A SPUR
GEAR BY PHOTOELASTIC AND NUMERICAL METHODS
BY

Sylvester Ani UGWU, B..Eng, (Nig.)

A Thesis Submitted To The Postgraduate
School of Ahmadu Bello University, Zaria, In
Partial Fulfillment Of The Requirements For The
Award of Master of Science (M.Sc.) Degree
(Mechanical) In Production Engineering.

July, 1990

DECLARATION

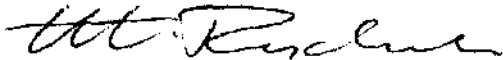
I hereby declare that this thesis has been prepared by myself and it is a record of my own research work. It has not been accepted in any previous application for a higher degree. All sources and information are specifically acknowledged by means of references.



S. A. UGWU.

July, 1990.

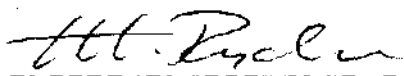
CERTIFIED BY:




Dr. W. R. RYCHWALSKI,
Supervisor.

CERTIFICATION

This project report entitled, "Determination of Stresses in a Spur Gear by Means of Photoelastic and Numerical Methods", by Sylvester Ani Ugwu, meets the regulations governing the award of the degree of Master of Science (Production Engineering) of Ahmadu Bello University, and is approved for its contribution to knowledge and literary presentation.


Date: 30-JULY-1990


Dr. W. R. Rychwalski,
Chairman, Supevisory Committee.


Date: 1/8/90

Dr. E. J. Bala,
Member, Supervisory Committee.

Date: _____

Professor C. O. Folayan,
Head of Department.


Date: 8-11-90

Dean, Postgraduate School.

DEDICATION

Dedicated To:

My Parents:

Mr. Ugwu Ngeeta

Mrs. Nogo-Arum Ugwu-Ngeeta;

My Brothers:

Jacob N. Ugwu

Moses C. Ugwu

Job N. Ugwu;

And My Sisters:

Miss Uchenwa Ugwu

Miss Calista Uruka Ugwu.

ACKNOWLEDGEMENT

I am highly indebted and with unreserved sincerity very grateful to my supervisor, Dr. W. R. Rychwalski, for his able, patient and intellectual assistance which immensely contributed towards elevating and developing my academic mind.

My sincere gratitude goes to Dr. E. J. Bala, Prof. S. Y. Aku, Prof. C. O. Folayan and all the members of staff of Mechanical Engineering Department, for their concern over the progress of this work.

I am also indebted to the following people:

- All my class mates whose advice spurred me on whenever things went wrong, especially Engr. Daniel Makundi, who helped me immensely on the computer aspect of my work.
- My brother, Jacob N. Ugwu, for his financial support.
- My cousin, Benjamin Odoh, my close friend Engr. Paul Eze, my parents, brothers and sisters, and others who provided the necessary moral support needed for the timely completion of this work.

S. A. UGWU.

JULY, 1990.

ABSTRACT

The new developments in mechanical engineering in Nigeria (Low Cost Vehicle project, aviation projects - AIR BEETLE, etc.), require in-house practical calculation techniques in design generally and calculation of stresses in machine components, particularly.

The machine components (Spur Gears) under operation are subjected to stresses which differ at different locations. These stresses are hereby determined with the use of photoelastic and numerical methods and compared with classical design formulae.

Gear Models made of photoelastic material (Columbia Resin CR-39) were produced and loaded in a specially built gear loading system. The stresses in the model were analysed using the photoelastic principles giving the stress difference ($\sigma_1 - \sigma_2$) at points. Next, numerical method (Finite Difference Method) was employed which gave ($\sigma_1 + \sigma_2$) values at the same points. The equations for ($\sigma_1 + \sigma_2$) and ($\sigma_1 - \sigma_2$) were solved for the individual stresses at the said points.

The stresses in the gear model were also determined using Finite Element Method, FEM. Later, the model stresses were applied to the steel prototype.

Finally, the results obtained using different methods and classical design formulae (Lewis, Modified Lewis and Sopwith Equations), were compared and inferences made. Some likely sources of error in the work were pinpointed.

TABLE OF CONTENTS

<u>CHAPTER:</u>	<u>PAGE</u>
TITLE PAGE	i
DECLARATION	ii
CERTIFICATION	iii
DEDICATION	iv
ACKNOWLEDGEMENT	v
ABSTRACT	vi
TABLE OF CONTENTS	vii
LIST OF TABLES	x
LIST OF FIGURES	xi
LIST OF PLATES	xiii
LIST OF SYMBOLS	xiv
1. Introduction	1
2. A review of Various Methods of Calculating Stresses in Spur Gears	5
2.1. Introduction	5
2.2. Strength of Gear - Lewis formula	7
2.3. Strength of Gear Teeth - Sopwith Equation	10
3. Application of Photoelastic and Numerical Methods for Determining Stresses	15
3.1. Field of Application of Photoelasticity	15
3.1.1. Limitations of Photoelastic Technique	16
3.2. Field of Application of Numerical Methods	16
4. Principles of Photoelasticity, Finite Difference Method and Finite Element Method	18

<u>CHAPTER</u>	<u>PAGE</u>
4.1. Photoelasticity	18
4.1.1. The Photoelastic Materials	21
4.2. The Finite Difference Method, FDM ..	22
4.2.1. Formulation of Finite Difference Equations	23
4.2.2. Computer Solution of FDM	27
4.2.3. Accuracy of Finite Difference Solution ..	27
4.3. The Finite Element Method FEM	27
4.3.1. Element Stiffness Matrix	28
4.3.2. Triangular Element	30
5. Experimental Results	36
5.1. Detailed Description of the Photoelastic Bench Used	36
5.2. Design and Fabrication of the Loading System	37
5.3. Preparation of the Models	38
5.4. Determination of Young's Modulus and Poisson's Ratio of the Model Material	45
5.5. Calibration of the Model	46
5.6. The Photoelastic Results	52
5.7. Separation of Principal Stresses with the use of FDM	66
5.7.1. Determination of Stresses at the nodal points 1, 2, 3, on the Model using Strain Gauges	66
5.7.2. Application of FDM	74
5.7.3. The Individual Stresses	79
5.8. Model Stresses Applied to the Prototype	83
6. Calculation of Stresses with the Use of FEM	85
7. Comparison of Results obtained by Different Methods	88

<u>CHAPTER</u>	<u>PAGE</u>
7.1. Calculating the Fillet Stresses with the use of Lewis formula	88
7.2. Calculating the Fillet Stresses with the use of Sopwith Equation	90
7.3. Comparison of the Fillet Stresses ..	91
7.4. Calculating the Contact Stress at the Point of Load Application with the use of Hertz Equation	91
7.5. Comparison of Contact Stresses	96
7.6. Inferences	96
8. Likely Sources of Error in this work ..	98
8.1. Likely Sources of Error in Photoelastic Results	98
8.2. Likely Sources of Error in Strain Measurement	100
8.3. Likely Sources of Error in Numerical Methods	101
9. Conclusion	103
REFERENCES	105

LIST OF TABLES

<u>TABLE</u>	<u>TITLE</u>	<u>PAGE</u>
5.1.	Tension test readings	46
5.2.	Fringe values for calibration	50
5.3.	Fringe values at 9% of full load	63
5.4.	Measured strains for Nodes 1, 2, 3,	71
5.5.	Corrected Strain Values	72
7.1.	Fillet stresses by different Methods	92
7.2.	Contact stresses by different Methods	96

LIST OF FIGURES

<u>FIGURE</u>	<u>TITLE</u>	<u>PAGE</u>
2.1.	Gear Nomenclature	6
2.2.	Lewis approach for Calculating Stresses..	8
2.3.	Dimensions required for Calculating Fillet Stresses	11
2.4.	Equivalent flat-sided projection constructed from Gear Tooth	13
4.1.	Plane Polariscope	19
4.2.	Toward Difference Formulae	23
4.3.	Square Mesh and Numbered Nodal Points ..	24
4.4.	Boundary not Coincident with Nodes ..	25
4.5.	Node Points on Arbitrarily Shaped Element	28
4.6.	Triangular Element	30
4.7a.	Uniform Stress Field of an Element resolved into Nodal Forces	33
4.7b.	Plane State Stress	33
5.1.	Assembly Drawing of the Loading System ..	39
5.2.	Fork-Shaped Component	40
5.3.	Model Hanger	41
5.4.	Model Hanger	42
5.5.	L-Shaped Component	43
5.6.	Gear Dimensions	44
5.7.	Tension Test Piece Dimensions ..	45
5.8.	Stress-Strain Curve	47
5.9.	Lateral Strain-Axial Strain Curve ..	47

<u>FIGURE</u>	<u>TITLE</u>	<u>PAGE</u>
5.10.	Caliberation Specimen Arrangement ..	48
5.11.	Detailed Drawing of Fig. 5.10	49
5.12.	Nodal points on the gear model	63
5.13.	Dimensions (square mesh) for generating difference equations	67
5.14a.	Force-Strain Curve for Node 1	68
5.14b.	Force-Strain Curve for Node 2	69
5.14c.	Force-Strain Curve for Node 3	70
6.1.	Computer Print-Out (Inside Back Cover Envelope)	
6.2.	Constant Strain Triangles on the Gear Model	86
7.1	Lewis approach for calculating stresses	89
7.2.	Equivalent flat-sided projection constructed from gear tooth for the calculation of fillet stress	91
7.3.	Dimensions required for the calculation of transmitted load	94
7.4.	Dimensions required for the calculation of Contact Stress	95

LIST OF PLATES

<u>PLATE</u>	<u>TITLE</u>	<u>PAGE</u>
I	- Zero order fringe at 0% load ..	53
II	- Half order fringes at 1% load ..	53
III	- Full order fringes at 1% load ..	54
IV	- Half order fringes at 1% load ..	54
V	- Full order fringes at 2% load ..	55
VI	- Half order fringes at 2% load ..	55
VII	- Full order fringes at 3% load ..	56
VIII	- Half Order fringes at 3% load ..	56
IX	- Full order fringes at 4% load ..	57
X	- Half order fringes at 4% load ..	57
XI	- Full order fringes at 5% load ..	58
XII	- Half order fringes at 5% load ..	58
XIII	- Full Order fringes at 6% load ..	59
XIV	- Half order fringes at 6% load ..	59
XV	- Full order fringes at 7% load ..	60
XVI	- Half order fringes at 7% load ..	60
XVII	- Full order fringes at 8% load ..	61
XVIII	- Half order fringes at 8% load ..	61
XIX	- Front view of the photoelastic bench	62
XX	- The models and the loading system on the straining frame	62

LIST OF SYMBOLS

<u>SYMBOL</u>	<u>MEANING</u>	<u>UNITS</u>
σ_1, σ_2	- Principal stresses	N/m ²
P	- Diametral pitch	mm
p	- Circular pitch	mm
N	- Number of teeth, fringe order	
d	- Pitch circle diameter	mm
t	- Thickness	mm
a	- Addendum distance	mm
b	- Dedendum distance	mm
m	- Module	mm
h_t	- Whole depth	mm
F	- Face width	mm
l	- Length	mm
W_p	- Applied load	N
W_t	- Tangential load component	N
W_r	- Radial load component	N
I	- Second moment of inertia	m ⁴
M	- Moment	Nm
σ	- Stress	N/m ²
Y	- Lewis form factor	
$\epsilon_1, \epsilon_2, \epsilon_1, \epsilon_2$	- Principal strains	
v	- Speed	m/s
δ	- Relative retardation; displacement	mm
n	- Index of refraction	
k	- Strain optical constant	

<u>SYMBOL</u>	<u>MEANING</u>	<u>UNITS</u>
K	- Stress optical constant	N/m ² /fringe
E	- Young's Modulus	N/m ²
μ	- Poisson's Ratio	
λ	- Wave length	mm
∇	- Harmonic operator	
$K^{(e)}, K$	- Element and global stiffness	Nm
[D]	- Element elastic property matrix	
A	- Surface area	m ²
[H]	- Stress-displacement matrix	
[B]	- Strain matrix	
K_{ij}	- Stiffness coefficients	Nm
{p}	- Column vector of loads	
{ δ }	- Column vector of displacement	
[K]	- Element stiffness matrix	
γ_{xy}	- Shear strain	
ϵ	- Strain	
Z	- Section Modulus	mm ³
R	- Fillet radius	mm

1. INTRODUCTION

In industries which require, in substantial quantities, gears which must combine minimum weight with consistent reliability or a predictable minimum life (such as the automobile and aircraft industries), gear stressing is the subject of specialist attention.

Essential limitations in the design of gear wheels are derived from kinematical conditions that the teeth must be so formed and disposed as to imitate the true rolling of the pitch circles, although the teeth may slide over one another, and of course, this normally happens. Although there are theoretically an infinite number of ways of satisfying the condition mentioned above, the great majority are shaped from curves described by points on the circles and straight lines when rolling without slipping on circles. The involute curves produced in this latter way are usually preferred, since a slight change in the distance between the wheel centres does not impair the transmission of true rolling motion, while the teeth, owing to the mode of formation, have their greatest breadth at the roots or junctions with the main body of the wheel, and are therefore well shaped to resist the maximum stresses which come upon them due to the sliding contact pressure between the surfaces.

Although in practice, the design of the teeth is thus limited, the stress distribution in them, and in the wheels themselves, afford a number of problems of

practical importance owing to wide use of gearing, often under particularly strenuous conditions.

The well-known Lewis formula for gear teeth is based on pure bending effect, and as such tends to produce low results. A further advancement in the Lewis formula was to take the component of the load producing compression into account. By introducing this term, the modified Lewis formula came into existence. These formulae are inaccurate because the effect of a high load in close proximity to the fillet is ignored, and because the simple bending theory formula is intended for beams whose depth is small compared with the length. To overcome these problems, the analysis of the stresses in spur gear has been done in this work using different other methods. These methods include numerical methods (Finite Difference Method, FDM and Finite Element Method, FEM); photoelastic technique and sorwith equation.

Photoelasticity and numerical methods (FDM and FEM) are individually or collectively used in stress analysis and proved to be very successful and efficient in calculation of stresses for parts of complex shape. Here the stress distribution in the teeth of a spur gear has been studied by both photoelastic technique combined with FDM and FEM.

In photoelastic method of stress analysis, stresses are inferred from the optical behaviour of stressed transparent materials. In this method of stress analysis, a model or detail of the structure is made from a suitable transparent plastic and loaded in such a way as to simulate

conditions in the prototype. When the model is placed in the polariscope and examined in the polarised light field provided by the instrument, coloured fringe patterns are seen which reveal a visible picture of the stress distribution over the whole area of the model and stress distribution which is accurately readable at any point in the model for both magnitude and direction. The key piece of equipment required for photoelastic studies is polariscope (photoelastic bench).

The photoelastic results give principal stress difference ($\sigma_1 - \sigma_2$) at any point in the model. For complete determination of separate principal stresses σ_1 and σ_2 FDM is used. This method gives the sum of principal stress ($\sigma_1 + \sigma_2$). The determination of sum of principal stresses by FDM was first developed by Shortly and Weller and was later improved upon by Frocht [ref. 7]. This method provides the most satisfactory method of determining the separate principal stresses from the photoelastic results alone without recourse to an auxiliary experiment, since the only data required are the boundary stresses from the fringe photography and partial fringe orders. It is beyond the scope of this chapter to deal, in detail, with the basic principles and theory of photoelasticity, FDM and FEM, since these are covered in Chapter Four of this work.

Nevertheless, it is worthy to note that in FDM, once the governing differential equations have been derived, no further reference is made to the physical problems; while FEM requires that the physical characteristics of the

problem be retained throughout the process of its solution. This results to a large number of simultaneous linear equations which must be solved for stresses and displacements of each element of the structure. This is a tedious task which is normally solved with the aid of a computer.

CHAPTER TWO

2.0. A REVIEW OF VARIOUS METHODS OF CALCULATING STRESSES IN SPUR GEARS

2.1. Introduction:

Gears are machine elements used in a wide range of engineering designs, so that power may be transmitted steadily and without slip, such as occurs with a belt drive. There are different types of gears; among which are spur gears, helical, spiral, worm and bevel gears.

Spur gears are those gears that have their teeth cut parallel to the axis of the shaft. A cross-section of the tooth is identical for both size and shape along the entire length. Spur gears are used to transmit rotary motion between parallel shafts. They are used over a wide range of articles from small watches and meters, gear trains on machine tools, in gear boxes as fitted to motor cars and aero-engines, to large drives as found in rolling mills and on board ships.

For the purpose of continuity, it is pertinent to define some of the terms used with gearing. These terms are explained with the aid of Fig. 2.1.

The pitch circle is a theoretical circle upon which all calculations are usually based. The pitch circles of a pair of mating gears are tangent to each other.

A pinion is the smaller of two mating gears while the larger is often called the gear.

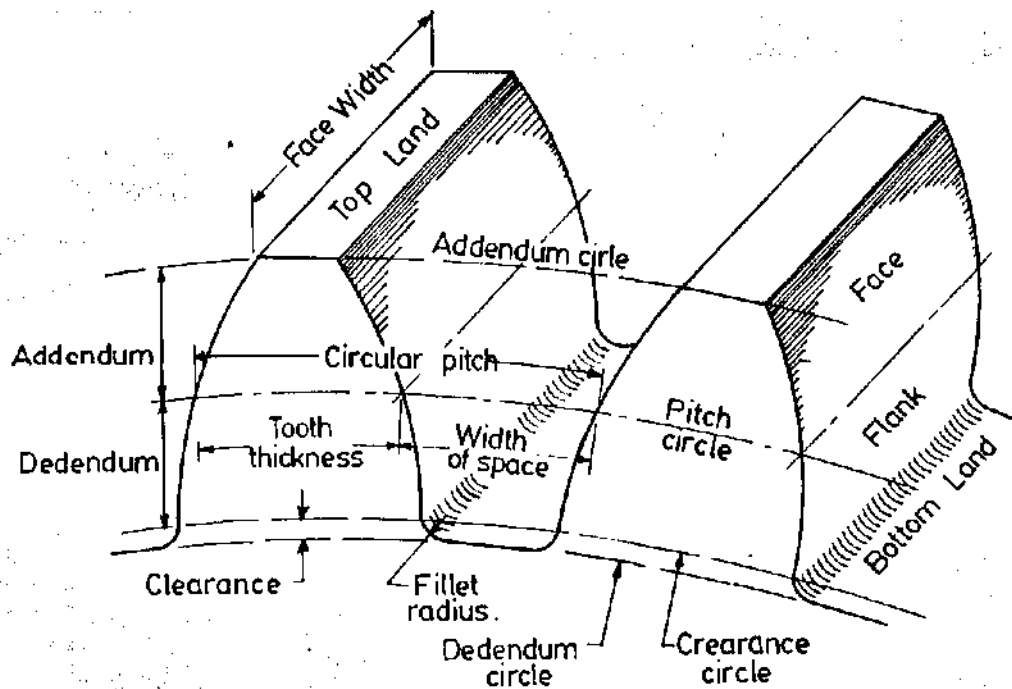


Fig. 2.1: Gear teeth nomenclature.

The circular pitch, p , is the distance measured on the pitch circle, from a point on one tooth to a corresponding point on an adjacent tooth. From Fig. 2.1, circular pitch p is equal to the sum of the tooth thickness and the width of space.

The diametral pitch, P , is the ratio of the number of teeth, N , on the gear to the pitch diameter, d .

The ratio of the pitch diameter to the number of teeth N is termed the module M . Hence, it is the reciprocal of diametral pitch.

The addendum ' a ' is the radial distance between the top-land and the pitch circle.

The dedendum b is the radial distance from the bottom land to the pitch circle.

The whole depth h_t is the sum of the addendum and dedendum.

The clearance circle is a circle that is tangent to the addendum circle of the mating gear.

The clearance is the amount by which the dedendum in a given gear exceeds the addendum of its mating gear.

The backlash is the amount by which the width of the tooth space exceeds the thickness of the engaging tooth measured on the pitch circle.

Having defined some of the terms which will be constantly referred to in this chapter, a review of some of the various methods of calculating stresses in spur gear now follows.

2.2. Strength of Gear - Lewis Formula:

The determination of maximum stresses in a loaded gear tooth is complicated by variation in magnitude and direction of the load on the tooth during contact and by the shape of the tooth, since it has varying width and is joined to the body of the gear by a fillet.

In 1892, Wilfred Lewis, in his paper titled, "Investigation of strength of gear teeth", to the Engineers Club of Philadelphia, made simplifying assumptions regarding the strength of gear teeth. This resulted in an equation which has been used extensively by industry in determining the size and proportions of gears up till now.

To derive the Lewis formula, refer to Fig. 2.2 which shows a cantilever of cross-sectional dimensions F and t , having a length l and a load W_t uniformly distributed across the distance F (face width). The section modulus is $Z = \frac{Ft^2}{6}$ and then the bending stress, σ , is:

$$\sigma = \frac{M}{Z} = \frac{6W_t \cdot l}{Ft^2} \text{ ----- (2.1)}$$

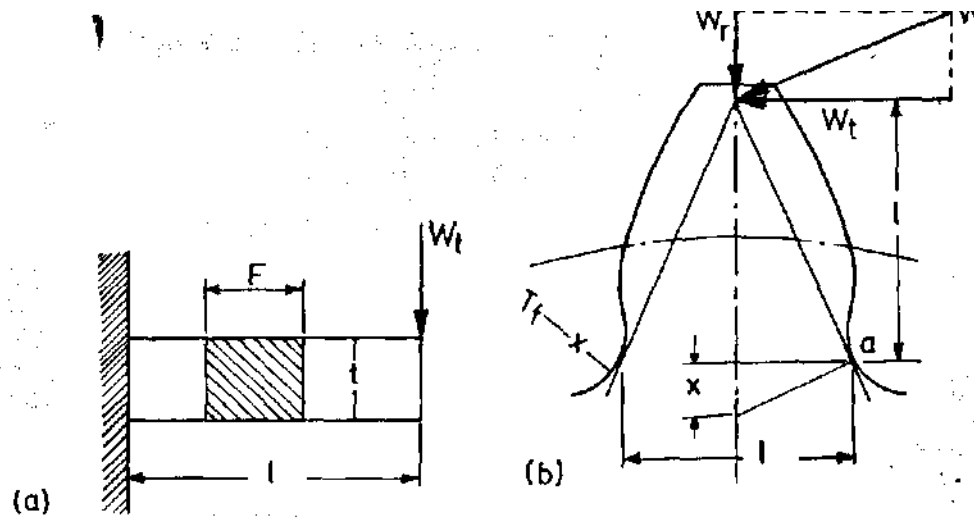


Fig. 2.2: Lewis Approach for Calculating Stresses.

Referring to Fig. 2.2.b, we assume that the maximum stress in gear tooth occurs at point 'a'. By similar triangles, one can write:

$$\frac{t/2}{x} = \frac{l}{t/2}$$

$$\Rightarrow x = \frac{t^2}{4l} \text{ ----- (2.2)}$$

Rearranging equation (2.1) we have

$$\sigma = \frac{6W_t l}{F t^2} = \frac{W_t}{F} \cdot \frac{1}{t^2/6l} = \frac{W_t}{F} \cdot \frac{1}{t^2/4l} \cdot \frac{1}{4/6} \text{ --- (2.3)}$$

Substituting the value of x from equation (2.2) into (2.3) and multiplying the numerator and the denominator by the circular pitch, p, we have

$$\sigma = \frac{W_t p}{F(2/3)xp} \text{ ----- (2.4)}$$

Letting $y = 2x/3p$, we have

$$\sigma = \frac{W_t}{Fpy} \text{ ----- (2.5)}$$

Equation (2.5) is the original Lewis equation. The factor y is called the Lewis form factor. Form factor may be obtained by either graphical layout of the gear tooth or digital computer.

At times the diametral pitch P is preferred to circular pitch p in determining the stresses. This is done by

substituting $P = \pi/p$ and $Y = \pi y$ in equation (2.5). This gives:

$$\sigma = \frac{W_t P}{F Y} \text{-----} (2.6)$$

Values of form factor Y are available in standard gear handbooks.

In the derivation of Lewis equation, a lot of assumptions were made which include the following:

The Lewis equation is solved by using tangential component of the load. If the radial component is considered, this would produce a uniform compressive stress to which must be added the bending stress. The effect of the radial component therefore is to increase the compression and decrease the tension.

In the derivation of Lewis formula, the greatest stress is assumed to occur when the load is at the tip of the tooth. If gears are cut with sufficient accuracy, the tip load condition is not the worst, because another pair of teeth will be in contact when this condition occurs. With this assumption, Lewis formula does not take into account the effect of high load in close proximity to the fillet.

Also, the tangential load W_t in Lewis formula, is assumed to be uniformly distributed across the full face of the gear. This statement is not completely true because gears and their supporting shafts are made of elastic materials which deflect under the application of loads. The effect of the deformations is to cause non-uniform distribution of the load.

In addition, the effects of stress concentration are neglected. Stress concentration factors are not taken into account and recent investigation indicates the advisability of doing so.

It has also been shown by photoelastic method that the stresses at the root of the tooth can be much greater than those allowed for by the Lewis formula. This is due to the change in the tooth contour as the form emerges into the root diameter.

Finally, the simple bending theory applied by Lewis here, is only applicable to beams of small t/l ratios. This ratio is not small for spur gears.

2.3. Strength Of Gear Teeth - Sopwith Equation:

The well-known Lewis formula for gear teeth is based on pure bending effect, and as such, tends to produce low results as mentioned in the introductory chapter. A further improvement in the Lewis formula took the component of the load producing compression into account. This gave birth to the modified Lewis formula. Both the original Lewis formula and modified Lewis formula are inaccurate because the effect of a high load in close proximity to the fillet is ignored and also because the simple bending theory formula is intended for beams whose depth is small compared with the length. To overcome this second difficulty, a more elaborate analysis on the lines suggested by D. G. Sopwith [ref. 12] was looked into.

A further requirement is that these formulae should take into account a stress concentration factor, the value of which should depend on the relative size of the fillet.

The above criticisms show that the basis of the Lewis-and modified Lewis formulae is unsound, and as such, serious errors in results may be obtained for certain cases.

To define the basis for the evaluation of Sopwith equation, the tensile fillet stresses produced by the loading of a single projection were analysed. The analysis showed that it was necessary to add to the usual bending term M , a term L which depended on the proximity of the load to the fillet, so giving the maximum calculated fillet stress to be $K(M + L)$, where K is the stress concentration factor or by using the actual dimensions that were found most suitable, tensile fillet stress is:

$$\sigma_f = K \left\{ \frac{1.5a}{e^2} + \sqrt{\frac{0.36}{b \cdot e}} \left(1 + \frac{1}{4} \sin \phi \right) \right\} \frac{W}{t} \text{ ----- (2.7)}$$

where: $K = 1 + 0.26 (e/R)^{0.7}$

W = Load applied to projection

t = thickness of the projection

and dimensions a , b , e , R and the angle ϕ are as indicated in Figure 2.3.

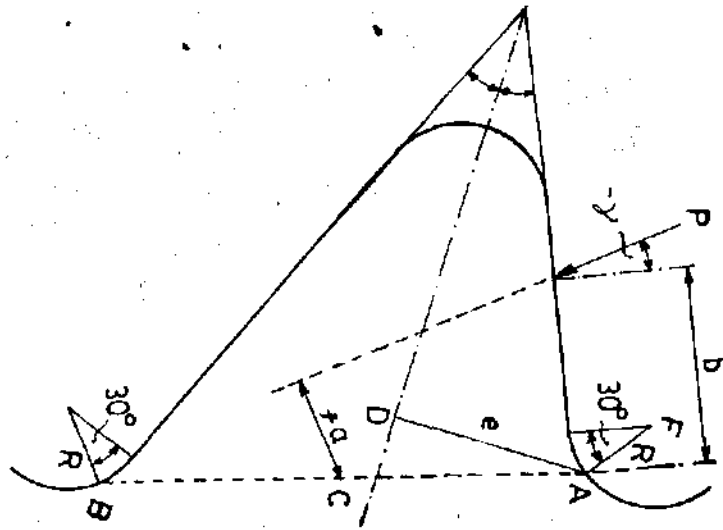


Fig. 2.3: Dimensions Required for Calculating Fillet Stresses.

ISRAELI LIBRARY
HMADU BELLO UNIVERSITY
ARIA, NIGERIA.

The formula, equation (2.7), can be simplified usually because frictional effects limit the angle ϕ to small value, so that the magnitude of $\frac{1}{4} \sin \phi$ is also small and can be neglected.

The formula embraces certain extreme conditions, such as a long cantilever subjected to a uniform bending moment (when the proximity term L vanishes); a stub-shaped projection loaded very close to the fillet and a projection with relatively large fillet radius having a stress concentration factor approaching unity. In effect, these conditions imply that the empirical formula must have a sound theoretical basis for its conception. The formula gives considerably greater accuracy than can be obtained by using the Lewis - or modified Lewis formula.

In Fig. 2.3, 'A' shows the point of maximum fillet stress, so the weakest semi-section is defined by the line AD of length 'e', this being the perpendicular from A on to the centre line of the projection. Note that the point A is found from the point of intersection of the fillet contour with a line AF drawn at 30° from the centre of the fillet radius. The particular angle of 30° was chosen so that the point A coincides with the point of maximum stress as determined from the fringe photographs. The arm of the bending moment 'a' is determined by perpendicular distance from the mid-point 'C' of AB to the line of action of the load.

This projection formula derived above was applied to gears with little modifications. Because of the curved

flanks of gear teeth, the tensile fillet stresses cannot be directly calculated from the projection formula. However, by transforming the gear tooth to an equivalent flat-sided projection, a close estimation of the maximum fillet stress can be made by using the conventions suggested in Fig. 2.4.

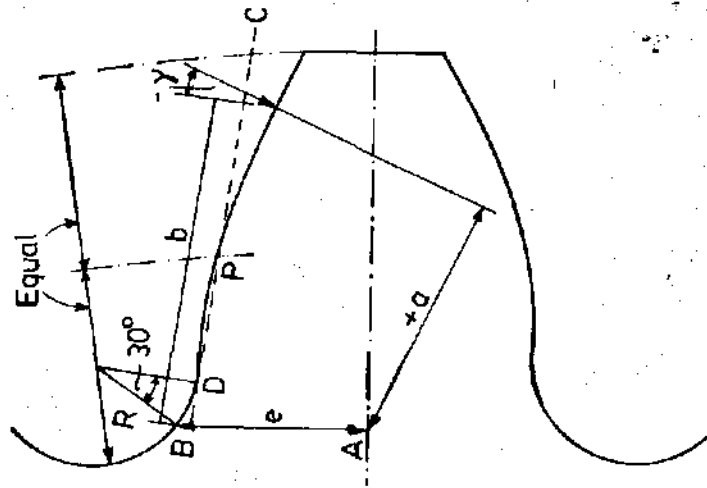


Fig. 2.4: Equivalent Flat-Sided Projection Constructed from Gear Tooth.

The point p on the flank is midway between the crest and the root, and from p , a line is drawn to touch the fillet at D . The line CD produces the flat side of the projection. By substituting values for the dimensions in the projection formula, equation (2.7), the maximum tensile fillet stress in gears can be calculated.

As could have been inferred from this review of various methods of calculating stresses in gears, there is no satisfactory analytical approach. The analytical methods presented here, especially the Lewis method, are useful in getting a ball-park answer and in predicting possible remedies when trouble is encountered. Hence in this project work, the author has decided to employ both

the laboratory testing and numerical methods to analyse stresses in a spur gear. It has been shown how they agree and disagree with traditional bending strength design (Lewis and Sopwith) formulae.

CHAPTER THREE

3.0. APPLICATION OF PHOTOELASTIC AND NUMERICAL METHODS FOR DETERMINING STRESSES

3.1. Field of Application of Photoelasticity:

For quite a long time now, the photoelastic method has been applied to a large number of engineering problems, particularly to the investigations of stress concentrations due to holes, notches and discontinuities in structural and machine elements, and to the stress analysis of rings, chains, links, hooks, and other parts of complicated shape not readily dealt with by analytical methods. Other problems investigated by photoelasticity range from the analysis of highly redundant bridge girders to the study of cutting stresses in machining operations.

Among the chief advantages of the photoelastic method of stress analysis are that it provides a means of: obtaining an overall visual picture of the shearing stress distribution throughout the body.

Measuring stress at a point with the consequent possibility of finding actual peak values even in regions of high stress gradient. Accurate stress determination in irregular members comparable to results obtained with precise strain gauge technique.

Readily obtaining qualitative results for location of minimum and maximum stress locations or for the determination of changes in stress distribution caused by minor alterations in shape of the model to aid in the process of developing a satisfactory design.

3.1.1. Limitations of Photoelastic Technique - Although photoelastic method has a very wide area of engineering application, it still has some shortcomings.

Photoelastic method of stress analysis is an indirect method of stress analysis requiring the use of accurate scale models and subsequent interpretation of data for the prototype. The experimental procedure is readily applied only to two-dimensional states since the three-dimensional methods require rather involved and carefully developed techniques. The separation of individual principal stresses at interior points in the model becomes rather troublesome when isoclinics are employed because of the unsharp loci (picture).

Minus these shortcomings of photoelasticity, it still remains a powerful method of stress analysis, particularly when supported by numerical techniques.

3.2. Field of Application of Numerical Methods:

Numerical methods consist of the Boundary Element Method, the Finite Difference Method and Finite Element Method. In this work, two of them were applied. They are the Finite Element and Finite Difference methods. Numerical methods for the solution of different equations have become particularly popular in recent times because modern technical problems require complex loading and shapes which seldom allow a closed solution.

It is believed that numerical applications in elasticity started as early as 1906, but was not efficiently applied until the introduction of computer hardware and software. From 50s, numerical methods are firmly established

in engineering. The numerical methods are now so efficiently used that they have rendered some analytical and some experimental procedures obsolete.

CHAPTER FOUR

4.0. PRINCIPLES OF PHOTOELASTICITY, FINITE DIFFERENCE METHOD, FDM, AND FINITE ELEMENT METHOD, FEM

4.1. Photoelasticity:

When a polarised beam passes through a transparent birefringent sheet (model) of thickness t , the light splits and two polarised beams propagate in planes x and y . x and y are the direction of principal strain at the point under consideration. Supposing the strain intensity along x and y is ϵ_1 and ϵ_2 , and the speed of the light in these directions is v_1 and v_2 , respectively; the time necessary to cross the plate for each of them will be t/v , and the relative retardation between these two beams will be:

$$\delta = c\left\{\frac{t}{v_1} - \frac{t}{v_2}\right\} = t\{n_1 - n_2\} \quad \text{----- (4.1)}$$

where n_1, n_2 , are the indices of refraction on x and y planes. Brewster showed in his work that the relative change in index of refraction is proportional to the difference of principal strains. Hence,

$$n_1 - n_2 = k(\epsilon_1 - \epsilon_2) \quad \text{----- (4.2)}$$

where k = strain optical coefficient. Combining equations (4.1) and (4.2) we have

$$\delta = tk(\epsilon_1 - \epsilon_2) \quad \text{----- (4.3)}$$

Hence, the basic relation for measuring strains using photoelastic method is:

$$\epsilon_1 - \epsilon_2 = \frac{\delta}{tk}$$

or

$$\sigma_1 - \sigma_2 = \frac{\delta}{t.k} \cdot \frac{E}{1+\mu} \quad \text{----- (4.4)}$$

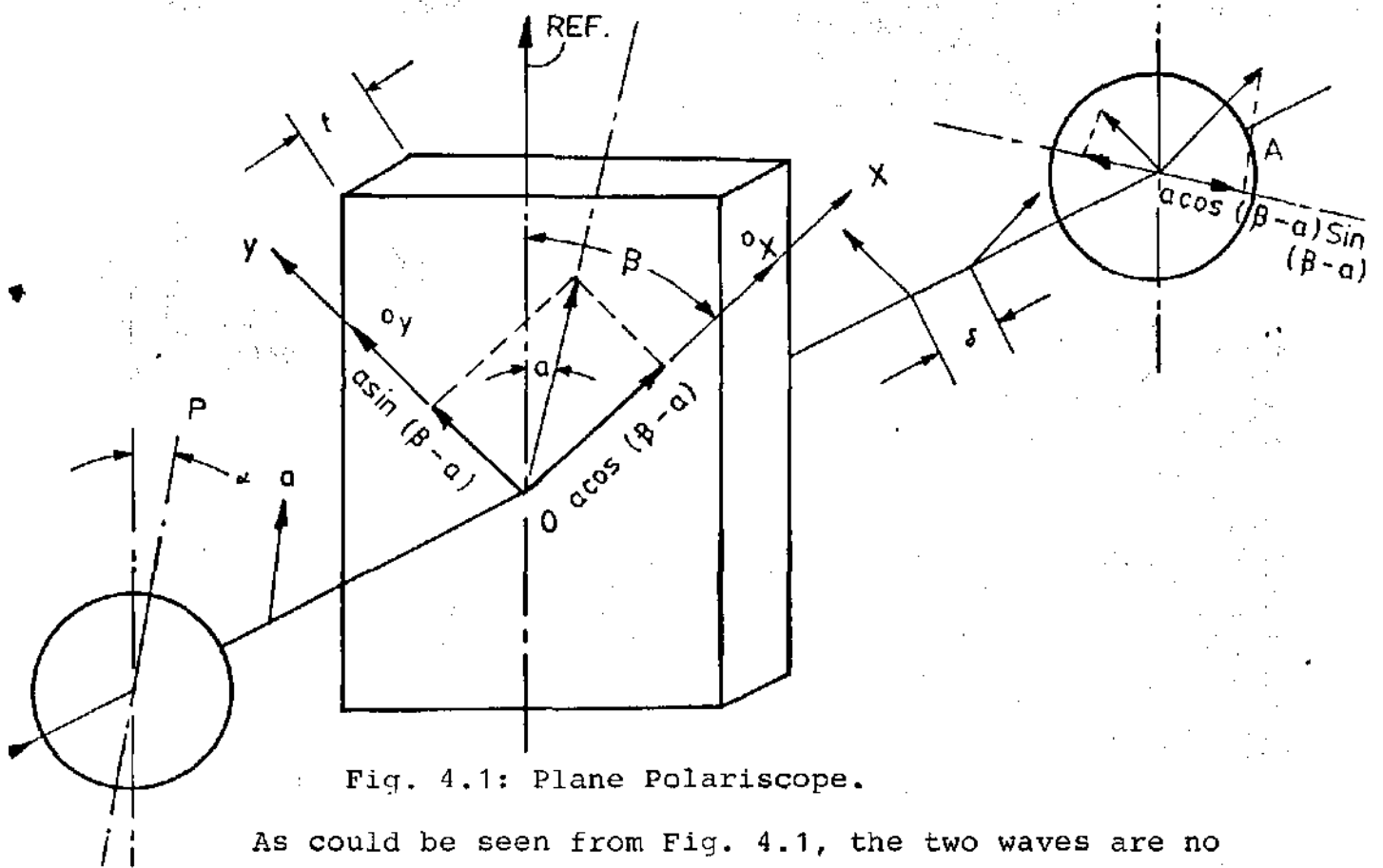


Fig. 4.1: Plane Polariscroscope.

As could be seen from Fig. 4.1, the two waves are no longer in phase when emerging from the model because of the relative retardation δ . The analyser A will transmit only one component of each of these waves, i.e. the one which is parallel to A. These waves will interfere and the resulting light intensity depends on the retardation δ and the angle between the analyser and direction of principal stresses $(\beta - \alpha)$. For plane polariscroscope, the intensity of light emerging will be

$$I = a^2 \sin^2 2(\beta - \alpha) \sin^2 \left(\frac{\pi \delta}{\lambda} \right) \text{ ----- (4.5)}$$

where $(\beta - \alpha)$ is the angle between the analyser and direction of principal stresses, δ = retardation and λ = wavelength.

When a quarter-wave plate is introduced in the path of light propagation, the plane polariscroscope changes to circular polariscroscope. Here, the emerging light intensity

is independent of the directions of principal stresses. Hence, from equation (4.5), the light intensity becomes

$$I = a^2 \sin^2 \left(\frac{\pi \delta}{\lambda} \right) \text{ ----- (4.6)}$$

From equation (4.5), the light intensity is zero when $(\beta - \alpha)$ is zero or when the crossed polariser-analyser is parallel to the directions of principal stresses.

This is for plane polariscope. Then for circular polariscope (equation (4.6)), the light intensity becomes zero when $\delta = 0$, $\delta = 1\lambda$; $\delta = 2\lambda$ or $\delta = N\lambda$ where N is 1, 2, etc. This number N which expresses the size of retardation is called the fringe order. Once $\delta = N\lambda$ is known, the strains are:

$$\epsilon_1 - \epsilon_2 = \frac{\delta}{t.k} = N \frac{\lambda}{t.k} = N.f \text{ ----- (4.7)}$$

where f contains all constants and N is the result of measurement.

Usually, in photoelastic analysis, the measured value is expressed in terms of stress rather than strain. Hence, in terms of stress, the basic equation becomes

$$\sigma_1 - \sigma_2 = N \cdot \frac{c}{t} = N.K \text{ ----- (4.8)}$$

$$\text{where } K = \frac{c}{t} \text{ ----- (4.9)}$$

K is the optical constant of the photoelastic model and t is the thickness of the model. K is either given by the manufacturer or can be simply determined by calibration as was the case in Chapter Five of this work. In photoelastic method of stress analysis, once the fringe order N is known, the stress difference $(\sigma_1 - \sigma_2)$ at any point in the model is completely defined using equation (4.8).

4.1.1. The Photoelastic Materials - The commonly employed photoelastic materials include Bakelite BT-61-893, Bakelite 48-005, Catalin, Celluloid, Glass, Columbia Resin CR-39, Unplasticised perspex, Marblette and Gelatin.

The choice of material for photoelastic model may be governed by the individual problem under consideration, that is, the type of model being investigated and the sensitivity. In addition, there are certain other general properties which should be sought for. These properties are summarised under the following headings:

The model material must transmit light. The material must be isotropic, that is to say that the material must not show any double refraction before the application of external loads. The material should be easy to fabricate into any desired shape for the model, either by machining, casting or joining of several pieces. The material must be hard enough to withstand the machining and clamping forces. A high modulus of elasticity is desirable to prevent excessive deflection of the model. Also desirable are moderate tensile strength and freedom from strain creep. The stress-optical sensitivity should be high and the optical creep effect small. The material selected is expected to have linear stress-strain and stress-retardation relations so as to conform to the elastic theory, on which this method of analysis is based, for similarity in stress pattern between model and prototype. The mechanical as well as the optical properties are expected to be constant at room temperature. Lastly, the cost of the material is expected to be moderate and the material must be readily available.

It may be difficult to have a single material that has all the properties enumerated above. The model material selected for this work is Columbia Resin CR-39 which has the following properties. CR-39 is a beautiful clear material. Optically, it is moderately sensitive to stress and it has relatively high modulus of elasticity. It is somewhat brittle and has the tendency to creep under load. The material was chosen on the ground that it was the model material available and because of its optical sensitivity.

4.2. The Finite Difference Method:

The partial differential equations presented for solution in stressing problems are typified by Poissons equations, laplace equations, harmonic and bia-harmonic equations in elasticity, etc., and none is likely to be capable of precise analytical solution for general problems of practical importance. An approximate numerical method of wide application is provided by Finite Difference Method, FDM. Essentially, these replace the (linear) governing equations and boundary conditions by finite difference approximation in terms of a finite number of unknown values of the dependent variables at a number of discrete points within or just outside the domain of integration. The finite difference equations form a set of linear algebraic equations to be solved for the set of unknowns. The task of accomplishing such numerical solution of large number of simultaneous linear equations can be achieved with the aid of an electronic computer; but before any discussion

of ways and means of solving the finite difference equations, either by the use of a computer or otherwise, some comments on their formulation are first called for.

4.2.1. Formulation of Finite Difference Equations -

As could have been inferred from the preceding section, FDM involves the replacement of the governing differential equation by a set of algebraic simultaneous linear equations which represent the value of the unknown variables (stress, strain, etc.), at some pivotal points which are normally referred to as nodes.

Making use of basic differential calculus, the definition of a derivative is given as follows:

$$\frac{df(x)}{dx} = \lim_{\Delta x \rightarrow 0} \frac{f(x + \Delta x) - f(x)}{\Delta x} \quad \text{----- (4.10)}$$

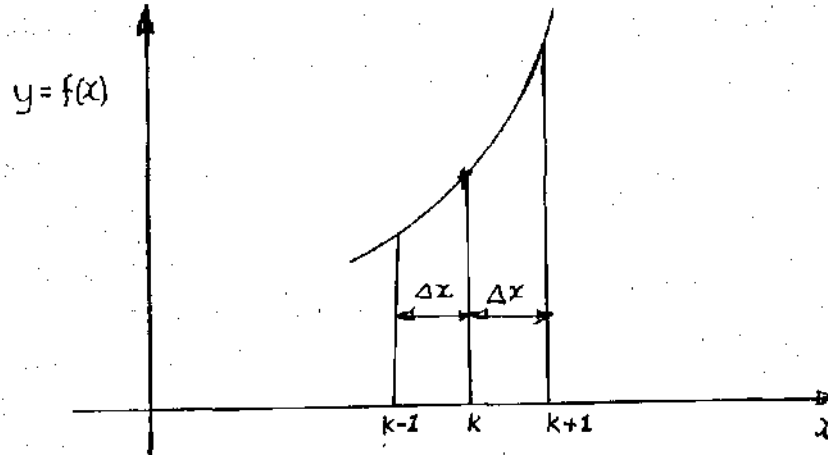


Fig. 4.2: Toward* Difference Formulae.

Referring to and making use of notations given in Fig. 4.2, we have:

$$\left(\frac{dy}{dx}\right)_K = \frac{Y_{K+1} - Y_{K-1}}{2 \Delta x} = \frac{Y_{K+\frac{1}{2}} - Y_{K-\frac{1}{2}}}{\Delta x} \quad \text{----- (4.11)}$$

Equation (4.11) is called difference formula.

Higher order differential coefficients can be derived in difference form in just the same way. For instance:

$$\left(\frac{d^2 y}{dx^2}\right)_K = \frac{d}{dx} \left(\frac{dy}{dx}\right)_K = \frac{\left(\frac{dy}{dx}\right)_{K+\frac{1}{2}} - \left(\frac{dy}{dx}\right)_{K-\frac{1}{2}}}{\Delta x}$$

But

$$\left(\frac{dy}{dx}\right)_{K+\frac{1}{2}} = \frac{Y_{K+1} - Y_K}{\Delta x} \quad \text{and} \quad \left(\frac{dy}{dx}\right)_{K-\frac{1}{2}} = \frac{Y_K - Y_{K-1}}{\Delta x}$$

$$\therefore \left(\frac{d^2 y}{dx^2}\right)_K = \frac{Y_{K+1} + Y_{K-1} - 2Y_K}{(\Delta x)^2} \quad \text{----- (4.12)}$$

The equations which normally occur in problems in elasticity are partial differential equations.

Figure 4.3 shows the conventional way of numbering the node points in order to obtain difference formula for point O. Note that non-strict adherence to this convention introduces no error.

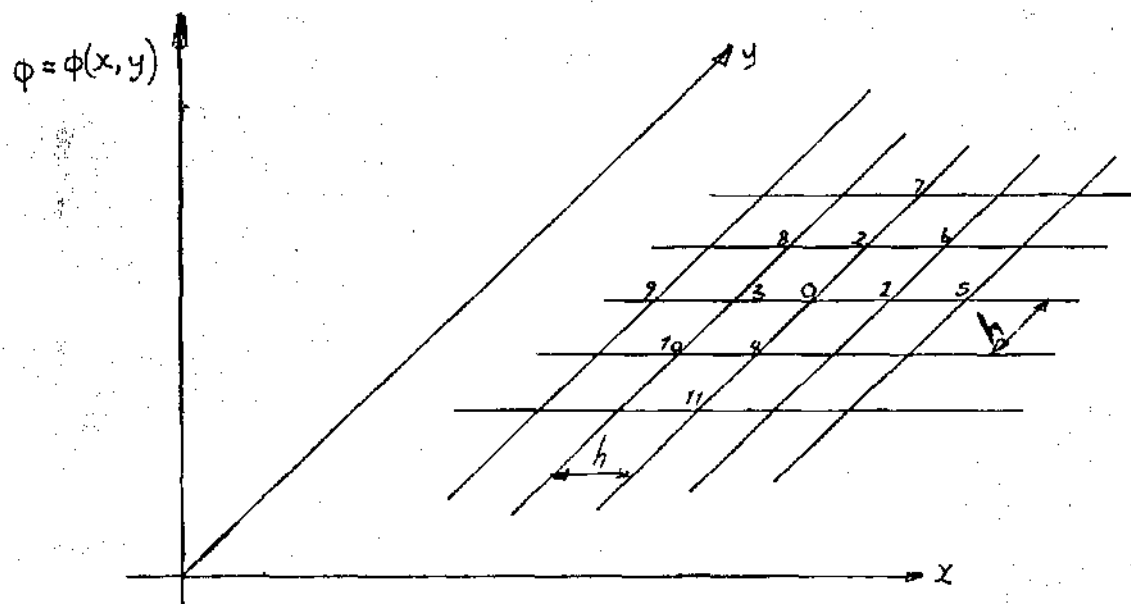


Fig. 4.3: Square Mesh and Numbered Nodal Points.

Extending the formulae (4.11) and (4.12) in terms of $\phi = \phi(x, y)$ for a square mesh gives:

$$\left(\frac{\partial^2 \phi}{\partial x^2}\right)_O = \frac{\phi_1 + \phi_3 - 2\phi_O}{h^2} \quad \text{----- (4.13)}$$

$$\left(\frac{\partial^2 \phi}{\partial y^2}\right)_0 \cong \frac{\phi_2 + \phi_4 - 2\phi_0}{h^2}$$

$$\begin{aligned} \therefore (\nabla^2 \phi)_0 &= \left(\frac{\partial^2 \phi}{\partial x^2}\right)_0 + \left(\frac{\partial^2 \phi}{\partial y^2}\right)_0 \\ &= \frac{\phi_1 + \phi_2 + \phi_3 + \phi_4 - 4\phi_0}{h^2} \end{aligned} \quad \text{----- (4.14)}$$

This can be extended to n-th order equation in the same manner. Hence:

$$\left(\frac{\partial^4 \phi}{\partial x^4}\right)_0 \cong \frac{\left(\frac{\partial^2 \phi}{\partial x^2}\right)_1 + \left(\frac{\partial^2 \phi}{\partial x^2}\right)_3 - 2\left(\frac{\partial^2 \phi}{\partial x^2}\right)_0}{h^2} \quad \text{----- (4.15)}$$

which gives:

$$\left(\frac{\partial^4 \phi}{\partial x^4}\right)_0 \cong \frac{6\phi_0 - 4\phi_1 - 4\phi_3 + \phi_5 + \phi_9}{h^4} \quad \text{----- (4.16)}$$

Similarly,

$$\left(\frac{\partial^4 \phi}{\partial y^4}\right)_0 \cong \frac{6\phi_0 - 4\phi_2 - 4\phi_4 + \phi_7 + \phi_{11}}{h^4} \quad \text{----- (4.17)}$$

The above equations were obtained on the ground that the boundaries of the cross-section or component being analysed are coincident with nodal points. In most engineering problems, the boundaries of the cross-section or component being analysed will not conveniently pass through the node points of the mesh and the difference equation must therefore be modified to allow for this.

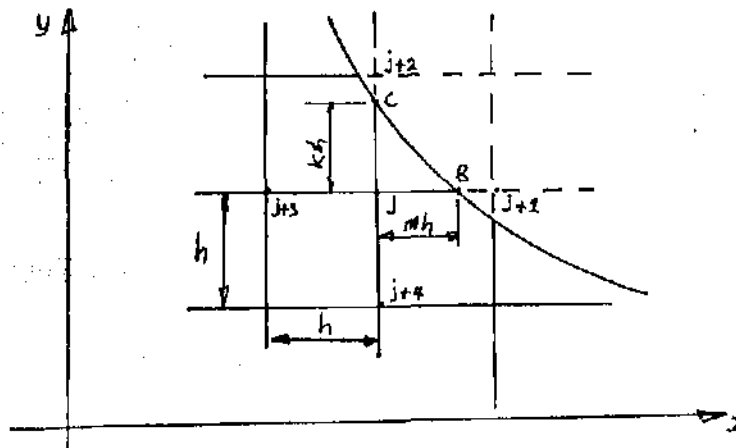


Fig. 4.4: Boundary not Coincident with Nodes.

In Fig. 4.4, B is a point on the boundary which does not coincide with the mesh; mh is the distance between j and B points in the x-direction ($m < 1$) and j+1 is an imaginary point on the mesh outside the boundary. In the same manner, C is another point on the boundary which does not coincide with the mesh; Kh is the distance between j and C in the y-direction while j+2 is another imaginary point on the mesh outside the boundary.

Employing the idea used in generating equations (4.14), (4.15), (4.16) and (4.17), the slope in the x- and y-directions at j are given by:

$$\left(\frac{\partial \phi}{\partial x}\right)_j \cong \frac{\phi_B - \phi_j}{mh}; \quad \left(\frac{\partial \phi}{\partial y}\right)_j \cong \frac{\phi_C - \phi_j}{Kh} \quad \text{----- (4.18)}$$

and hence the value of ϕ at the imaginary mesh point j+1 and j+2 can be extrapolated as:

$$\phi_{j+1} \cong \phi_j + h\left(\frac{\partial \phi}{\partial x}\right)_j + \left(1 - \frac{1}{m}\right)\phi_j$$

$$\phi_{j+2} \cong \phi_j + h\left(\frac{\partial \phi}{\partial y}\right)_j + \left(1 - \frac{1}{K}\right)\phi_j$$

Hence,

$$\left(\frac{\partial^2 \phi}{\partial x^2}\right)_j \cong \frac{\phi_{j+3} + \frac{1}{m}\phi_B - \left(1 + \frac{1}{m}\right)\phi_j}{h^2} \quad \text{----- (4.19)}$$

$$\left(\frac{\partial^2 \phi}{\partial y^2}\right)_j = \frac{\phi_{j+4} + \frac{1}{K}\phi_C - \left(1 + \frac{1}{K}\right)\phi_j}{h^2}$$

$$\begin{aligned} \therefore (\nabla^2 \phi)_j &= \left(\frac{\partial^2 \phi}{\partial x^2}\right)_j + \left(\frac{\partial^2 \phi}{\partial y^2}\right)_j \\ &= \frac{\phi_{j+3} + \phi_{j+4} + \frac{1}{m}\phi_B + \frac{1}{K}\phi_C - 2\phi_j - \left(\frac{1}{m} + \frac{1}{K}\right)\phi_j}{h^2} \quad \text{--- (4.20)} \end{aligned}$$

With equations (4.14) and (4.20), any stress problem can be solved by FDM by generating the mesh and finding the difference equations which give n-equations in n-unknowns which could be solved manually or with the use of computer.

4.2.2. Computer Solution of FDM - Once the set of simultaneous linear algebraic equations to be solved are written in the right order, it will be found that the matrix dimension corresponds to the number of nodes. These equations can be solved by Gaussian elimination process either manually for rough meshes or by the use of computer for fine meshes. Computer programmes have been written which are capable of solving large sets of equations.

4.2.3. Accuracy of Finite Difference Solution - It has been pointed out that the FDM contains an essential approximation, consequently solutions obtained by its use must be in some error no matter how small. The error can be made small and in the past, two extreme ways of doing so have been advocated: (i) by taking the mesh sufficiently fine; (ii) by including sufficiently high order differences in finite difference formulae based on a coarse mesh.

4.3. The Finite Element Method (FEM);

The basis of FEM is the element stiffness matrix. It involves dividing physical systems such as structure, solid, etc., into a finite number of relatively simple elements whose load-displacement characteristics are known, can easily be derived or approximated using well tried method in the theory of elasticity. These elements are connected at a discrete number of points along their periphery known as nodal points.

When a problem is being solved with the use of FEM, it is important to be aware of the physics and engineering assumptions of it. This method offers a unifying approach to the solution of diverse engineering problems. Two basic

features make the FEM to be superior to other competing methods. First, a geometrically complex domain of the problem is represented as a collection of geometrically simple subdomains called finite elements. Second, over each finite element the approximations are derived using the basic idea that any continuous function can be represented by a linear combination of algebraic polynomials.

4.3.1. The Element Stiffness Matrix - As said in the preceding section, any structure being analysed with the use of FEM may be broken down into finite number of relatively simple elements whose load-displacement characteristics are known, can easily be derived or approximated. The structure or component is then re-assembled using the chosen elements and the overall or structure stiffness equations thus derived. These equations linking the structure loads and structure displacements are approximate, the degree of approximation depending on how well the assembly elements accommodate the loading and boundary conditions and obey the rules of compatibility. Hence, the element stiffness matrix is the basic building block of the FEM.

Let us take for instance, an arbitrarily shaped element with n nodes as shown in Figure 4.5.

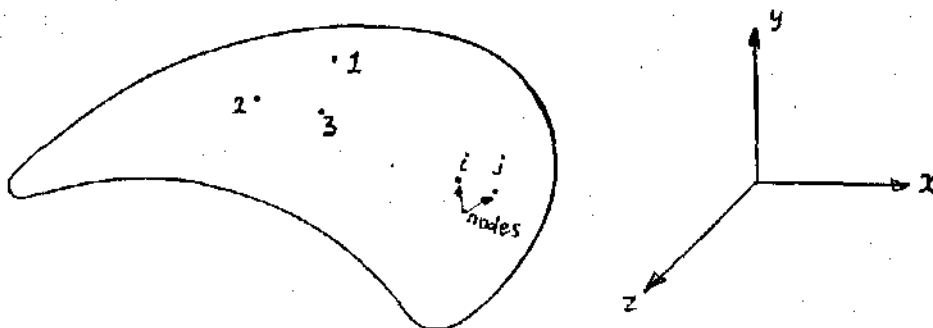


Fig. 4.5: Node Points on Arbitrarily Shaped Element.

Each node is, in general, free to move in several directions and thus each node will have a number of element displacement (δ) associated with it and with each displacement will be associated an element load (p). Each element load p_i will depend upon every element displacement ($\delta_1, \delta_2, \dots, \delta_n$) and for a linear elastic solid a typical equation would be:

$$p_i = K_{i1}\delta_1 + K_{i2}\delta_2 + \dots + K_{in}\delta_n \text{ ----- (4.21)}$$

where $i = 1, 2, \dots, n$. The coefficients K_{ij} in equations (4.21) are called stiffness coefficients and the whole of n equations would be written

$$\begin{array}{l} p_1 = K_{11}\delta_1 + K_{12}\delta_2 + \dots + K_{1n}\delta_n \\ p_2 = K_{21}\delta_1 + K_{22}\delta_2 + \dots + K_{2n}\delta_n \\ \vdots \\ p_n = K_{n1}\delta_1 + K_{n2}\delta_2 + \dots + K_{nn}\delta_n \end{array} \quad \text{ } \text{----- (4.22)}$$

Equation (4.22) written in short matrix form gives:

$$\{p\} = [K]\{\delta\} \text{ ----- (4.23)}$$

where $\{p\}$ is the column vector of loads, $\{\delta\}$ is the column vector of displacements and $[K]$ is the element stiffness matrix.

Calculation of element stiffness matrix $[K]$ is the starting point of FEM. In the following section, the stiffness matrix is calculated for two-dimensional element used in plane elasticity (triangular element).

4.3.2. Triangular Element -

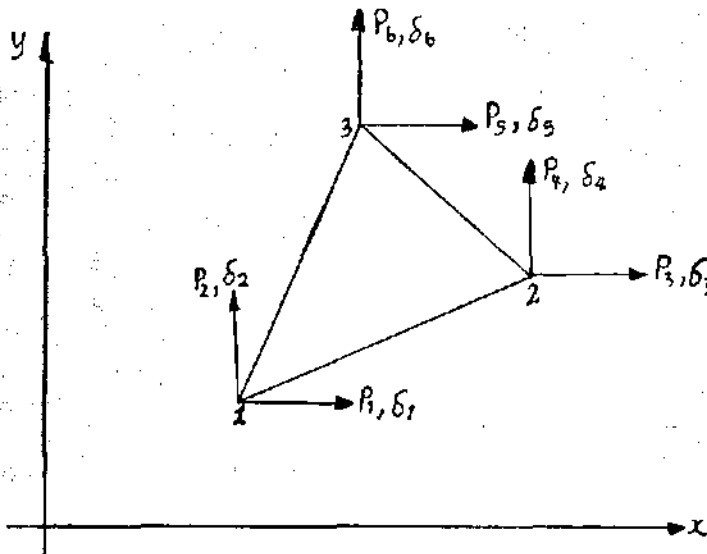


Fig. 4.6: Triangular Element.

A typical triangular element normally used in the analysis of two-dimensional problems is shown in Figure 4.6. The element is referenced to x-y system of coordinates. Nodes are numbered in counter-clockwise direction. The thickness of the element is t , the area is A . Loads and displacements follow the node numbering but have their own separate numeration.

In this two-dimensional element analysis, we assume a function for the displacements: The displacement function here selected (equation (4.24)) is the lowest order one and is outstanding as it provides constant strain throughout the element (consequently constant stress). A triangular element with displacement function (4.24) is known as CST - (Constant-Strain-Triangle).

We have six degrees of freedom involved, six unknown coefficients are required.

$$\left. \begin{aligned} \delta_x &= \alpha_1 + \alpha_2 x + \alpha_3 y \text{ (in x-direction)} \\ \delta_y &= \alpha_4 + \alpha_5 x + \alpha_6 y \text{ (in y-direction)} \end{aligned} \right\} \text{----- (4.24)}$$

where $\alpha_1 \dots \alpha_6$ are the six unknowns and are found by evaluating displacements at each of the nodes as follows:

$$\begin{Bmatrix} \delta_1 \\ \delta_3 \\ \delta_5 \end{Bmatrix} = \begin{bmatrix} 1 & x_1 & y_1 \\ 1 & x_2 & y_2 \\ 1 & x_3 & y_3 \end{bmatrix} \begin{Bmatrix} \alpha_1 \\ \alpha_2 \\ \alpha_3 \end{Bmatrix} \quad \text{and}$$

$$\begin{Bmatrix} \delta_2 \\ \delta_4 \\ \delta_6 \end{Bmatrix} = \begin{bmatrix} 1 & x_1 & y_1 \\ 1 & x_2 & y_2 \\ 1 & x_3 & y_3 \end{bmatrix} \begin{Bmatrix} \alpha_4 \\ \alpha_5 \\ \alpha_6 \end{Bmatrix} \quad \text{----- (4.25)}$$

The first set of equations (4.25) solved for $\alpha_1, \alpha_2, \alpha_3$ (by Gaussian elimination or matrix inversion) gives:

$$\begin{Bmatrix} \alpha_1 \\ \alpha_2 \\ \alpha_3 \end{Bmatrix} = \frac{1}{2A} \begin{bmatrix} x_2 y_3 - x_3 y_1 & x_3 y_1 - x_1 y_2 & x_1 y_2 - y_1 x_3 \\ -y_2 x_3 & -y_3 x_1 & -y_1 x_2 \\ y_2 - y_3 & y_3 - y_1 & y_1 - y_2 \\ x_3 - x_2 & x_1 - x_3 & x_2 - x_1 \end{bmatrix} \begin{Bmatrix} \delta_1 \\ \delta_2 \\ \delta_3 \end{Bmatrix} \quad \text{---- (4.26)}$$

where $2A = (x_2 y_3 - x_3 y_2) - (x_1 y_3 - x_3 y_1) + (x_1 y_2 - y_1 x_2) = 2 \times \text{area of triangular element.}$

Similarly, the second set of (4.25) is solved and the full solution becomes:

$$\begin{Bmatrix} \alpha_1 \\ \alpha_2 \\ \alpha_3 \\ \alpha_4 \\ \alpha_5 \\ \alpha_6 \end{Bmatrix} = \frac{1}{2A} \begin{bmatrix} x_2 y_3 - & 0 & x_3 y_1 - & 0 & x_1 y_2 - & 0 \\ y_2 x_3 & & y_3 x_1 & & y_1 x_2 & \\ b_1 & 0 & b_2 & 0 & b_3 & 0 \\ a_1 & 0 & a_2 & 0 & a_3 & 0 \\ 0 & x_2 y_3 - & 0 & x_3 y_1 - & 0 & x_1 y_2 - \\ & y_2 x_3 & & y_3 x_1 & & y_1 x_2 \\ 0 & b_1 & 0 & b_2 & 0 & b_3 \\ 0 & a_1 & 0 & a_2 & 0 & a_3 \end{bmatrix} \begin{Bmatrix} \delta_1 \\ \delta_2 \\ \delta_3 \\ \delta_4 \\ \delta_5 \\ \delta_6 \end{Bmatrix} \quad \text{----- (4.2)}$$

where

$$\begin{aligned} a_1 &= x_3 - x_2; & b_1 &= y_2 - y_3 \\ a_2 &= x_1 - x_3; & b_2 &= y_3 - y_1 \\ a_3 &= x_2 - x_1; & b_3 &= y_1 - y_2 \end{aligned} \quad \text{----- (4.28)}$$

Nodal displacements $\delta_1 \dots \delta_6$ are not yet known.

From strain-displacement equations,

$$\epsilon_x = \frac{\partial \delta_x}{\partial x}, \quad \epsilon_y = \frac{\partial \delta_y}{\partial y}, \quad \gamma_{xy} = \frac{\partial \delta_x}{\partial y} + \frac{\partial \delta_y}{\partial x} \quad \text{----- (4.29)}$$

we get (from equations (4.24) and (4.27))

$$\begin{Bmatrix} \epsilon_x \\ \epsilon_y \\ \gamma_{xy} \end{Bmatrix} = \frac{1}{2A} \begin{bmatrix} b_1 & 0 & b_2 & 0 & b_3 & 0 \\ 0 & a_1 & 0 & a_2 & 0 & a_3 \\ a_1 & b_1 & a_2 & b_2 & a_3 & b_3 \end{bmatrix} \begin{Bmatrix} \delta_1 \\ \delta_2 \\ \delta_3 \\ \delta_4 \\ \delta_5 \\ \delta_6 \end{Bmatrix} \quad \text{----- (4.30)}$$

or

$$\{\epsilon(e)\} = [B(e)] \{\delta(e)\} \quad \text{----- (4.31)}$$

For a plane state the stress-strain relationship is:

$$\{\sigma(e)\} = \begin{Bmatrix} \sigma_x \\ \sigma_y \\ \tau_{xy} \end{Bmatrix} = [D(e)] \begin{Bmatrix} \epsilon_x \\ \epsilon_y \\ \gamma_{xy} \end{Bmatrix} \quad \text{----- (4.32)}$$

or

$$\{\sigma(e)\} = [D(e)] \{\epsilon(e)\} \quad \text{----- (4.33)}$$

where, for plane state of stress

$$[D(e)] = \frac{E}{(1+\mu)(1-2\mu)} \begin{bmatrix} 1-\mu & \mu & 0 \\ \mu & 1-\mu & 0 \\ 0 & 0 & \frac{1-2\mu}{2} \end{bmatrix} \quad \text{--- (4.34)}$$

For a plane state of stress

$$[D(e)] = \frac{E}{1-\mu^2} \begin{bmatrix} 1 & \mu & 0 \\ \mu & 1 & 0 \\ 0 & 0 & \frac{1-\mu}{2} \end{bmatrix} \quad \text{--- (4.35)}$$

Equations (4.34) and (4.35) are derived from three-dimensional Hooke's Law, E and μ being the Young's modulus and Poisson's ratio, respectively.

The next step in the derivation is to find a set of nodal forces which are statically equivalent to the stress field acting. Refer to Figure 4.7.

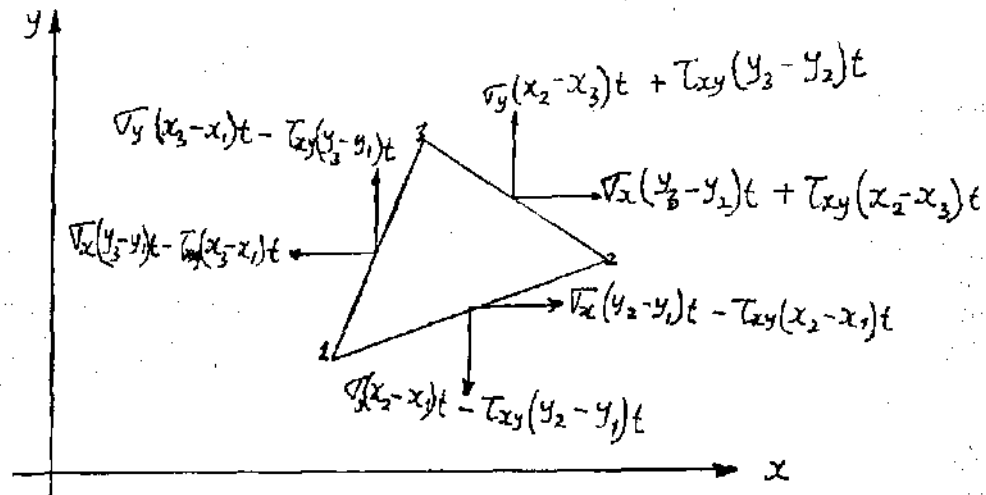


Fig. 4.7a: Uniform Stress Field of an Element resolved into nodal forces.

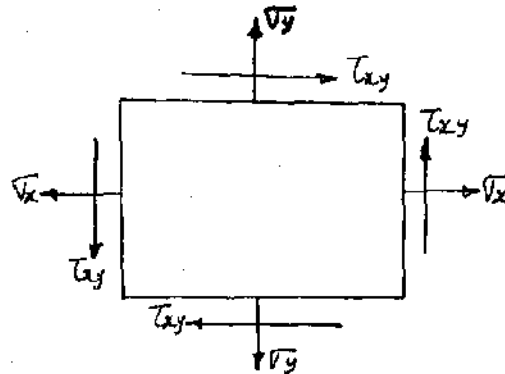


Fig. 4.7b: Plane State Stress.

As mentioned earlier, the stresses are uniform within the triangle, hence the mid-side forces are now divided equally between their adjacent nodes. Also equation (4.22) is applied.

$$\{p^{(e)}\} = \begin{Bmatrix} p_1 \\ p_2 \\ p_3 \\ p_4 \\ p_5 \\ p_6 \end{Bmatrix} = \frac{-t^{(e)}}{2} \begin{bmatrix} b_3+b_2 & 0 & a_3+a_2 \\ 0 & a_3+a_2 & b_3+b_2 \\ b_1+b_3 & 0 & a_1+a_3 \\ 0 & a_1+a_3 & b_1+b_3 \\ b_1+b_2 & 0 & a_1+a_2 \\ 0 & a_1+a_2 & b_1+b_2 \end{bmatrix} \begin{Bmatrix} \sigma_x \\ \sigma_y \\ \tau_{xy} \end{Bmatrix} \quad \text{--- (4.36)}$$

Again noting that $b_3+b_2 = -b_1$ (from equation (4.28)), this becomes:

$$\{p^{(e)}\} = \frac{t^{(e)}}{2} \begin{bmatrix} b_1 & 0 & a_1 \\ 0 & a_1 & b_1 \\ b_2 & 0 & a_2 \\ 0 & a_2 & b_2 \\ b_3 & 0 & a_3 \\ 0 & a_3 & b_3 \end{bmatrix} \{\sigma^{(e)}\} \quad \text{--- (4.37)}$$

From matrix algebra transposing a matrix simply means interchanging its rows and columns. Comparing matrices in equations (4.37) and (4.30) we conclude;

$$\{p^{(e)}\} = \frac{t^{(e)}}{2} \cdot 2A^{(e)} \cdot [B^{(e)}]^T \cdot \{\sigma^{(e)}\} \quad \text{--- (4.38)}$$

where

$$[B^{(e)}]^T = \frac{1}{2A^{(e)}} \begin{bmatrix} -b_1 & 0 & a_1 \\ 0 & a_1 & b_1 \\ b_2 & 0 & a_2 \\ 0 & a_2 & b_2 \\ b_3 & 0 & a_3 \\ 0 & a_3 & b_3 \end{bmatrix} \quad \text{--- (4.39)}$$

is the transpose of matrix $[B^{(e)}]$.

Substituting now equations (4.31) and (4.33) in equation (4.38) gives:

$$\{p^{(e)}\}_j = t^{(e)} A^{(e)} [B^{(e)}]^T [D^{(e)}] [B^{(e)}] \{\delta^{(e)}\} \quad \text{--- (4.40)}$$

or

$$\{p^{(e)}\}_j = [K^{(e)}] \{\delta^{(e)}\} \quad \text{----- (4.41)}$$

and the element stiffness matrix is therefore:

$$[K^{(e)}] = t^{(e)} A^{(e)} [B^{(e)}]^T [D^{(e)}] [B^{(e)}] \quad \text{---- (4.42)}$$

The final step is to determine the element stress from the element nodal displacements. This is done from equations (4.33) and (4.31):

$$\{\sigma^{(e)}\}_j = [D^{(e)}] [B^{(e)}] \{\delta^{(e)}\} \quad \text{----- (4.43)}$$

or

$$\{\sigma^{(e)}\}_j = [H^{(e)}] \{\delta^{(e)}\} \quad \text{----- (4.44)}$$

where $[H^{(e)}]$ is the stress-displacement matrix. Note that if:

the material of each element is the same, $[D^{(e)}] = [D]$ throughout the calculations;

the thickness of all elements is the same, $t^{(e)} = t$ throughout the calculations;

all triangle areas are the same, $A^{(e)} = A$ and one realizes how powerful the method is.

Also it should be noted that the element stiffness matrix $[K^{(e)}]$ can be calculated without knowing nodal displacements. Stresses and strains, however, can be calculated only if nodal displacements are known.

CHAPTER FIVE

5.0. EXPERIMENTAL RESULTS

5.1. Detailed Description Of The Photoelastic Bench Used:

Model 061 Polariscopes was used for this experimental work (see Plate xix). The model required no assembly operations. The polariscopes was simply set on a table and the power line connected to a 110 volt A/C supply. The parts of the instrument are as follows:

(i) A diffused light source consisting of six fluorescent tubes equally spaced about the optical centre of the instrument. The tubes are cool while General Electric F15T12-CW bulbs.

(ii) Two polarising filters (polariser and analyser) laminated between glass which are mechanically linked together and may be rotated in unison for the observation of isoclinics.

(iii) Two quarter wave plates positioned between the polariser and analyser which are also mechanically coupled.

(iv) Around the analyser is a graduated color-coded dial to indicate the quantity measured.

(v) A mechanical drive system that provides for remote control of all four filters.

(vi) Straining frame - Model 062, highly overdesigned structure to incorporate a screw-operated loading system for producing constant deformation of the model. The model 062 has a built in vertical and lateral travel adjustment for ease and versatility of model positioning. The frame is mounted on the base of the polariscopes between the

polariser and analyser housings.

(vii) Electrical load cell readout system-Model 062A consisting of a compact universal strain gauge transducer coupled to an indicator to provide a highly accurate load indication. The indicator is equipped with a tension-compression selector switch.

(viii) Camera-Model 066, which was not used in the analysis due to unavailability of the film for it. The particulars of the camera, film and film developer used are as follows: Camera used is Pentax E II M with rings and 135 mm telephoto lens. The film is ORWO Blanck and White - NP 22 $\frac{135}{36}$. The developer is Eukobrom while the Fixer is Superfix. The paper used in printing the photographs is Tura Paper - RR 111.

(ix) Monochromator - Model 068 which was fitted to the point of light source housing.

5.2. Design and Fabrication of the Loading System:

In Figure (5.1), the loading system made up of the loading fixtures, the straining frame and the models is shown. The loading fixtures include two triangular plates used as model hangers, a fork-shaped component and L-shaped component, all used for load application to the models.

Triangular Plates (Model Hangers)- On Figure 5.1, these plates are identified as item Nos. (1) and (6). The dimensions of the two plates are shown in Figures 5.3 and 5.4. They are constructed by marking out the triangular shape on a half-inch thick plates. They are cut and welded to a rectangular bar. The bar serves as a means of support of the hangers to the straining frame.

Fork-Shaped Component - This is identified as item No. (5) on Figure 5.1. The dimensions of the component can be seen on Fig. 5.2. Using the drawing for the component, the dimensions were marked on the bar and cut to shape.

It is used to apply load to one of the models as shown in Figure 5.1. It is connected to the load cell for proper recording of the amount of load applied.

L-Shaped Component - This component is identified as item no. (2) on Figure 5.1. The method of production is the same as the fork. As can be seen from Figure 5.1, it is used to apply load to one of the models. It is connected to the adjustable screw head. The dimensions of the component are seen on Figure 5.5.

5.3. Preparation Of The Models:

A CR-39 photoelastic sheet of 5 mm thickness was used. The dimensions of the gear-models used are shown on Figure 5.6. The pitch circle diameter for both gears is 74 mm. A hole of 9 mm diameter was drilled through the centre of the cut-out sheet and a 9 mm bolt passed through it to help hold it to the headstock of the lathe machine on which the gear-models were turned to shape. The involute shape of the teeth was traced on the blank and the teeth cut using hacksaw and filed to shape. After the filing, the central hole of 9 mm diameter was enlarged to 10 mm to enable the models fit very well in the fixture as shown in Figure 5.1 and Plate xx. For the load application to the gears, the second holes of 8 mm diameter were drilled for the connection of L-shaped and fork-shaped components as shown in Figure 5.1. Finally, the teeth edges and holes were polished with fine emery cloth to reduce friction between surfaces. No annealing of the models was carried out since the models did not show any residual stresses when examined in the polariscope before being stressed.

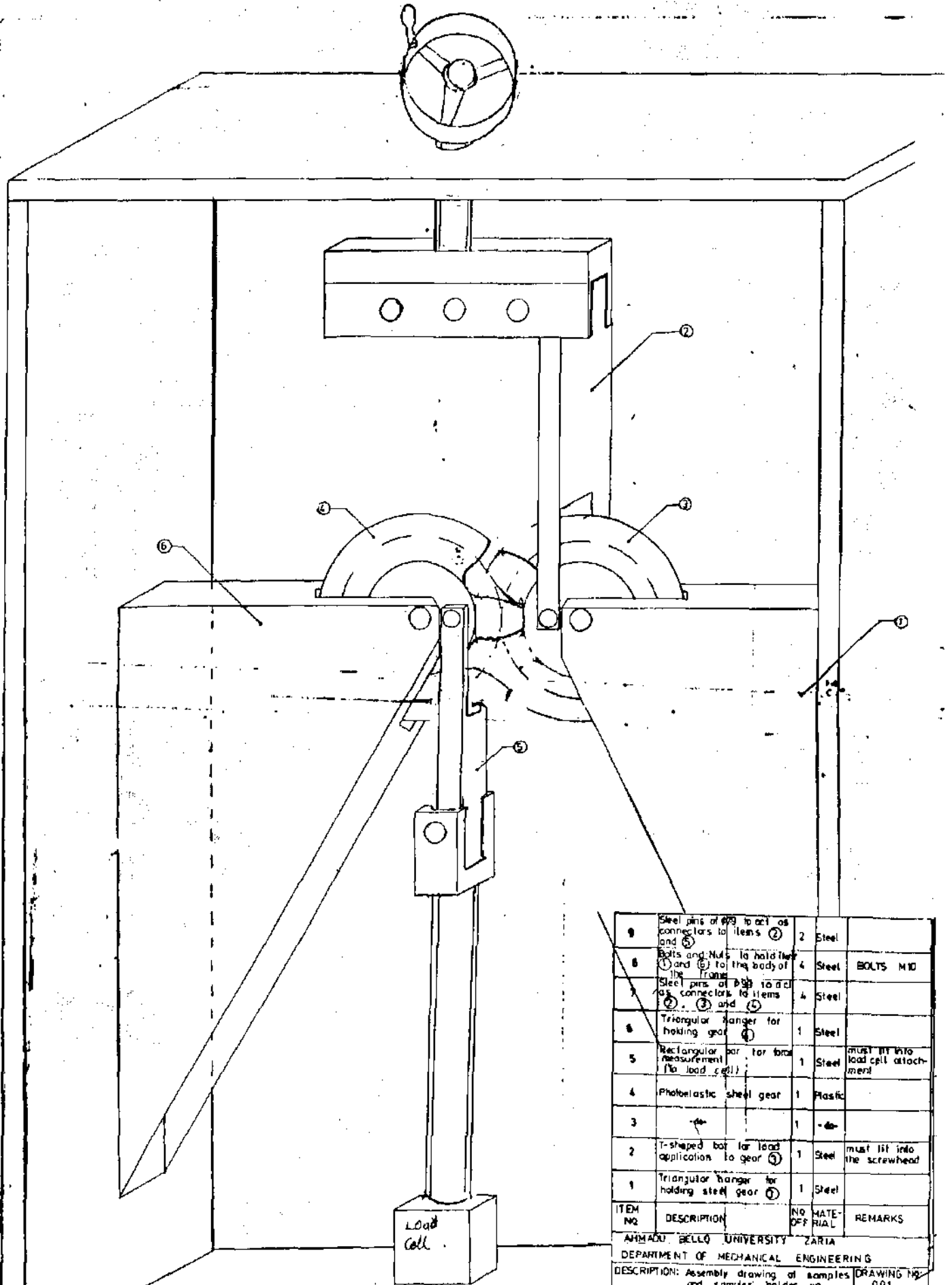
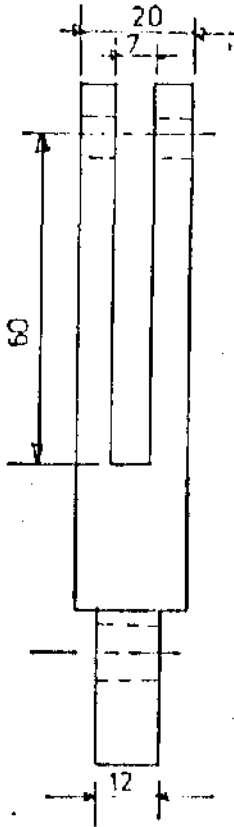
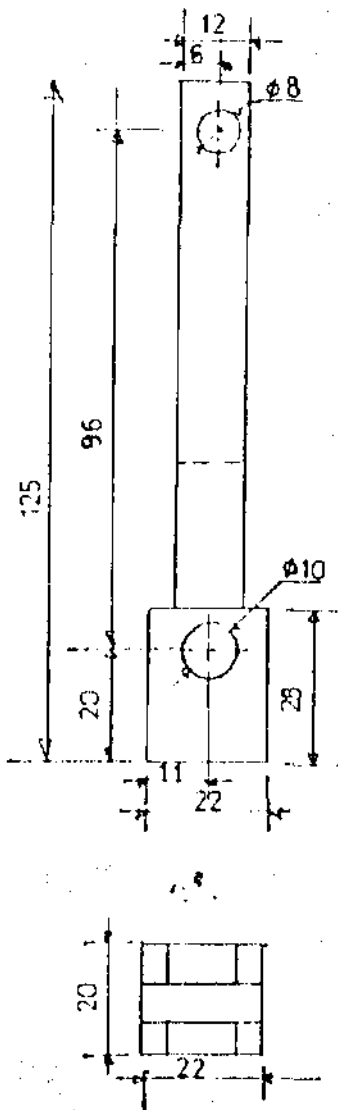


FIG. 51 ASSEMBLY DRAWING

9	Steel pins of 1/8" to act as connectors to items 2 and 5	2	Steel	
8	Bolts and Nuts to hold item 1 and 6 to the body of the frame	4	Steel	BOLTS MID
7	Steel pins of 1/8" to act as connectors to items 2, 3 and 5	4	Steel	
6	Triangular hanger for holding gear 4	1	Steel	
5	Rectangular bar for force measurement (No load cell)	1	Steel	MUST FIT INTO LOAD CELL ATTACHMENT
4	Photoelastic steel gear	1	Plastic	
3		1	-	
2	T-shaped bar for load application to gear 3	1	Steel	MUST FIT INTO THE SCREWHEAD
1	Triangular hanger for holding steel gear 3	1	Steel	
ITEM NO	DESCRIPTION	NO	MATERIAL	REMARKS
AHMADU BELLO UNIVERSITY ZARIA				
DEPARTMENT OF MECHANICAL ENGINEERING				
DESCRIPTION: Assembly drawing of samples holder on photoelastic bench				DRAWING No: 001
NAME		SIGNATURE	DATE	SCALE: 1:1
DRAWN: Ugwu, S. A.			26/09	TOTAL WEIGHT:
TRACED: Ikwere, S. A.			26/09	



AHMADU BELLO UNIVERSITY ZARIA				
DEPARTMENT OF MECHANICAL ENGINEERING				
DESCRIPTION: Detail drawing of item ⑤				DRAWING No: 002
				MATERIAL: STEEL
	NAME	SIGNATURE	DATE	SCALE: 1:1
DRAWN:	Ugwu, S. A.	<i>[Signature]</i>	12:6:89	WEIGHT:
TRACED:	Ugwu, S. A.	<i>[Signature]</i>	12:6:89	
CHECKED:	DR. W. Rychwalski	<i>[Signature]</i>		
APPROVED:	DR. W. Rychwalski	<i>[Signature]</i>		

FIG. 5.2: FORK_SHAPED COMPONENT

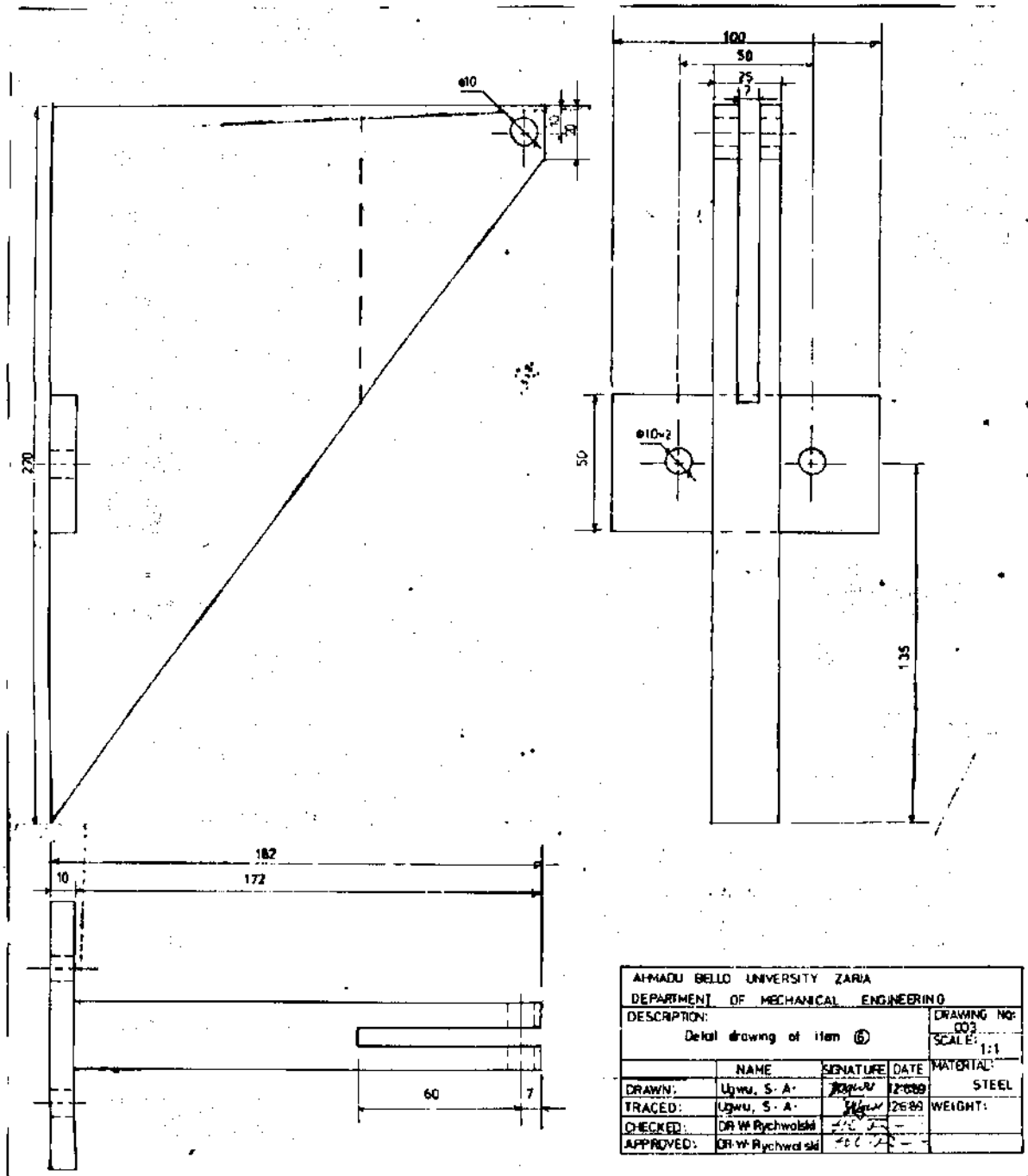


FIG. 5.3: MODEL HANGER

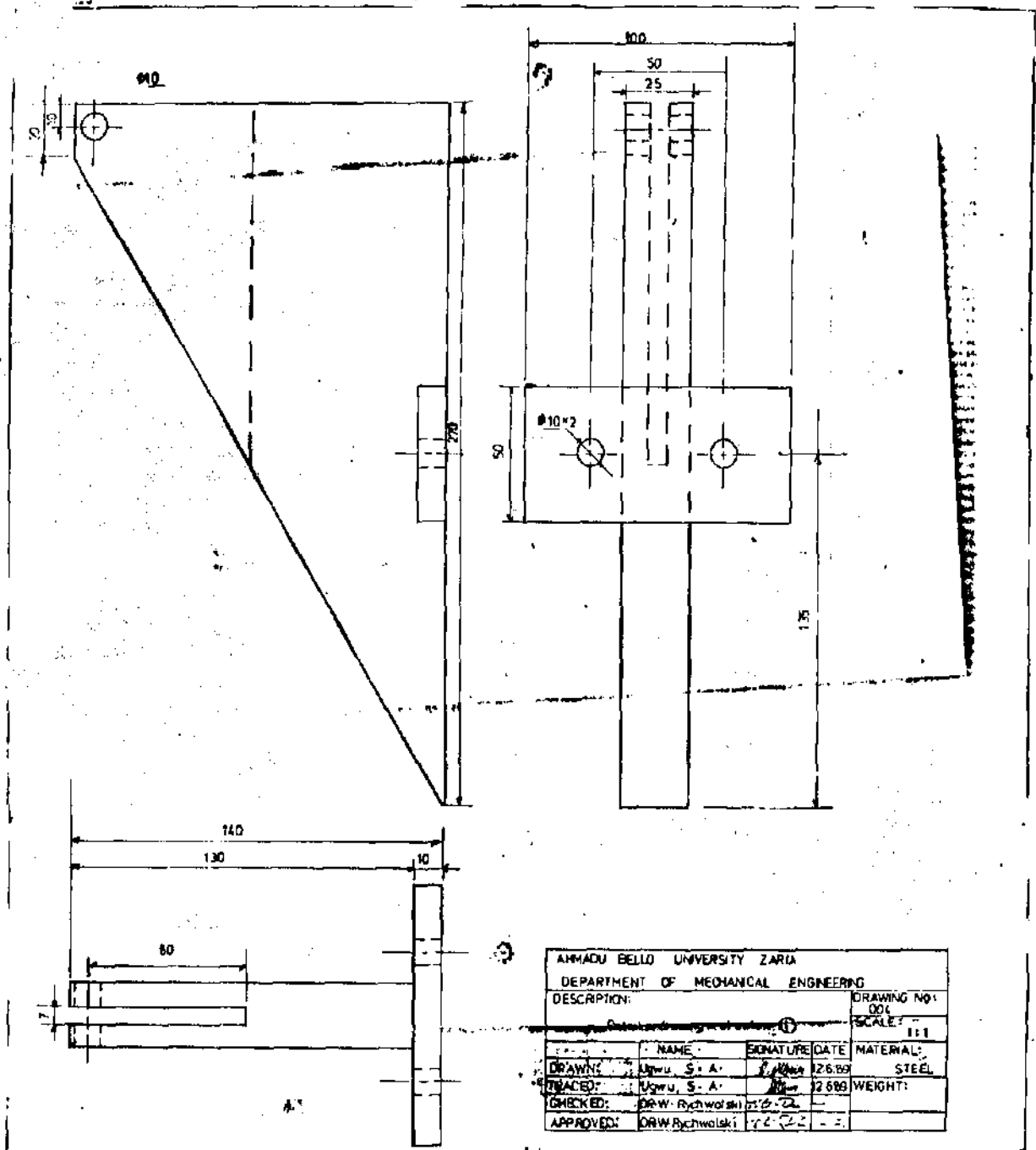
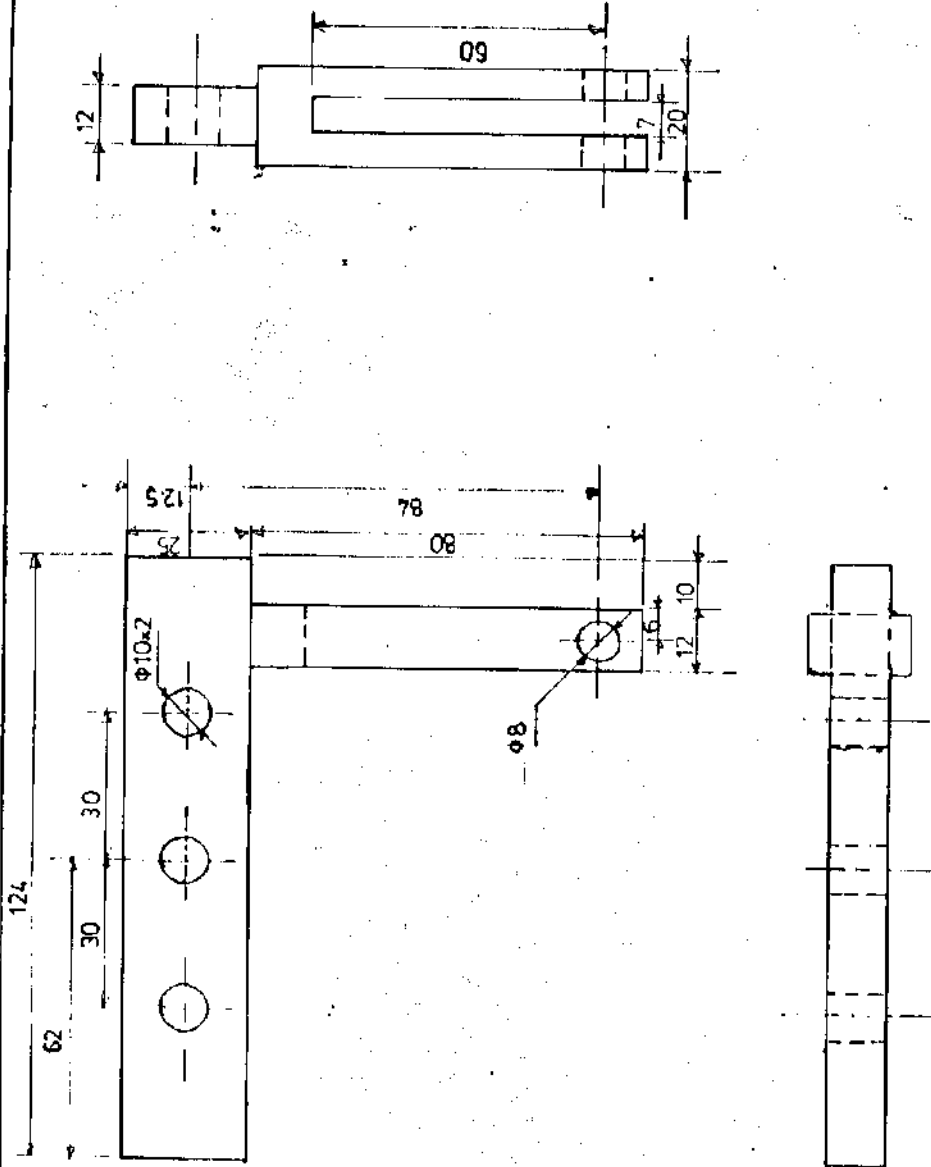


FIG. 5. 4: MODEL HANGER



AHMADU BELLO UNIVERSITY ZARIA		DRAWING NO:	
DEPARTMENT OF MECHANICAL ENGINEERING		005	
DESCRIPTION: Detail drawing of Item ②		SCALE: 1:1	
NAME	SIGNATURE	DATE	MATERIAL:
Ugwu, S. A.	<i>[Signature]</i>	12/6/89	STEEL
Ugwu, S. A.	<i>[Signature]</i>	12/6/89	WEIGHT:
DR. W. Rychwalski	<i>[Signature]</i>		
APPROVED:	DR. W. Rychwalski		

FIG. 5.5: L-SHAPED COMPONENT

DIMENSION OF THE GEARS

No OF TEETH $N = 6$

DIAMETRAL PITCH $P = 2 \text{teeth/in}$

PITCH CIRCLE DIAMETER $d = \frac{N}{P} = \frac{6}{2} = 3 \text{in} = 76.2 \text{mm}$

CIRCULAR PITCH $p = \frac{\pi d}{N} = \frac{\pi \times 75.2}{6} = 39.90 \text{mm} = 1.57 \text{in}$

TOOTH THICKNESS $t = \frac{p}{2} = \frac{39.90}{2} = 19.90 \text{mm} = 0.785 \text{in}$

ADDENDUM DISTANCE $a = \frac{1}{P} = \frac{1}{2} = 0.5 \text{in} = 12.7 \text{mm}$

DEDENDUM DISTANCE $b = \frac{1.25}{P} = \frac{1.25}{2} = 0.625 \text{in} = 15.87 \text{mm}$

EXTERNAL DIAMETER OF THE GEAR BLANK:

ADDENDUM CIRCLE DIAMETER $= d + 2a = 76.2 + 2 \times 12.7 = 101.6 \text{mm}$

DEDENDUM CIRCLE DIAMETER $= d - 2b = 76.2 - 15.87 = 44.45 \text{mm}$

CLEARANCE $= b - c = 0.625 - 0.5 = 0.025 \text{in} = 0.635 \text{mm}$

PRESSURE ANGLE $\phi = 20^\circ$

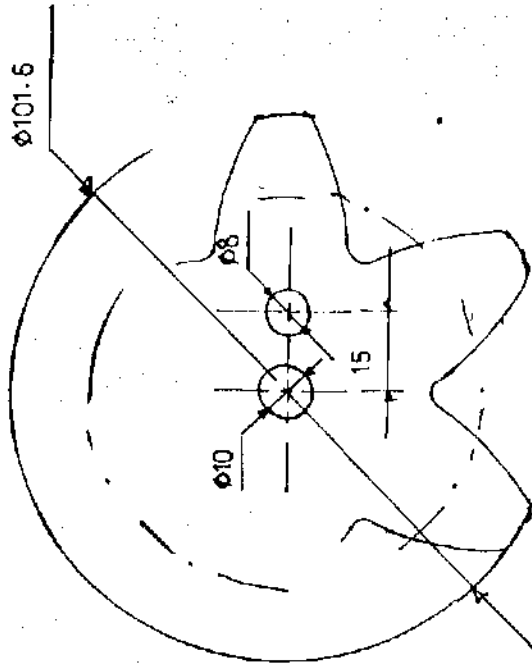


FIG. 5.6: DIMENSION OF THE GEARS

5.4. Determination Of Young's Modulus And Poisson's Ratio Of The Model Material:

For the determination of E and μ , one specimen of length 121 mm, width 14 mm and thickness 5 mm (model thickness) was cut and subjected to tensile load using Monsanto Tensometer W. On the specimen were mounted two strain gauges - one in axial direction and the other in radial direction, as shown in Figure 5.7, to read axial and lateral strains, respectively.

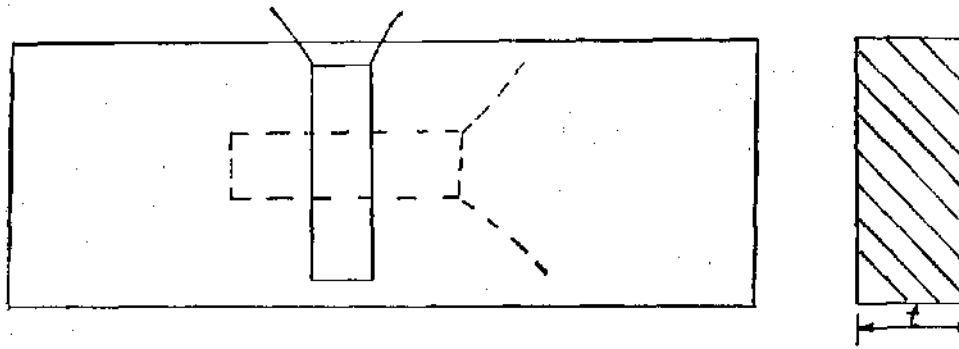


Fig. 5.7: Tension Test Piece Dimensions.

Table 5.1 shows the readings taken during the test. From the analysis that follows, E and μ were found to be 4.444 GN/m² and 0.325, respectively. From these results, the material is suspected to be Columbia Resin CR-39. The values do not very much agree with the values in standard textbooks because there are bound to be some human errors in carrying out the experiment. These may be due to the use of the strain gauges or the tensometer.

Readings:

$$\text{Area} = W.t = 14 \times 10^{-3} \times 5 \times 10^{-3} = 7 \times 10^{-5} \text{ m}^2$$

APPLIED LOAD (N)	MEASURED STRAIN (x 10 ⁻⁶)		CORRECTED STRAIN = MEASURED x $\frac{1.94}{2.00}$		STRESS P/A (MN/m ²)
	Axial Strain e _a	Lateral Strain e _l	e' _a	e' _l	
50	170	- 60	164.90	- 58.20	0.71
100	330	-110	320.10	-106.70	1.43
150	510	-165	494.70	-160.05	2.14
200	685	-215	664.45	-208.55	2.86

TABLE 5.1: TENSION TEST READINGS:

These readings were taken and with them graphs shown in Figures 5.8 and 5.9 were plotted.

Under elastic limit, stress is proportional to strain. Hence $\sigma = Ee$. Young's Modulus $E = \frac{\sigma}{e}$ = slope of the graph = 4.444 GN/m².

$$\begin{aligned} \text{Poisson's ratio } \mu &= - \frac{\text{Lateral Strain}}{\text{Axial Strain}} \\ &= \text{Slope of graph (Fig. 5.9)} \\ &= -(-0.325) = \underline{0.325} \end{aligned}$$

5.5. Calibration Of The Model:

For the purpose of calibration, a test piece of rectangular cross-section, width 25 mm, thickness 5 mm and length 150 mm was cut and subjected to pure bending.

As there was not any effective means of subjecting the test piece to pure bending provided on the straining frame of the photoelastic bench, a way was devised. Referring to Figures 5.10 and 5.11, the arrangement consists of two rectangular bars with grooves and four rollers. Having made the loading system, the model was put in place and subjected to pure bending. The resulting

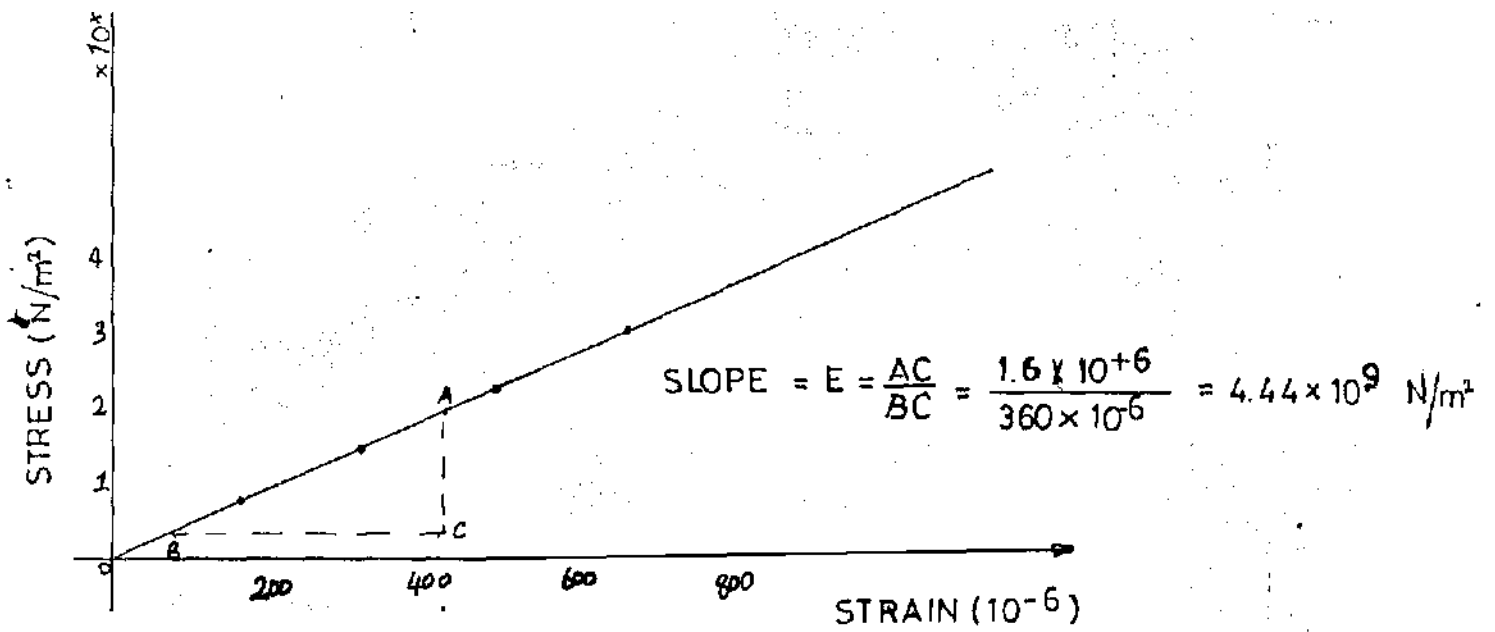


FIG.5.8: STRESS-STRAIN CURVE

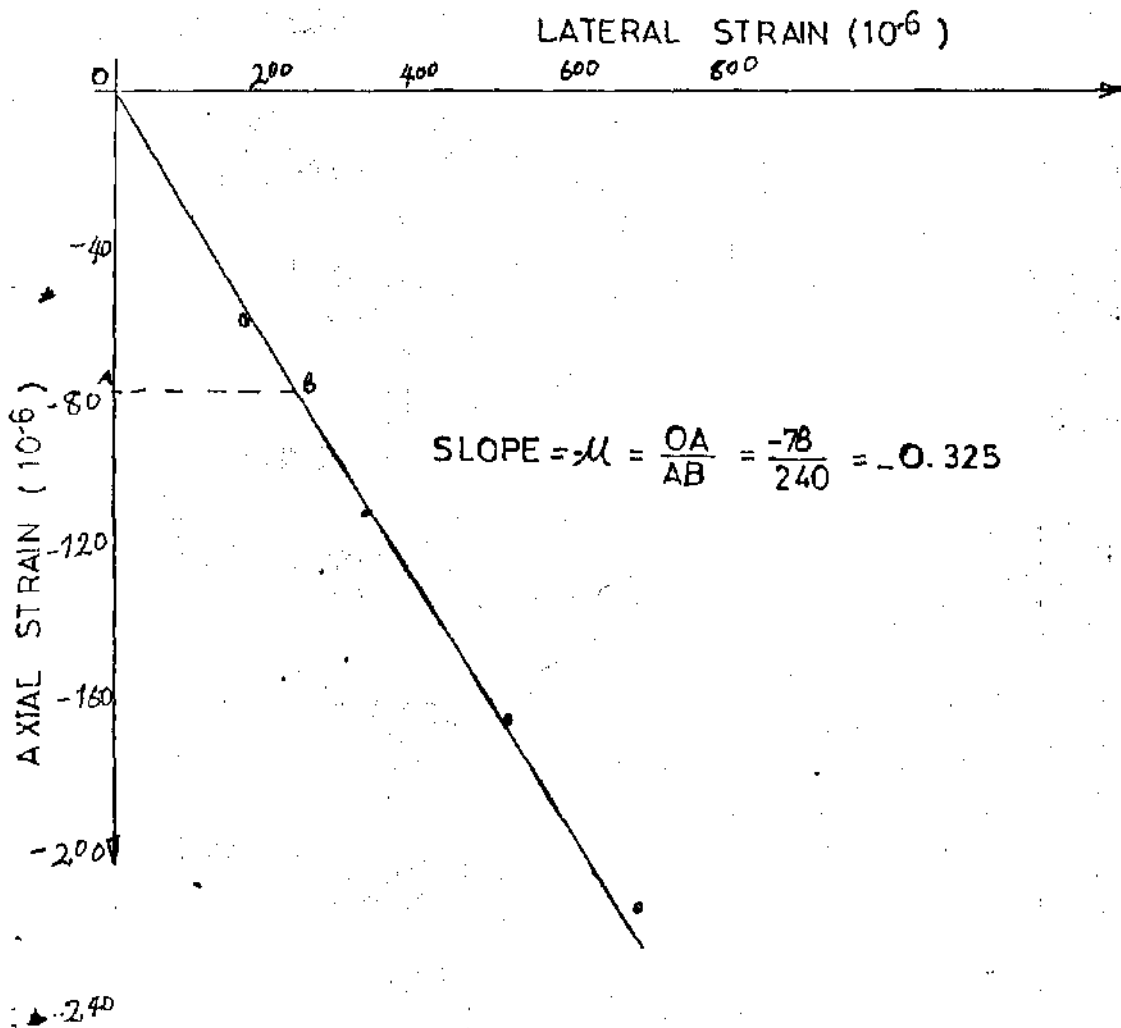


FIG.5.9: LATERAL STRAIN - AXIAL STRAIN CURVE:

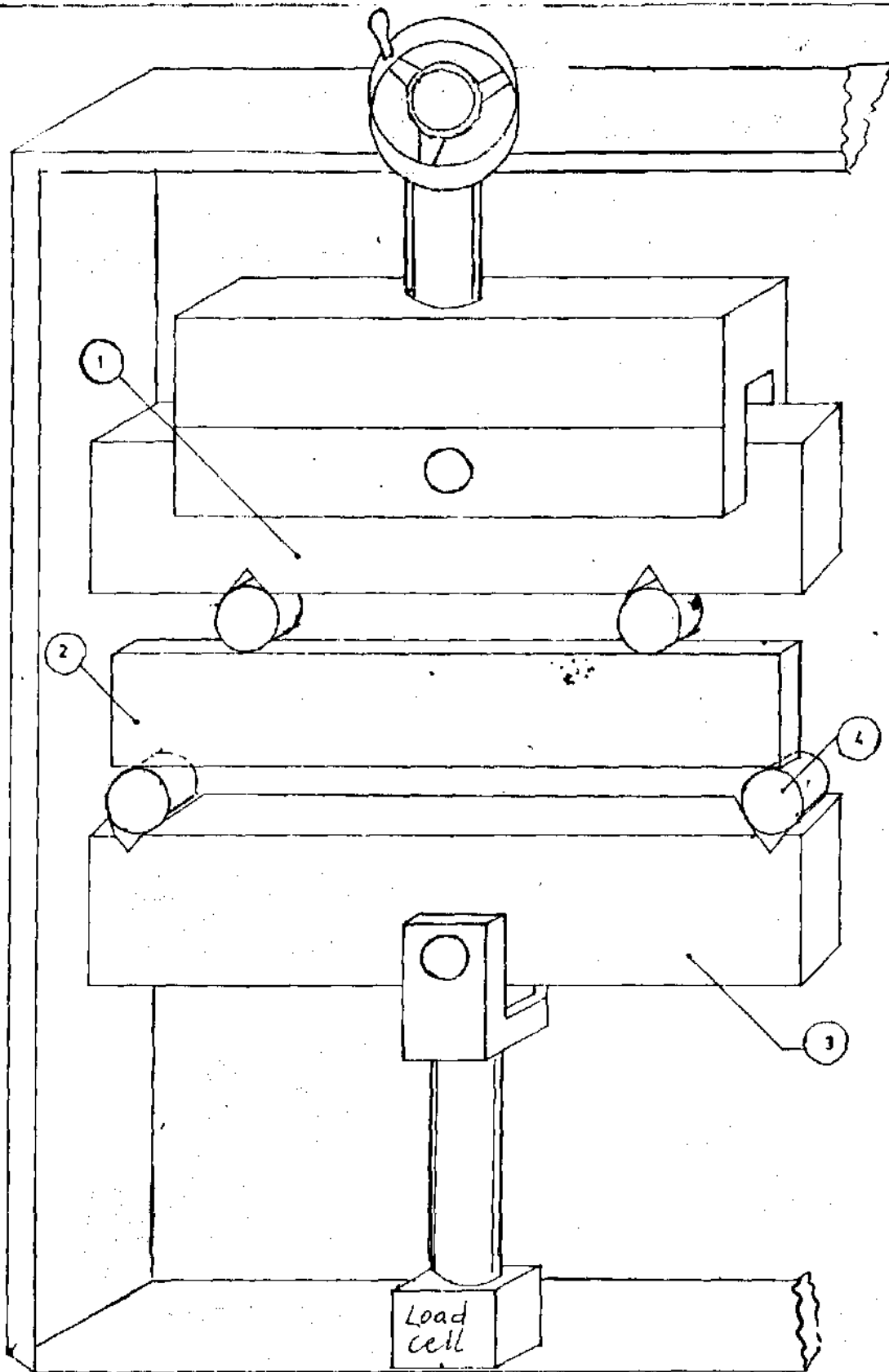


FIG.5.10: Calibration Specimen arrangement

ITEM 3 STEEL BAR

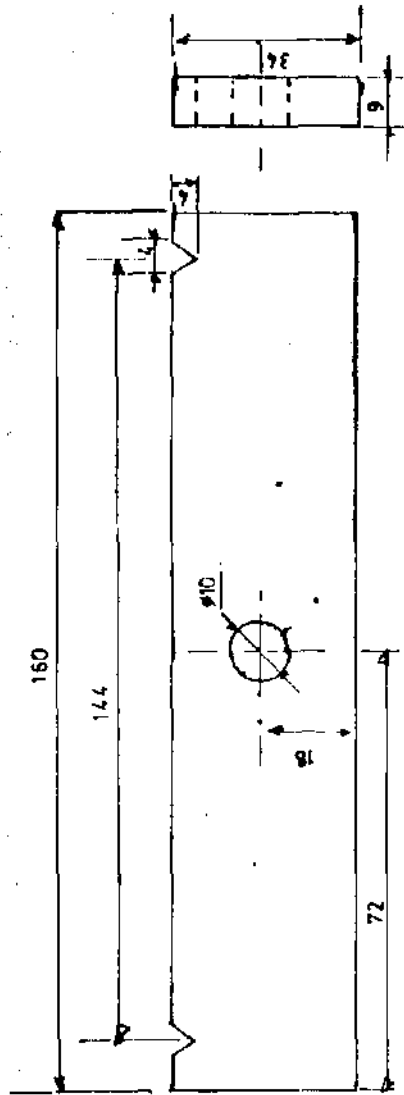


FIG. 5.11a

ITEM 2 PLASTIC SHEET

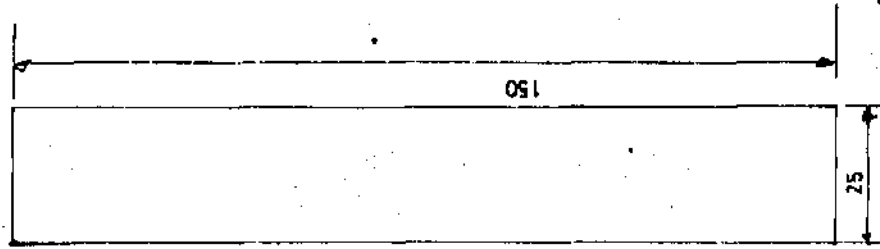


FIG. 5.11c

ITEM 1 STEEL BAR

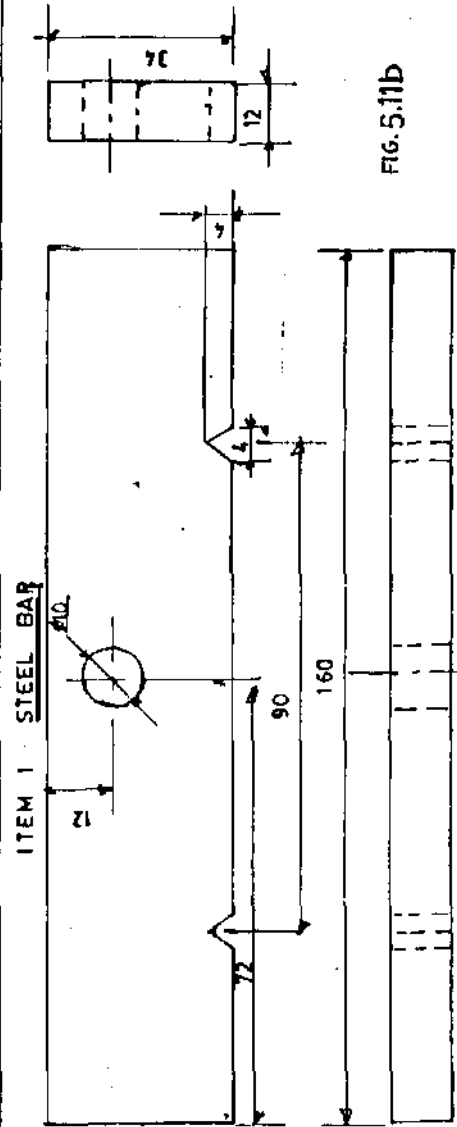


FIG. 5.11b

FIG. 5.11 : Detailed drawing of fig-10

fringes were noted as the force applied increases. Table 5.2 shows the readings obtained at 5% load. The readings were analysed and stress-optical constant K found as shown in the following analysis.

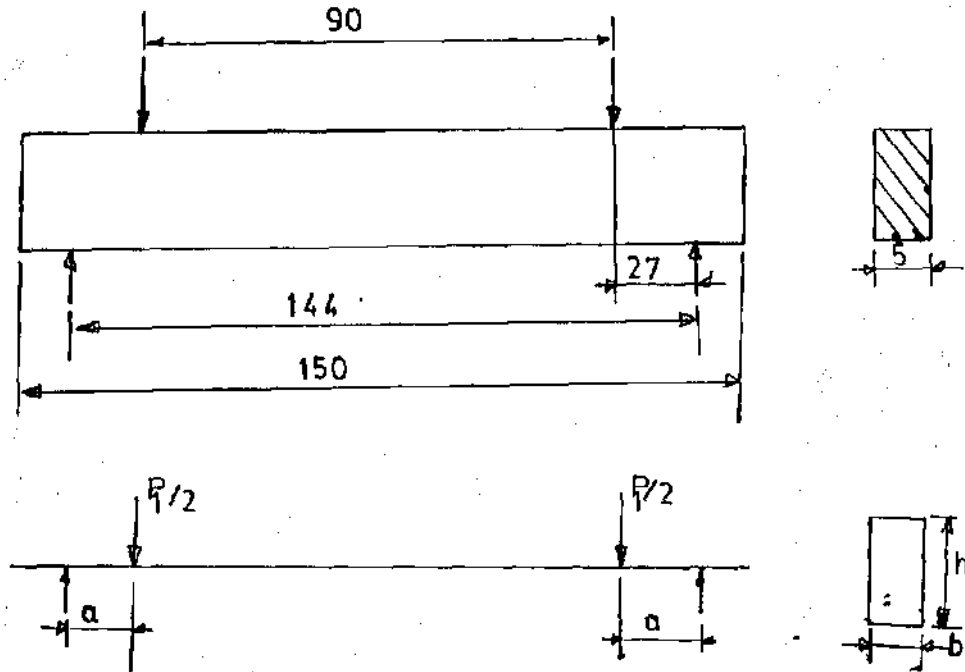
Readings

Full load $p = 2000 \text{ lb} = 8900 \text{ N}$

PERCENTAGE LOAD APPLIED (% p)	ACTUAL LOAD APPLIED p_1 (N)	FRINGE ORDER OBSERVED (N)
1%	89	1
2%	178	2
3%	267	3
4%	356	4
5%	445	5

TABLE 5.2: FRINGE VALUES FOR CALIBERATION

Specimen Arrangement



Dimensions: $a = 27 \text{ mm}; b = 5 \text{ mm}$

$p_1 = \text{as given in Table 5.2/}$

Using equation (4.8), the stress optical constant K is given by:

$$\sigma_1 - \sigma_2 = \frac{C}{t} \cdot N = N \cdot K \quad \text{----- (4.8)}$$

In pure bending, $\sigma_2 = 0$, Hence, $\sigma_1 = \frac{M}{Z} = N \cdot K$ ----- (5.1)

Bending Moment, $M = \frac{P_1}{2 \cdot a}$ ----- (5.2)

Moment of Inertia, $Z = \frac{bh^2}{6}$ ----- (5.3)

Substituting equations (5.2) and (5.3) into equation (5.1), we have:

$$N \cdot K = \frac{P_1 \cdot a \cdot 6}{2 \cdot b \cdot h^2} \quad \text{----- (5.4)}$$

$$K = \frac{3 P_1 a}{b h^2 N} \quad \text{----- (5.5)}$$

= Optical Constant.

Substituting the values of the constants in equation (5.5), for individual fringe value, we have,

For N = 1

$$K_1 = \frac{3 \times 89 \times 27 \times 10^{-3}}{5 \times 10^{-3} \times (25 \times 10^{-3})^2 \times 1} = \underline{\underline{2306880 \text{ N/m}^2/\text{fringe}}}$$

For N = 2

$$K_2 = \frac{3 \times 178 \times 27 \times 10^{-3}}{5 \times 10^{-3} \times (25 \times 10^{-3})^2 \times 2} = \underline{\underline{2306880 \text{ N/m}^2/\text{fringe}}}$$

For N = 3

$$K_3 = \frac{3 \times 267 \times 27 \times 10^{-3}}{5 \times 10^{-3} \times (25 \times 10^{-3})^2 \times 3} = \underline{\underline{2306880 \text{ N/m}^2/\text{fringe}}}$$

For N = 4

$$K_4 = \frac{3 \times 356 \times 27 \times 10^{-3}}{5 \times 10^{-3} \times (25 \times 10^{-3})^2 \times 4} = \underline{\underline{2306880 \text{ N/m}^2/\text{fringe}}}$$

For N = 5

$$K_5 = \frac{3 \times 445 \times 27 \times 10^{-3}}{5 \times 10^{-3} \times (25 \times 10^{-3})^2 \times 5} = \underline{\underline{2306880 \text{ N/m}^2/\text{fringe}}}$$

$$K = \frac{K_1 + K_2 + K_3 + K_4 + K_5}{5} = \underline{\underline{2306880 \text{ N/m}^2/\text{fringe}}}$$

5.6. The Photoelastic Results:

Having prepared the models and the loading system as discussed in Sections 5.1 and 5.2, the models were first examined for machining residual stresses which were found to be absent. Then load was applied to the gears using the straining frame. The development of the fringes as the applied load was being increased was noted and photographed. The photographs are shown in Plates I to XVIII.

Whole and fractional fringes at different nodal points were measured using Tardy Compensation Method. For fractional fringe order measurement, the points of interest were marked as 1, 2, ..., 12 and A, B, ..., K, on the model. Starting with point 1, an isoclinic was brought to the point. Then the common rotation of polariser-analyser was locked thereby aligning them with the direction of principal stresses σ_1 and σ_2 . The quarter wave plates were then placed at 45° to the direction of the principal stresses using an in-built mechanism for this purpose. Now the analyser is separately rotated to move a fringe to the point 1. When a fringe is brought to the point, the pointer on the Tardy Compensation (SM) Scale indicates the fractional fringe order. The fractional fringe order added to the whole

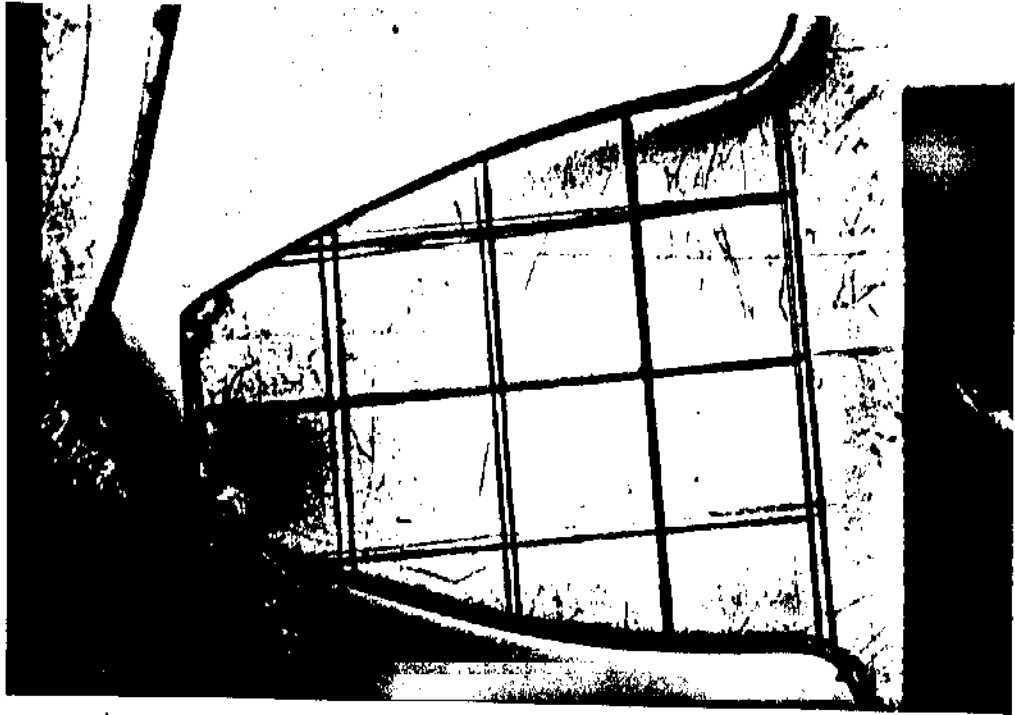


PLATE II: HALF ORDER FRINGES AT $\frac{1}{8}$ LOAD

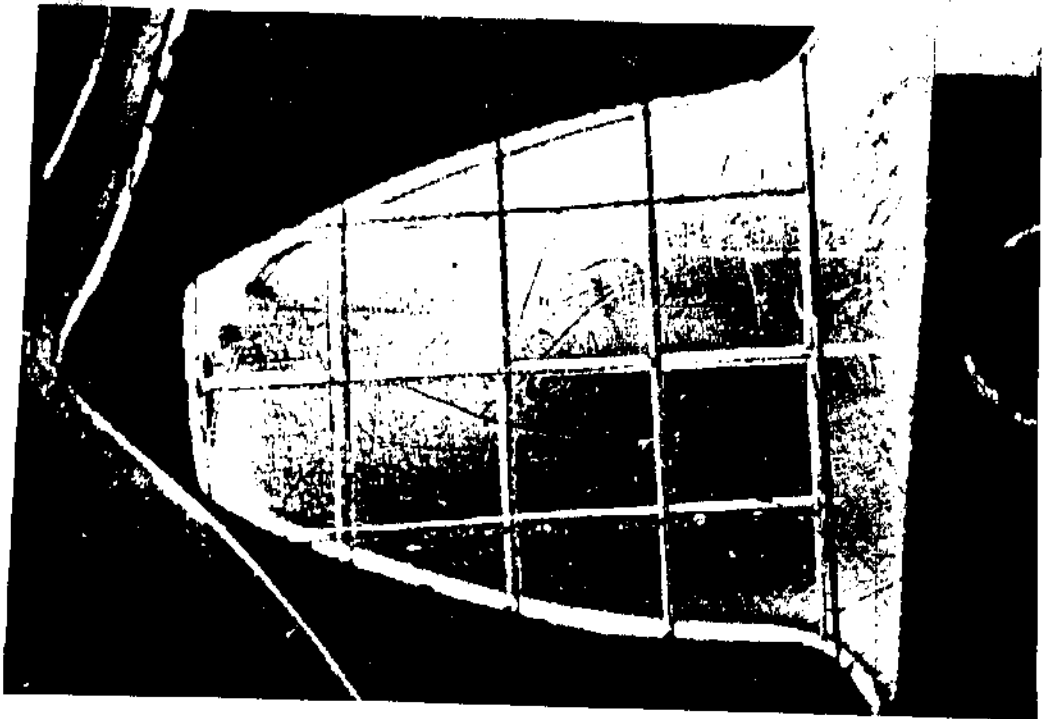


PLATE I: ZERO ORDER FRINGE AT 0/8 LOAD

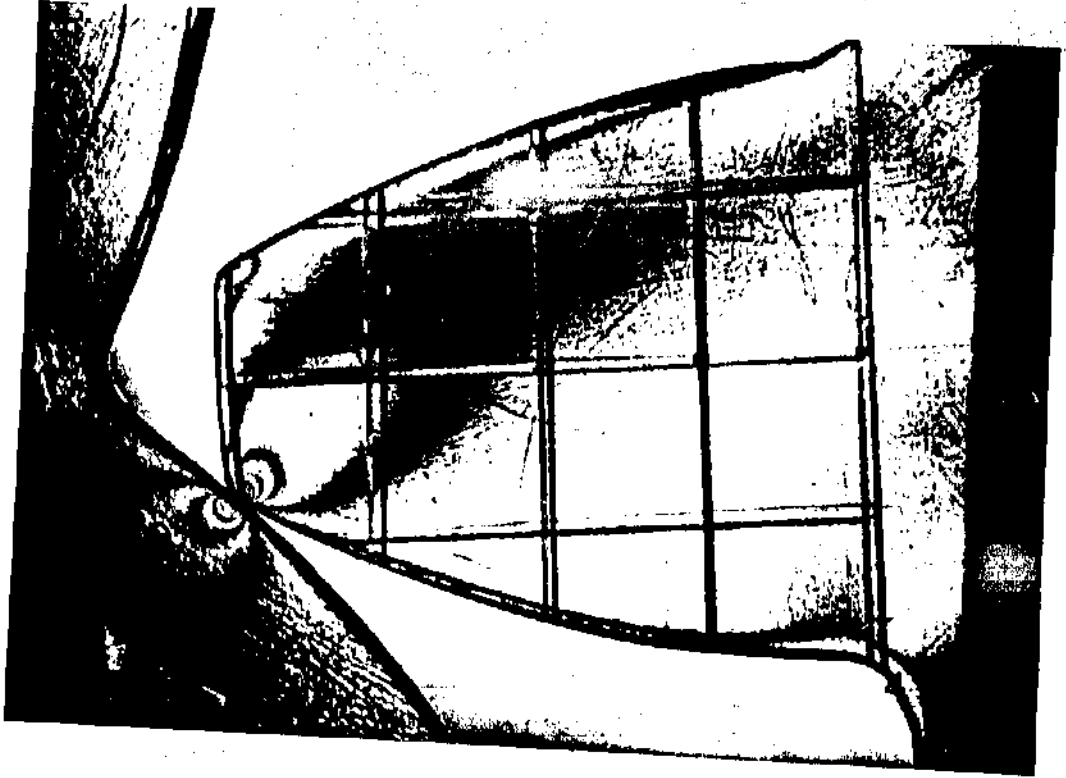


PLATE IV: HALF ORDER FRINGES AT $1/8$ LOAD

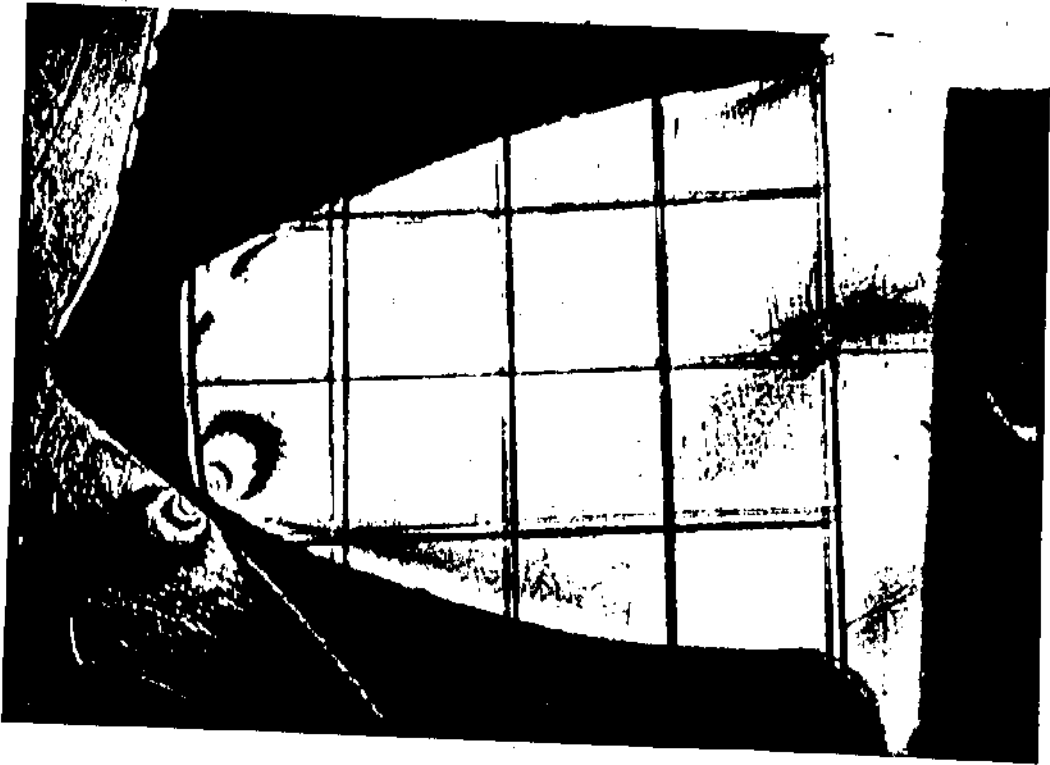


PLATE III: FULL ORDER FRINGES AT $1/8$ LOAD

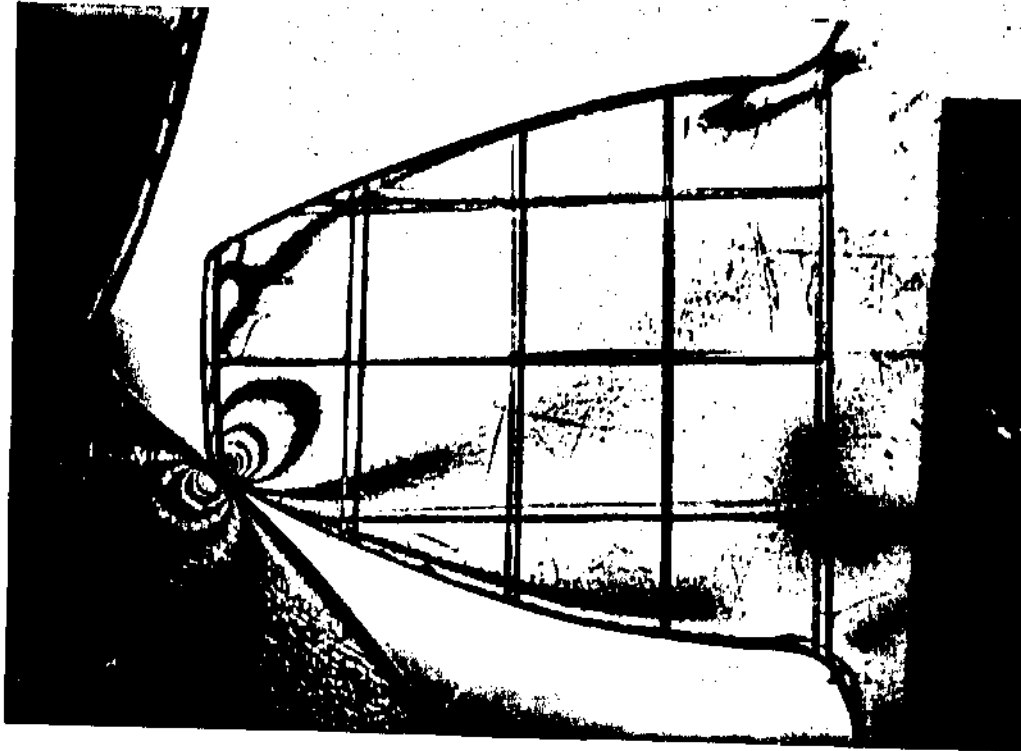


PLATE VI: HALF ORDER FRINGES AT 2% LOAD



PLATE V: FULL ORDER FRINGES AT 2% LOAD

KASHIM IBRAHIM LIBRARY
AHMADU BELLO UNIVERSITY
ZARIA, N.D.



PLATE VII: FULL ORDER FRINGES AT 3% LOAD

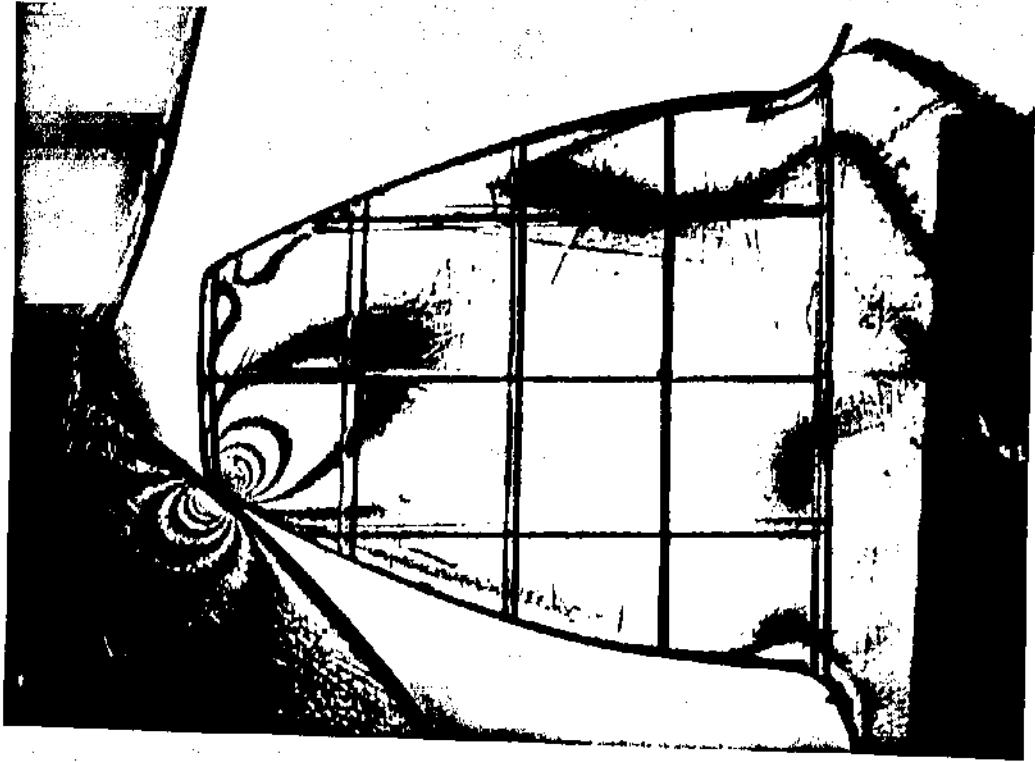


PLATE VIII: HALF ORDER FRINGES AT 3% LOAD

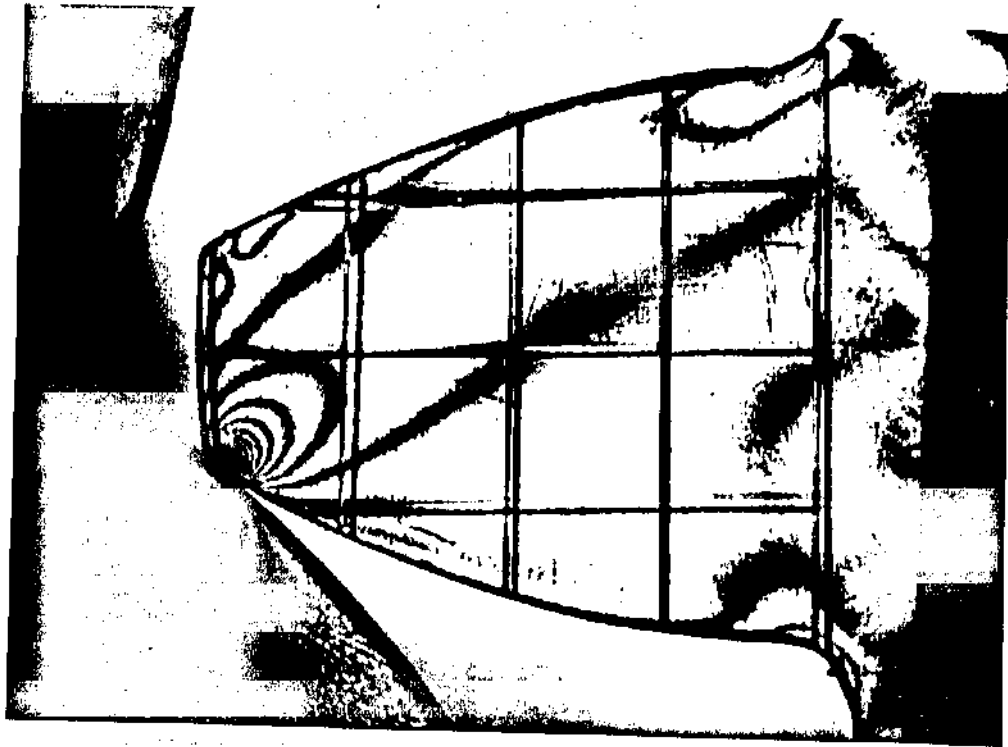


PLATE X: HALF ORDER FRINGES AT 4x LOAD



PLATE IX: FULL ORDER FRINGES AT 4x LOAD

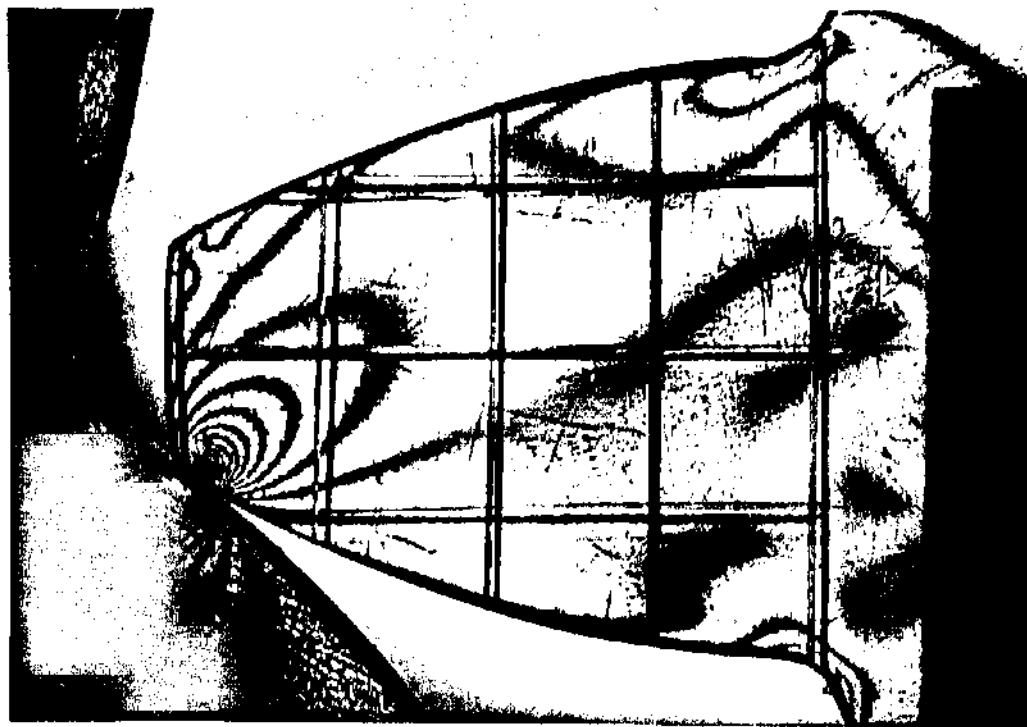


PLATE XII: HALF ORDER FRINGES AT 5% LOAD



PLATE XI: FULL ORDER FRINGES AT 5% LOAD

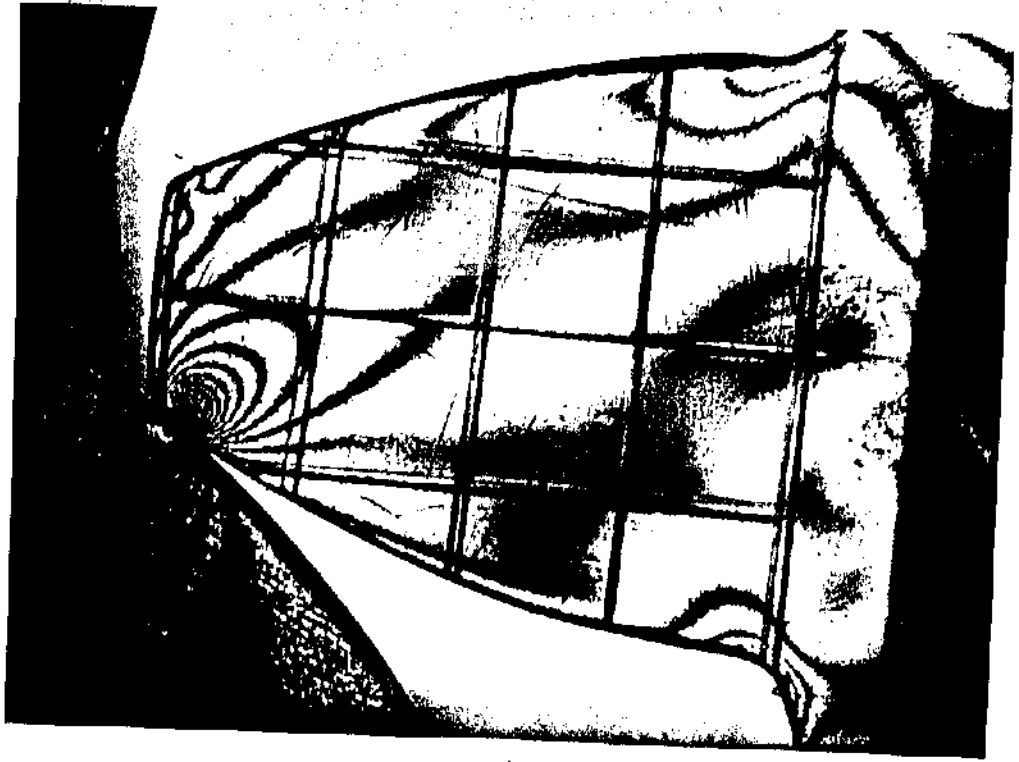


PLATE XIV: HALF ORDER FRINGES AT 6% LOAD



PLATE XIII: FULL ORDER FRINGES AT 6% LOAD

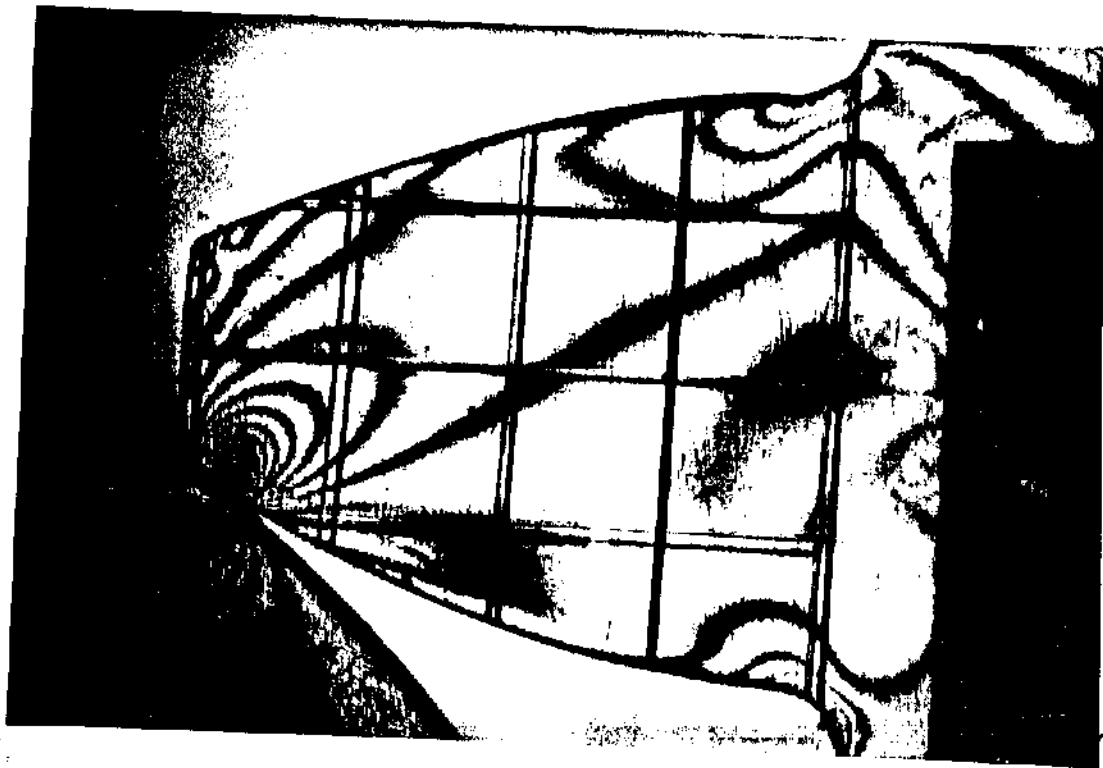


PLATE XVI: HALF ORDER FRINGES AT $7/8$ LOAD

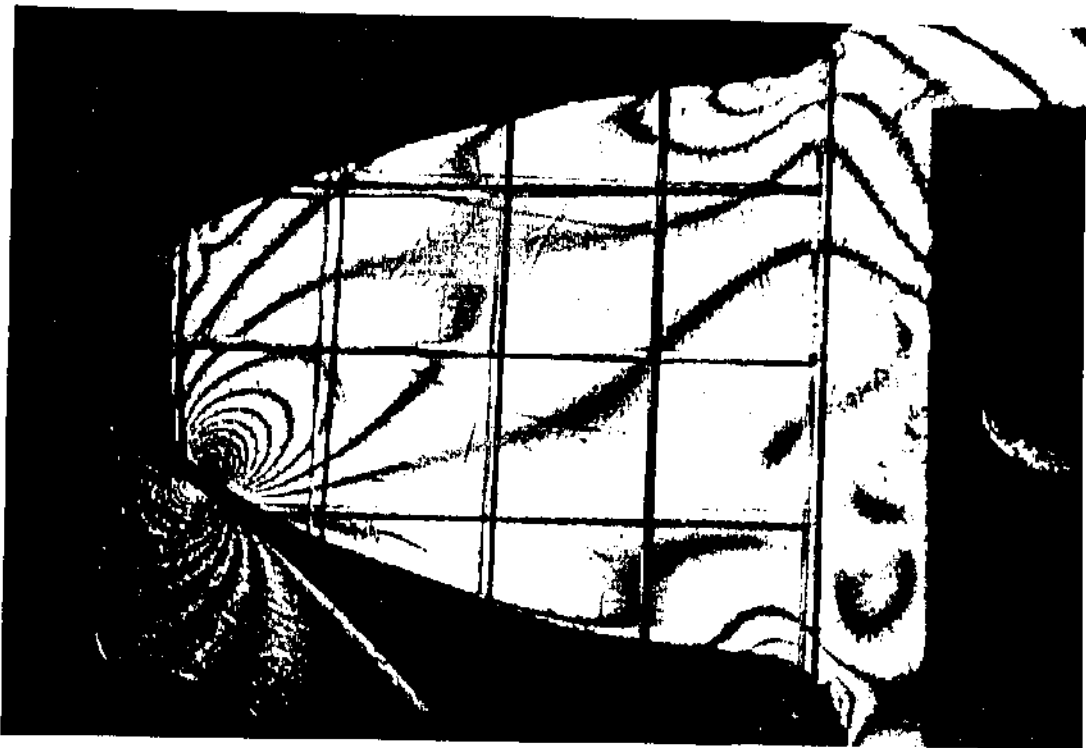


PLATE XV: FULL ORDER FRINGES AT $7/8$ LOAD

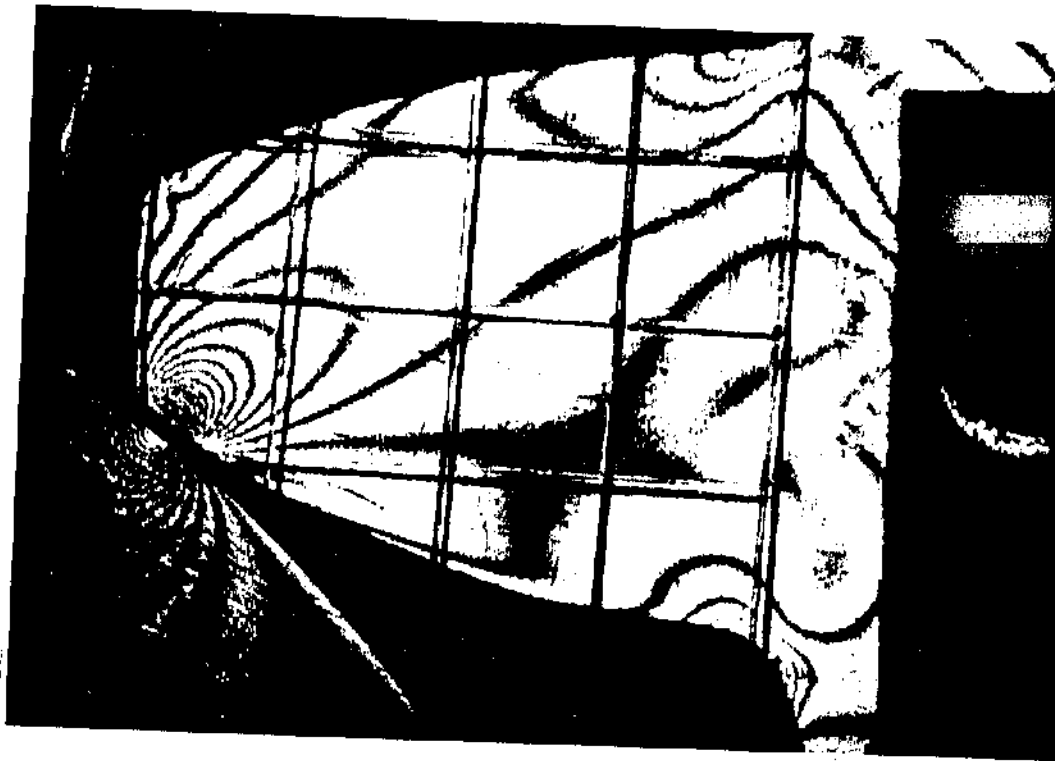


PLATE XVII: FULL ORDER FRINGES AT 8% LOAD

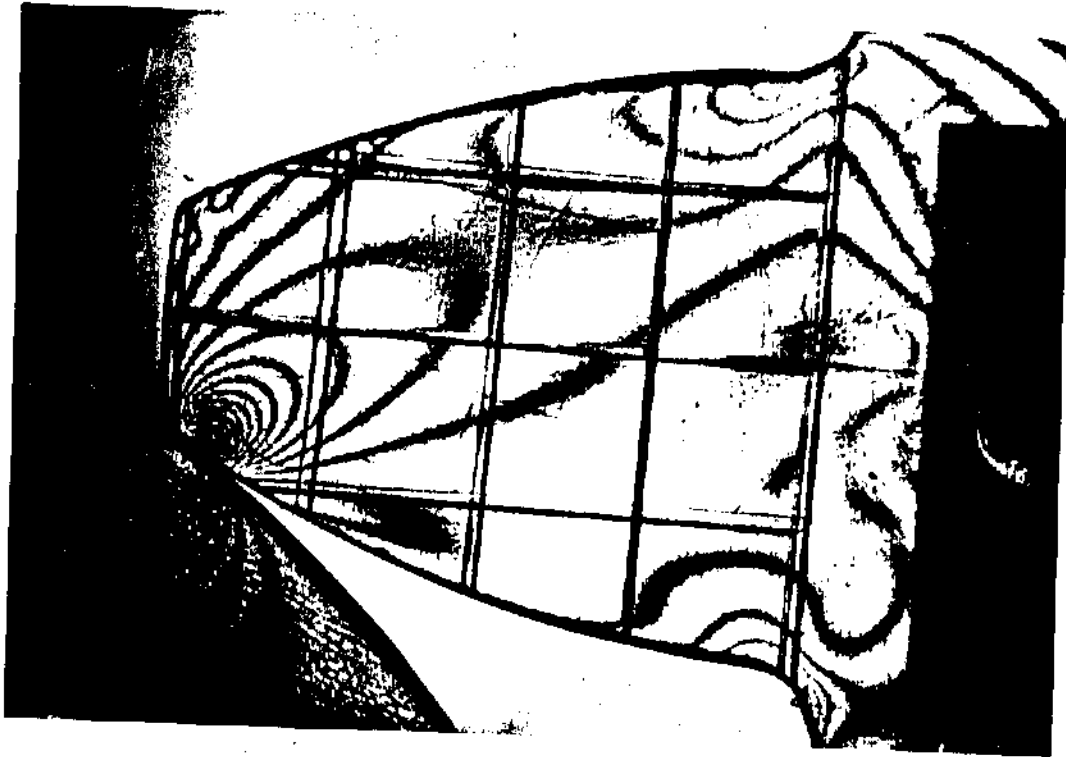


PLATE XVIII: HALF ORDER FRINGES AT 8% LOAD

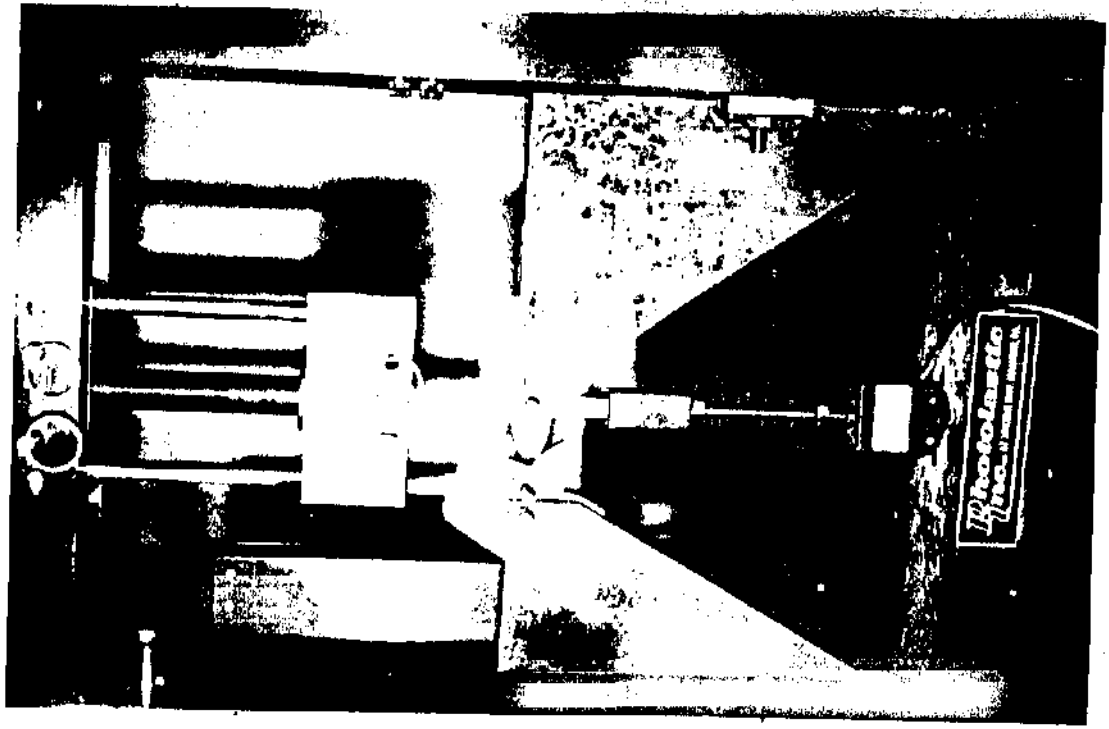


PLATE XX: THE MODELS & LOADING SYSTEM ON STRAINING FRAME

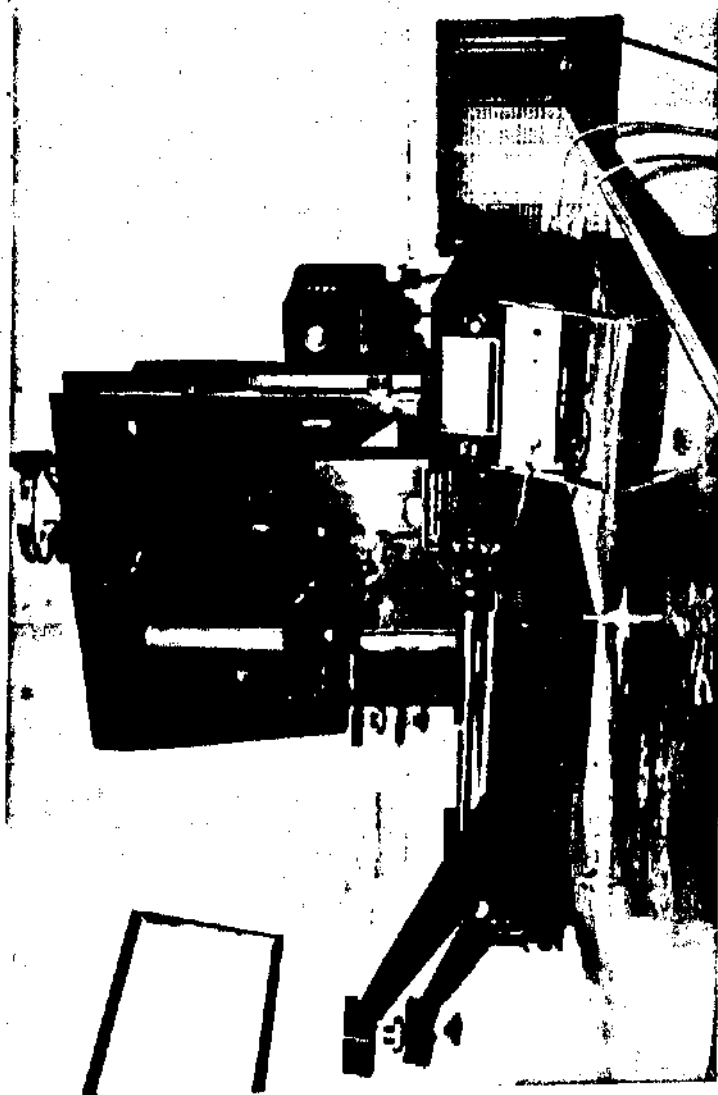


PLATE XIX: FRONT VIEW OF THE PHOTOELASTIC BENCH

fringe order gives the result tabulated in Table 5.3. The SM scale is calibrated to read in hundreds of a fringe. The total resulting fringe order is either negative or positive depending on whether it is the lower order - or higher order fringe that moved to the point when the analyser is rotated.

Readings

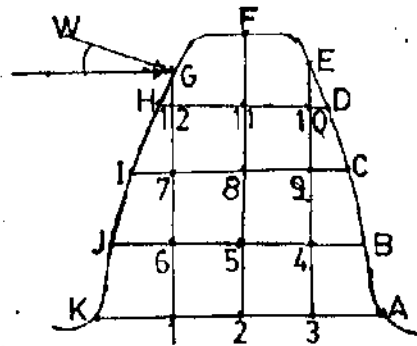


Fig. 5.12: Nodal Points on the Gear Model.

Nodal Points*	A	B	C	D	E	F
Fringe Order*	- 9.10	-4.25	-3.505	-2.41	-1.35	-1.95

G	H	I	J	K	1
-19.26	+7.15	+4.565	+5.315	+9.00	+1.21

2	3	4	5	6	7
+0.805	+1.30	+3.245	+2.39	+2.52	+2.40

8	9	10	11	12
+3.63	+3.75	+2.80	+4.32	+2.16

TABLE 5.3: FRINGE VALUES AT 9% OF FULL LOAD

Boundary Stresses:

At the boundary, one of the principal stresses is zero. This implies that:

$$\sigma_1 - \sigma_2 = \sigma = \sigma_1 + \sigma_2 = \phi = K.N$$

$$K = 2306880 \text{ N/m}^2/\text{fringe}$$

N = fringe order indicated in Table 5.3. Hence:

$$\sigma_1 + \sigma_2 = \sigma = \phi = K.N \quad (5.6)$$

Point A:

$$\phi_A = K.N_A = 2306880 \times (-9.10) = \underline{\underline{-20992608 \text{ N/m}^2}}$$

Point B:

$$\phi_B = K.N_B = 2307880 \times (-4.25) = \underline{\underline{-9804240 \text{ N/m}^2}}$$

Point C:

$$\phi_C = K.N_C = 2306880 \times (-3.505) = \underline{\underline{-8085614.4 \text{ N/m}^2}}$$

Point D:

$$\phi_D = K.N_D = 2306880 \times (-2.41) = \underline{\underline{-5559580.8 \text{ N/m}^2}}$$

Point E:

$$\phi_E = K.N_E = 2306880 \times (-1.35) = \underline{\underline{-3114288 \text{ N/m}^2}}$$

Point F:

$$\phi_F = K.N_F = 2306880 \times (-1.95) = \underline{\underline{-4498416 \text{ N/m}^2}}$$

Point G:

$$\phi_G = K.N_G = 2306880 \times (-19.26) = \underline{\underline{-44430509 \text{ N/m}^2}}$$

Point H:

$$\phi_H = K.N_H = 2306880 \times (4.15) = \underline{\underline{9573552 \text{ N/m}^2}}$$

Point I:

$$\phi_I = K.N_I = 2306880 \times 4.365 = \underline{\underline{10069531 \text{ N/m}^2}}$$

Point J:

$$\phi_J = K.N_J = 2306880 \times 5.315 = \underline{\underline{12261067 \text{ N/m}^2}}$$

Point K:

$$\phi_K = K.N_K = 2306880 \times 9.0 = \underline{\underline{20761920 \text{ N/m}^2}}$$

Stresses at the Interior Nodal Points:

The principal stress differences at the nodal points are as follows:

Point 1:

$$\sigma_1 - \sigma_2 = K.N_1 = 2306880 \times 1.21 = \underline{\underline{2791324.8 \text{ N/m}^2}}$$

Point 2:

$$\sigma_1 - \sigma_2 = K.N_2 = 2306880 \times 0.805 = \underline{\underline{1857038.4 \text{ N/m}^2}}$$

Point 3:

$$\sigma_1 - \sigma_2 = K.N_3 = 2306880 \times 1.30 = \underline{\underline{2998944 \text{ N/m}^2}}$$

Point 4:

$$\sigma_1 - \sigma_2 = K.N_4 = 2306880 \times 3.245 = \underline{\underline{7485825.6 \text{ N/m}^2}}$$

Point 5:

$$\sigma_1 - \sigma_2 = K.N_5 = 2306880 \times 2.39 = \underline{\underline{5513443.2 \text{ N/m}^2}}$$

Point 6:

$$\sigma_1 - \sigma_2 = K.N_6 = 2306880 \times 2.52 = \underline{\underline{5813337.6 \text{ N/m}^2}}$$

Point 7:

$$\sigma_1 - \sigma_2 = K.N_7 = 230688 \times 2.40 = \underline{\underline{5536512.0 \text{ N/m}^2}}$$

Point 8:

$$\sigma_1 - \sigma_2 = K.N_8 = 2306880 \times 3.63 = \underline{\underline{8373974.4 \text{ N/m}^2}}$$

Point 9:

$$\sigma_1 - \sigma_2 = K.N_9 = 2306880 \times 3.75 = \underline{\underline{8650800 \text{ N/m}^2}}$$

Point 10:

$$\sigma_1 - \sigma_2 = K.N_{10} = 2306880 \times 2.8 = \underline{\underline{6459264.0 \text{ N/m}^2}}$$

Point 11:

$$\sigma_1 - \sigma_2 = K.N_{11} = 2306880 \times 4.32 = \underline{\underline{9965721.6 \text{ N/m}^2}}$$

Point 12:

$$\sigma_1 - \sigma_2 = K.N_{12} = 2306880 \times 2.16 = \underline{\underline{4982860.8 \text{ N/m}^2}}.$$

5.7. Separation Of Principal Stresses With The Use of Finite Difference Method:

It has been found by the theory of elasticity that the governing differential equation (Compatibility Condition) for plane state of stress and plane state of strain, in the absence of body forces, is the Laplace equation:

$$\nabla^2 \phi = \frac{\partial^2 \phi}{\partial x^2} + \frac{\partial^2 \phi}{\partial y^2} = 0 \text{ ----- (5.7)}$$

where

$$\phi = \sigma_1 + \sigma_2 = \sigma_x + \sigma_y \text{ ----- (5.8)}$$

To obtain an approximate numerical solution of this equation using finite difference method, it is necessary to know the values of $(\sigma_1 + \sigma_2)$ along the boundary of the model, as has been done in Section 5.6. Also, the stresses at the nodal points 1, 2 and 3 are needed. The stresses at these nodes are determined using strains gauges as shown in the following sub-section.

5.7.1. Determination of Stresses at Nodal Points 1, 2, 3, On the Model Using Strain Gauges - Using finite difference method, a set of algebraic simultaneous linear equations are generated by considering the different

nodal points. To obtain the required n -equations in n -unknowns, specific values of stress at some reference points (1, 2 & 3) are needed. Hence, the stresses at nodal points 1, 2, 3, are determined using strain gauges.

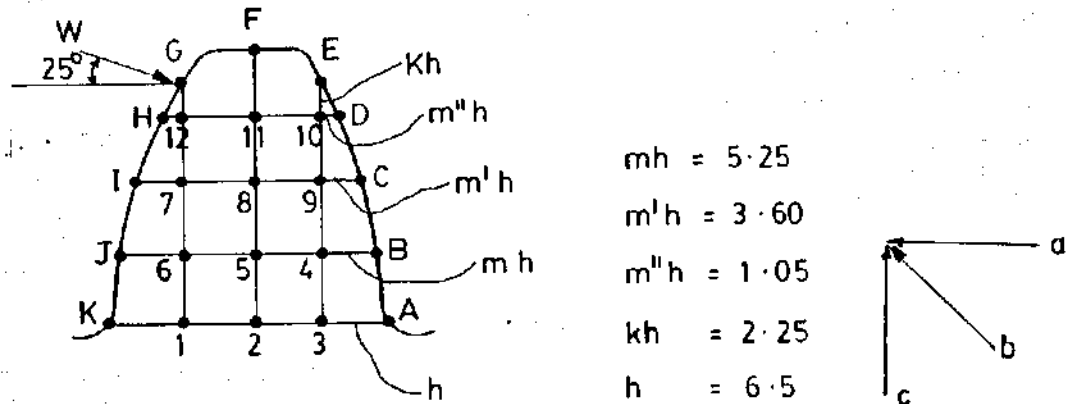


Fig. 5.13: Dimensions (Square Mesh) for Generating Difference Equations.

Three strain gauges were mounted at the points on the model in the directions marked a, b, c. These were connected to the strain indicator and load was applied to the model. Table 5.4 shows the readings taken. Table 5.5 shows the corrected strain. The readings were corrected because of the difference in gauge factor of strain indicator and strain gauges. The gauge factor of the indicator is 2.0 while that of the strain gauges is 1.91. Figures 5.14 show the relationship between the applied force and the resulting strains.

Using these readings shown in the tables below, the principal stresses at each of the three points were calculated as follows:

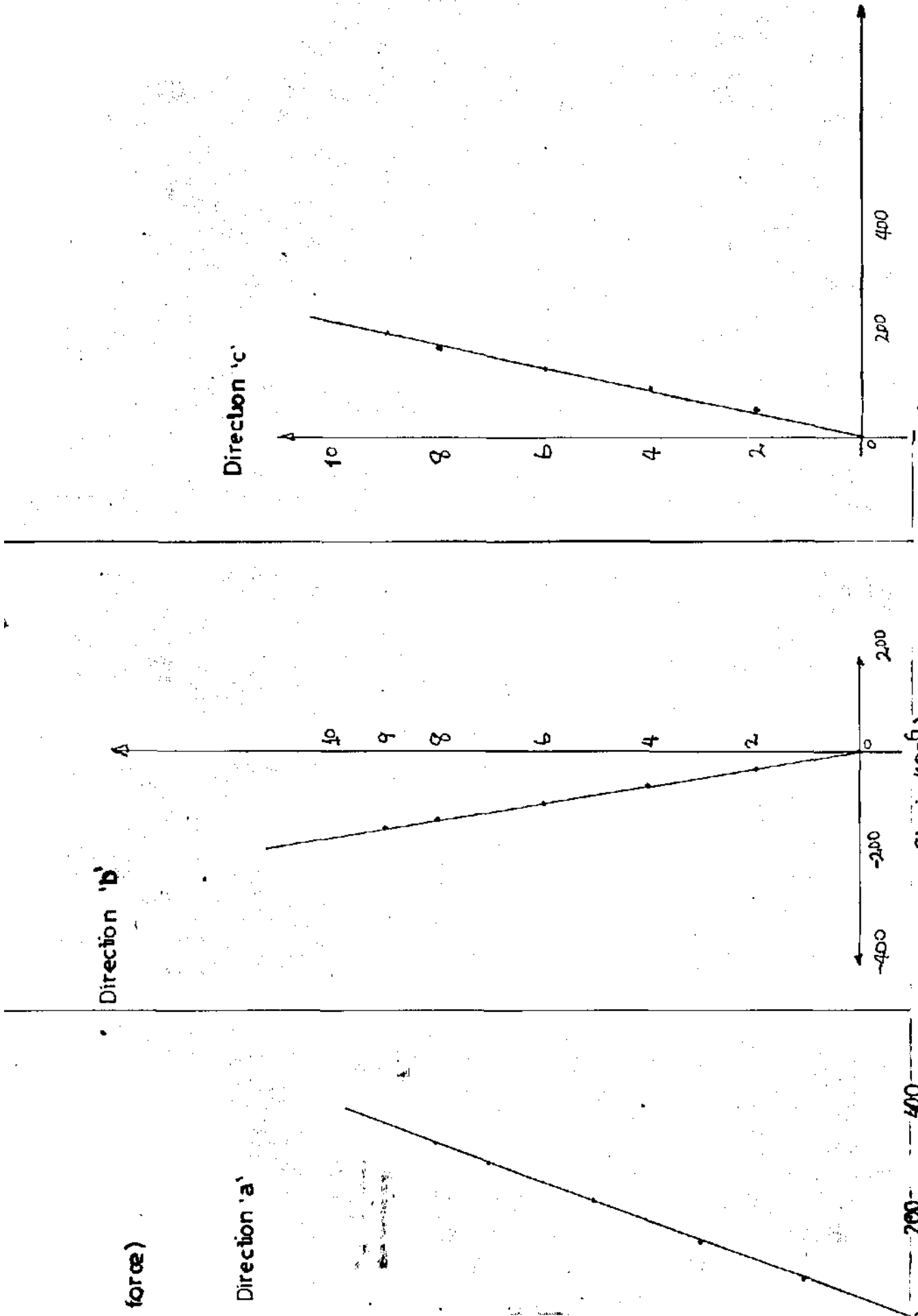


FIG. 5.14 a: FORCE - STRAIN CURVE FOR NODE 1

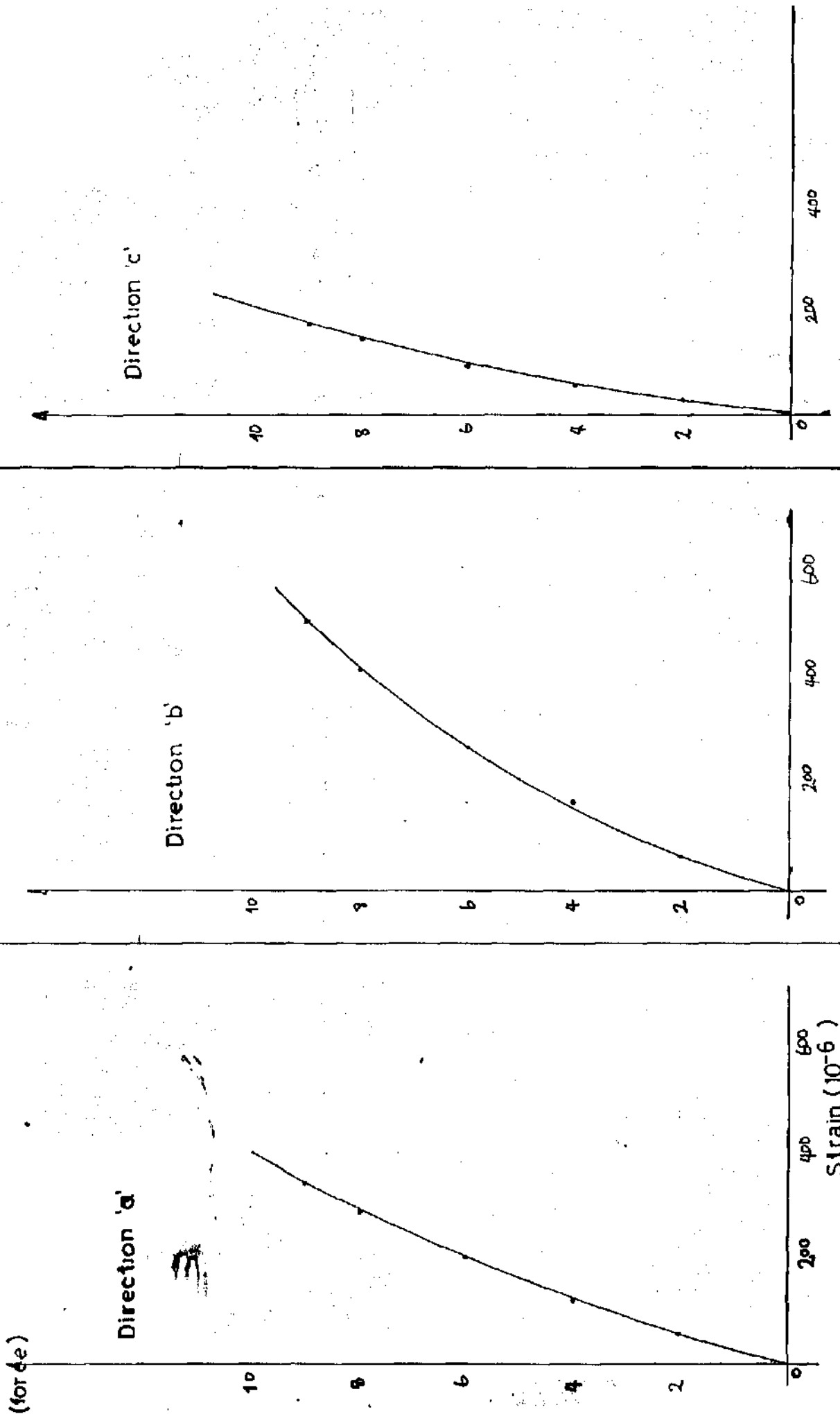


FIG. 5.14 b: FORCE - STRAIN CURVE FOR NODE 2

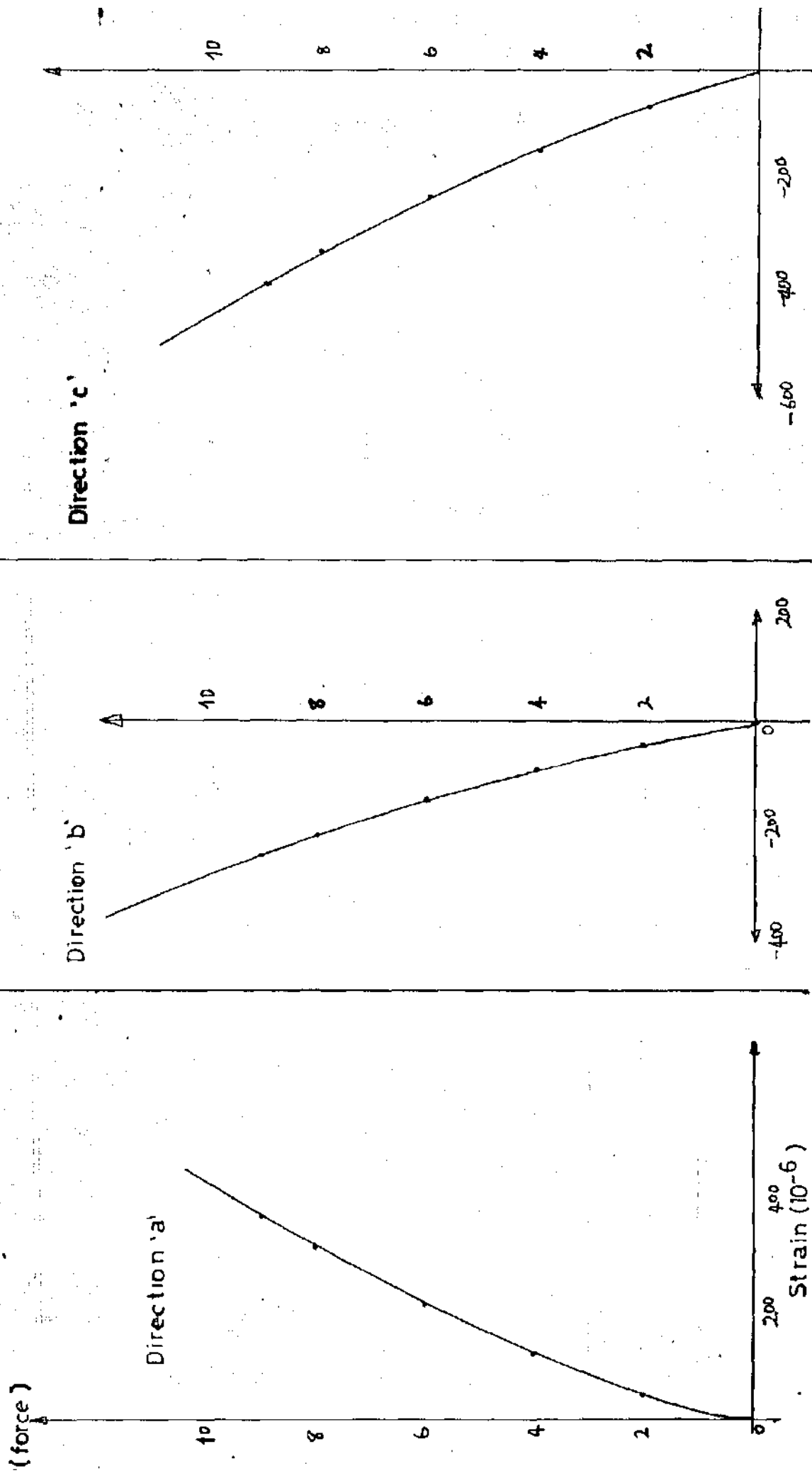


FIG. 5.14c: FORCE - STRAIN CURVE FOR NODE 3

Readings

MEASURED STRAINS ($\times 10^{-6}$)									
Points	1			2			3		
Strain %p	e_a	e_b	e_c	e_a	e_b	e_c	e_a	e_b	e_c
2%p = 178N	70	- 35	50	55	65	25	40	- 45	- 70
4%p = 356N	150	- 70	90	115	165	50	125	- 90	-150
6%p = 534N	230	-100	130	200	270	85	215	-145	-235
8%p = 712N	305	-135	170	285	410	140	320	-210	-330
9%p = 801N	345	-150	200	340	505	165	380	-250	-390

TABLE 5.4: MEASURED STRAINS FOR POINTS 1, 2, 3:

Calculation of Principal Strains and Stresses:

Note that corrected values of strains at 9% (810N) of full load are used in the calculations.

In the calculation of principal strains e_1 and e_2 , the following equations apply:

$$e_{1,2} = \frac{e_a + e_c}{2} \pm \frac{\sqrt{2}}{2} \sqrt{[(e_a - e_b)^2 + (e_b - e_c)^2]} \quad \text{--- (5.9)}$$

In the calculation of principal stresses σ_1 and σ_2 , the following equations apply:

$$\sigma_1 = \frac{E(e_1 + \mu e_2)}{1 - \mu^2}$$

$$\sigma_2 = \frac{E(e_2 + \mu e_1)}{1 - \mu^2} \quad \text{--- (5.10)}$$

$$\sigma_1 + \sigma_2 = \frac{E(e_1 + e_2)}{1 - \mu}$$

CORRECTED STRAIN = MEASURED STRAIN x $\frac{1.91}{2.00}$															
Nodes				1				2				3			
%p	Strain			e _a	e _b	e _c	e _a	e _b	e _c	e _a	e _b	e _c			
	e _a	e _b	e _c												
2%p = 178N	66.85	- 33.425	47.75	52.525	62.075	23.875	38.20	- 42.975	- 66.85						
4%p = 356N	143.25	- 66.85	85.95	109.825	157.575	47.75	119.375	- 85.95	- 143.25						
6%p = 534N	219.63	- 95.5	124.15	191	257.85	81.175	205.325	- 138.475	- 224.425						
8%p = 712N	291.275	- 128.925	162.35	272.175	391.55	133.70	305.60	- 200.55	- 315.15						
9%p = 801N	329.475	- 143.25	191.00	324.7	482.275	157.52	362.90	- 238.75	- 372.42						

TABLE 5.5: CORRECTED STRAIN VALUES

Node Point 1:

Applying equations (5.9) and (5.10) to node point 1, we have:

$$e_{1,2} = \frac{329.475 \times 10^{-6} + 191 \times 10^{-6}}{2} \\ \pm \frac{\sqrt{2}}{2} \sqrt{\{(329.475 \times 10^{-6} + 143.25 \times 10^{-6})^2 + (-143.25 \times 10^{-6} - 191 \times 10^{-6})^2\}} \\ = 2.602375 \times 10^{-4} \pm 4.093849 \times 10^{-4} \\ \therefore e_1 = \underline{\underline{6.696224 \times 10^{-4}}} \\ \therefore e_2 = \underline{\underline{-1.491474 \times 10^{-4}}}$$

Now the stresses:

$$\sigma_1 + \sigma_2 = \frac{E(e_1 + e_2)}{1 - \mu} \\ = \frac{4.4444 \times 10^9 (6.696224 \times 10^{-4} - 1.491474 \times 10^{-4})}{1 - 0.325} \\ = \underline{\underline{3426992.5 \text{ N/m}^2}} = \phi_1$$

Node Point 2:

Applying equations (5.9) and (5.10) to node 2, we have:

$$e_{1,2} = \frac{324.7 \times 10^{-6} + 157.575 \times 10^{-6}}{2} \\ \pm \frac{\sqrt{2}}{2} \sqrt{\{(324.7 \times 10^{-6} - 482.275 \times 10^{-6})^2 + (482.275 \times 10^{-6} - 157.58 \times 10^{-6})^2\}} \\ = 2.411375 \times 10^{-4} \pm 2.5520577 \times 10^{-4} \\ \therefore e_1 = \underline{\underline{4.9634327 \times 10^{-4}}} \\ \therefore e_2 = \underline{\underline{1.4068271 \times 10^{-5}}}$$

Now the stresses:

$$\begin{aligned}\sigma_1 + \sigma_2 &= \frac{E(e_1 + e_2)}{1 - \mu} \\ &= \frac{4.4444 \times 10^9 (4.9634327 \times 10^{-4} + 1.4068271 \times 10^{-5})}{1 - 0.325} \\ &= \underline{\underline{3175441.5 \text{ N/m}^2}} = \phi_2\end{aligned}$$

Node Point 3:

Also applying equations (5.9) and (5.10) to node point 3, we have:

$$\begin{aligned}e_{1,2} &= \frac{362.9 \times 10^{-6} - 372.45 \times 10^{-6}}{2} \\ &\pm \frac{\sqrt{2}}{2} \sqrt{(362.5 \times 10^{-6} + 238.75 \times 10^{-6})^2 + (-238.75 \times 10^{-6} + 372.45 \times 10^{-6})^2} \\ &= -4.775 \times 10^{-6} \pm 4.3580868 \times 10^{-4}\end{aligned}$$

$$\therefore e_1 = \underline{\underline{4.3103368 \times 10^{-4}}}$$

$$\therefore e_2 = \underline{\underline{-4.4058368 \times 10^{-4}}}$$

Now the stresses:

$$\begin{aligned}\sigma_1 + \sigma_2 &= \frac{E(e_1 + e_2)}{1 - \mu} \\ &= \frac{4.4444 \times 10^9 (4.3103368 \times 10^{-4} - 4.4058 \times 10^{-4})}{1 - 0.325} \\ &= \underline{\underline{-62880.047 \text{ N/m}^2}} = \phi_3\end{aligned}$$

5.7.2. Application Of FDM - Having calculated the sum of principal stresses at the node points 1, 2 and 3, we now proceed with the finite difference analysis.

Applying equations (4.14) and (4.20), the following finite difference equations are generated for the nodal points 1 to 12.

Point 1: $\phi_1 = 3426992.5$

Point 2: $\phi_2 = 3175441.5$

Point 3: $\phi_3 = -62880.1$

Point 4: $\phi_5 + \frac{1}{m}\phi_B - (\frac{1}{m} + 1)\phi_4 + \phi_9 + \phi_3 - 2\phi_4 = 0$

Point 5: $\phi_4 + \phi_6 - 4\phi_5 + \phi_8 + \phi_2 = 0$

Point 6: $\phi_5 + \frac{1}{m}\phi_J - (\frac{1}{m} + 1)\phi_6 + \phi_7 + \phi_1 - 2\phi_6 = 0$

Point 7: $\phi_8 + \frac{1}{m'}\phi_I - (\frac{1}{m'} + 1)\phi_7 + \phi_{12} + \phi_6 - 2\phi_7 = 0$

Point 8: $\phi_{11} + \phi_5 + \phi_7 + \phi_9 - 4\phi_8 = 0$

Point 9: $\phi_8 + \frac{1}{m''}\phi_C - (\frac{1}{m''} + 1)\phi_9 + \phi_{10} + \phi_4 - 2\phi_9 = 0$

Point 10: $\phi_{11} + \frac{1}{m'''}\phi_D - (\frac{1}{m'''} + 1)\phi_{10} + \phi_9 + \frac{1}{K}\phi_E - (\frac{1}{K} + 1)\phi_{10} = 0$

Point 11: $\phi_{10} + \phi_{12} + \phi_F + \phi_8 - 4\phi_{11} = 0$

Point 12: $\phi_{11} + \frac{1}{m'''}\phi_H - (\frac{1}{m'''} + 1)\phi_{12} + \phi_7 + \frac{1}{K}\phi_G - (\frac{1}{K} + 1)\phi_{12} = 0.$

As indicated on Figure 5.13:

$$mh = 5.25 \text{ mm and } h = 6.5 \text{ mm}$$

$$\therefore m = \frac{5.25}{6.5} = \underline{\underline{0.808}}$$

$$m'h = 3.6 \text{ mm, } h = 6.5 \text{ mm}$$

$$\therefore m' = \frac{3.6}{6.5} = \underline{\underline{0.554}}$$

$$m''h = 1.05 \text{ mm, } h = 6.5 \text{ mm}$$

$$\therefore m'' = \frac{1.05}{6.5} = \underline{\underline{0.162}}$$

$$Kh = 2.5 \text{ mm, } h = 6.5$$

$$\therefore K = \frac{2.5}{6.5} = \underline{\underline{0.385}}$$

Substituting the values of the stresses at the boundary of the model as calculated in Section 5.6, the values of m , m' , m'' and K as calculated above, and the values of ϕ_1 , ϕ_2 and ϕ_3 as calculated above, into the equations for the nodal points 4 - 12, we have:

- Point 4: $-4.24\phi_4 + \phi_5 + \phi_9 = 12196840$
- Point 5: $\phi_4 - 4\phi_5 + \phi_6 + \phi_8 = -3175441.5$
- Point 6: $\phi_5 - 4.24\phi_6 + \phi_7 = -12891482$
- Point 7: $\phi_6 - 4.805\phi_7 + \phi_8 + \phi_{12} = -10680771$
- Point 8: $\phi_5 + \phi_7 - 4\phi_8 + \phi_9 + \phi_{11} = 0$
- Point 9: $\phi_4 + \phi_8 - 4.805\phi_9 + \phi_{10} = 14594972$
- Point 10: $\phi_9 - 11.06\phi_{10} + \phi_{11} = 43319232$
- Point 11: $\phi_8 + \phi_{10} - 4\phi_{11} + \phi_{12} = -4498416$
- Point 12: $\phi_7 + \phi_{11} - 11.06\phi_{12} = -1.71 \times 10^8$

The above equations put in matrix form look as follows:

EQUATION ↓ →	4	5	6	7	8	9	10	11	12	ϕ_i	C_i
4	-4.24	1	0	0	0	1	0	0	0	ϕ_4	12196840
5	1	-4	1	0	1	0	0	0	0	ϕ_5	- 3175441.5
6	0	1	-4.24	1	0	0	0	0	0	ϕ_6	-12891482
7	0	0	1	-4.81	1	0	0	0	1	ϕ_7	-19680771
8	0	1	0	1	-4	1	0	1	0	ϕ_8	= 0
9	1	0	0	0	1	-4.81	1	0	0	ϕ_9	14594972
10	0	0	0	0	0	1	-11.06	1	0	ϕ_{10}	43319232
11	0	0	0	0	1	0	1	-4	1	ϕ_{11}	- 4498416
12	0	0	0	1	0	0	0	1	-11.06	ϕ_{12}	- 1.71 x 10 ⁸

Using Gaussian elimination method triangularization of the matrix is achieved.

EQUATION ↓	4	5	6	7	8	9	10	11	12	ϕ_i	C_i
4	1	-4	1	0	1	0	0	0	0	ϕ_4	- 3175441.5
5	0	1	-4.24	1	0	0	0	0	0	ϕ_5	-12891482
6	0	0	1	-4.81	1	0	0	0	1	ϕ_6	-10680771
7	0	0	0	1	0	0	0	1	-11.06	ϕ_7	- 1.71 x 10 ⁸
8	0	0	0	0	1	0	1	-4	1	ϕ_8	= - 4498416
9	0	0	0	0	0	1	-11.06	1	0	ϕ_9	43319232
10	0	0	0	0	0	0	1	3.64	-22.21	ϕ_{10}	- 3.53 x 10 ⁸
11	0	0	0	0	0	0	0	1	- 5.32	ϕ_{11}	- 8333333.3
12	0	0	0	0	0	0	0	0	1	ϕ_{12}	16040178

Now by back substitution ϕ_i are found.

$$\phi_{12} = \underline{\underline{16040178 \text{ N/m}^2}}$$

$$\phi_{11} = -8333333.3 + 5.32(16040178) = \underline{\underline{2000414 \text{ N/m}^2}}$$

$$\begin{aligned} \phi_{10} &= -3.53 \times 10^8 - 3.64(2000414) + 22.21(16040178) \\ &= \underline{\underline{-4029153.6 \text{ N/m}^2}} \end{aligned}$$

$$\begin{aligned} \phi_9 &= 43319232 + 11.06(-4029153.6) - 2000414 \\ &= \underline{\underline{-3243620.8 \text{ N/m}^2}} \end{aligned}$$

$$\begin{aligned} \phi_8 &= -4498416 - (-4029153.6) + 4(2000414) - 16040178 \\ &= \underline{\underline{-8507784.4 \text{ N/m}^2}} \end{aligned}$$

$$\begin{aligned} \phi_7 &= -1.71 \times 10^8 - 2000414 + 11.06(16040178) \\ &= \underline{\underline{4403954.7 \text{ N/m}^2}} \end{aligned}$$

$$\begin{aligned} \phi_6 &= -10680771 + 4.81(4403954.7) - (-8507784.4) - 16040178 \\ &= \underline{\underline{2969857.5 \text{ N/m}^2}} \end{aligned}$$

$$\begin{aligned} \phi_5 &= -12891482 + 4.24(2969857.4) - 4403954.7 \\ &= \underline{\underline{-4703241.3 \text{ N/m}^2}} \end{aligned}$$

$$\begin{aligned} \phi_4 &= -3175441.5 + 4(-4703241.3) - 2969857.4 - (-8507784.4) \\ &= \underline{\underline{-16450480 \text{ N/m}^2}} \end{aligned}$$

$$\phi_3 = \underline{\underline{-62880.1 \text{ N/m}^2}}$$

$$\phi_2 = \underline{\underline{3175441.5 \text{ N/m}^2}}$$

$$\phi_1 = \underline{\underline{3426992.5 \text{ N/m}^2}}$$

5.7.3. The Individual Stresses - By combining the result from the photoelastic analysis and that obtained using finite difference method, the individual stresses can be calculated. Photoelastic readings gave $(\sigma_1 - \sigma_2)$ for the nodal points while FDM gave $(\sigma_1 + \sigma_2)$ values for the same nodal points. By solving the two equations,

separate principal stresses are found as follows:

Point 1:

$$\begin{array}{r} \sigma_1 - \sigma_2 = 2791324.8 \\ + \end{array}$$

$$\sigma_1 + \sigma_2 = 3426992.5$$

$$2\sigma_1 = 62183173$$

$$\sigma_1 = \underline{\underline{3109158.7 \text{ N/m}^2}}$$

$$\sigma_2 = \underline{\underline{317833.85 \text{ N/m}^2}}$$

Point 2:

$$\begin{array}{r} \sigma_1 - \sigma_2 = 1857038.4 \\ + \end{array}$$

$$\sigma_1 + \sigma_2 = 3175441.5$$

$$2\sigma_1 = 5032479.9$$

$$\sigma_1 = \underline{\underline{2516240 \text{ N/m}^2}}$$

$$\sigma_2 = \underline{\underline{659201.55 \text{ N/m}^2}}$$

Point 3:

$$\begin{array}{r} \sigma_1 - \sigma_2 = 2998944 \\ + \end{array}$$

$$\sigma_1 + \sigma_2 = 62880.1$$

$$2\sigma_1 = 3061824.1$$

$$\sigma_1 = \underline{\underline{1530912.10 \text{ N/m}^2}}$$

$$\sigma_2 = \underline{\underline{-1468032.0 \text{ N/m}^2}}$$

Point 4:

$$\begin{array}{r} \sigma_1 - \sigma_2 = 7485825.6 \\ + \end{array}$$

$$\sigma_1 + \sigma_2 = -16450480$$

$$2\sigma_1 = -8964654.4$$

$$\sigma_1 = \underline{\underline{-4482327.2 \text{ N/m}^2}}$$

$$\sigma_2 = \underline{\underline{-11968153 \text{ N/m}^2}}$$

Point 5:

$$\begin{array}{r} \sigma_1 - \sigma_2 = 5513443.2 \\ + \\ \sigma_1 + \sigma_2 = -4703241.3 \\ \hline \end{array}$$

$$2\sigma_1 = 810201.9$$

$$\therefore \sigma_1 = \underline{\underline{405700.95 \text{ N/m}^2}}$$

$$\sigma_2 = \underline{\underline{-5108342.3 \text{ N/m}^2}}$$

Point 6:

$$\begin{array}{r} \sigma_1 - \sigma_2 = 5813337.6 \\ + \\ \sigma_1 + \sigma_2 = 2969857.5 \\ \hline \end{array}$$

$$2\sigma_1 = 8783195.1$$

$$\therefore \sigma_1 = \underline{\underline{4391597.6 \text{ N/m}^2}}$$

$$\sigma_2 = \underline{\underline{-1421740.1 \text{ N/m}^2}}$$

Point 7:

$$\begin{array}{r} \sigma_1 - \sigma_2 = 5536512.0 \\ + \\ \sigma_1 + \sigma_2 = 4403954.7 \\ \hline \end{array}$$

$$2\sigma_1 = 9940466.7$$

$$\therefore \sigma_1 = \underline{\underline{4970233.4 \text{ N/m}^2}}$$

$$\sigma_2 = \underline{\underline{-566278.65 \text{ N/m}^2}}$$

Point 8:

$$\begin{array}{r} \sigma_1 - \sigma_2 = 8373974.4 \\ + \\ \sigma_1 + \sigma_2 = -8507784.4 \\ \hline \end{array}$$

$$2\sigma_1 = -133810$$

$$\therefore \sigma_1 = \underline{\underline{-66905 \text{ N/m}^2}}$$

$$\sigma_2 = \underline{\underline{-8440879.4 \text{ N/m}^2}}$$

Point 9:

$$\begin{array}{r} \sigma_1 - \sigma_2 = 8650800 \\ + \\ \sigma_1 + \sigma_2 = -3243620.8 \\ \hline \end{array}$$

$$2\sigma_1 = 5407179.2$$

$$\therefore \sigma_1 = \underline{\underline{2703589.6 \text{ N/m}^2}}$$

$$\sigma_2 = \underline{\underline{-5947210.4 \text{ N/m}^2}}$$

Point 10:

$$\begin{array}{r} \sigma_1 - \sigma_2 = 6459264.0 \\ + \\ \sigma_1 + \sigma_2 = -4029153.6 \\ \hline \end{array}$$

$$2\sigma_1 = 2430110.4$$

$$\therefore \sigma_1 = \underline{\underline{1215055.2 \text{ N/m}^2}}$$

$$\sigma_2 = \underline{\underline{-5244208.8 \text{ N/m}^2}}$$

Point 11:

$$\begin{array}{r} \sigma_1 - \sigma_2 = 9965721.6 \\ + \\ \sigma_1 + \sigma_2 = 2000414 \\ \hline \end{array}$$

$$2\sigma_1 = 11966136$$

$$\therefore \sigma_1 = \underline{\underline{5983067.8 \text{ N/m}^2}}$$

$$\sigma_2 = \underline{\underline{-3982653.8 \text{ N/m}^2}}$$

Point 12:

$$\begin{array}{r} \sigma_1 - \sigma_2 = 4982860.8 \\ + \\ \sigma_1 + \sigma_2 = 16040178 \\ \hline \end{array}$$

$$2\sigma_1 = 21023039$$

$$\therefore \sigma_1 = \underline{\underline{10511519 \text{ N/m}^2}}$$

$$\sigma_2 = \underline{\underline{5528658.6 \text{ N/m}^2}}$$

Overall Results Compiled:

±

STRESSES AT THE POINTS ON THE BOUNDARY (N/m ²)			STRESSES AT THE INTERIOR POINTS (N/m ²)		
NODE	σ_1	σ_2	NODE	σ_1	σ_2
A	0	-20992608	1	3109158.7	317833.85
B	0	-98004240	2	2516240	659201.55
C	0	-8085614.4	3	1530912.1	-1468032
D	0	-5559580.8	4	-4482327.2	-11968153
E	0	-3114288	5	405100.95	-5108342.3
F	0	-4498416	6	4391597.6	-1421740
G	0	-44430509	7	4970233.4	-566278.65
H	9573552	0	8	-66905	-8440879
I	10069531	0	9	2703589.6	-5947210.4
J	12261067	0	10	1215055.2	-5244208.8
K	20761920	0	11	5983067.8	-3982653.8
			12	10511519	5528658.6

5.8. Model Stresses Applied To The Prototype:

The results from the 2-D photoelastic model now have to be interpreted to stress values in the metal part. The model may differ from the metal part in respect of scale, thickness, applied load and elastic constants.

Various methods for transposing the stresses to the new conditions have been suggested. The problem as applied to photoelastic work has been specifically considered by J. N. Godier [ref. 12]. He suggested that for the straight-forward 2-D case, the stress at a point

is proportional to the quantity $(W/t.l)$ so that the stress in the engineering part can be derived from the relationship:

$$\sigma = \sigma_m \times \frac{W_p}{W_m} \times \frac{t_m}{t_p} \times \frac{l_m}{l_p} \text{-----(5.11)}$$

where the suffix 'p' and 'm' refers to prototype and model, respectively and σ = stress at a point. W is the transmitted load, t = thickness, l = typical length dimension.

Assuming the prototype to be made of steel, the transmitted load to be 2 kN, the gear wheel thickness to be 25 mm, the thickness of the gear tooth to be 6.6 mm. With these values and the corresponding values in the model, the stress developed, for example, at the fillet of the prototype is calculated as:

Data for the Model

$\sigma_m = 20.33 \text{ MPa (tension)}$

Tooth thickness along the pitch line $t_m = 20 \text{ mm}$

The face width $l_m = 5 \text{ mm}$

Transmitted load $W_m = 282.705 \text{ N.}$

Data for the Prototype

$\sigma_p = ?$

Tooth thickness along the pitch line $t_p = 6.6 \text{ mm}$

The face width $l_p = 25 \text{ mm}$

Transmitted load $W_p = 2000 \text{ N}$

Substituting these values into equation (5.11), the fillet stress (tension) on the prototype is calculated as follows:

$$\sigma = 20.33 \times \frac{2000}{282.705} \times \frac{5}{25} \times \frac{20}{6.6} = \underline{\underline{87.167 \text{ MPa}}}$$

CHAPTER SIX

6.0. CALCULATION OF STRESSES WITH THE USE OF FEM

In calculating stresses using an in-plane constant strain triangle CST Finite Element Method, FEM, computer programme (ref.3) was employed. A mainframe computer Cyber 932-11 installed at Ahmadu Bello University Computer Centre was used to run the computation.

The programme is completely listed in Figures 6.1a to 6.1g enclosed at the end of the volume, and is divided into three main parts, namely:

- (i) Calculation of the element stiffness matrices and assemblage into the overall structural stiffness matrix.
- (ii) Solution of the set of simultaneous linear equations to determine the nodal point displacement.
- (iii) Evaluation of stresses in the individual elements.

The flow chart of the programme is enclosed at the end of the volume along with the programme (Fig. 6.1a-g, Fig. 6.1w)

The analysis is carried out in a single pass using input data (Figures 6.1g to 6.1n) which provide a geometrical description of the structure (Figure 6.2) and its loading (Figure 6.2) and producing an output consisting of tabulated nodal point deflections (Fig. 6.1p to 6.1r) and element stresses (Fig. 6.1r to 6.1v).

After the subdivision of the structure into 242 triangular elements (CST) as shown in Figure (6.2)

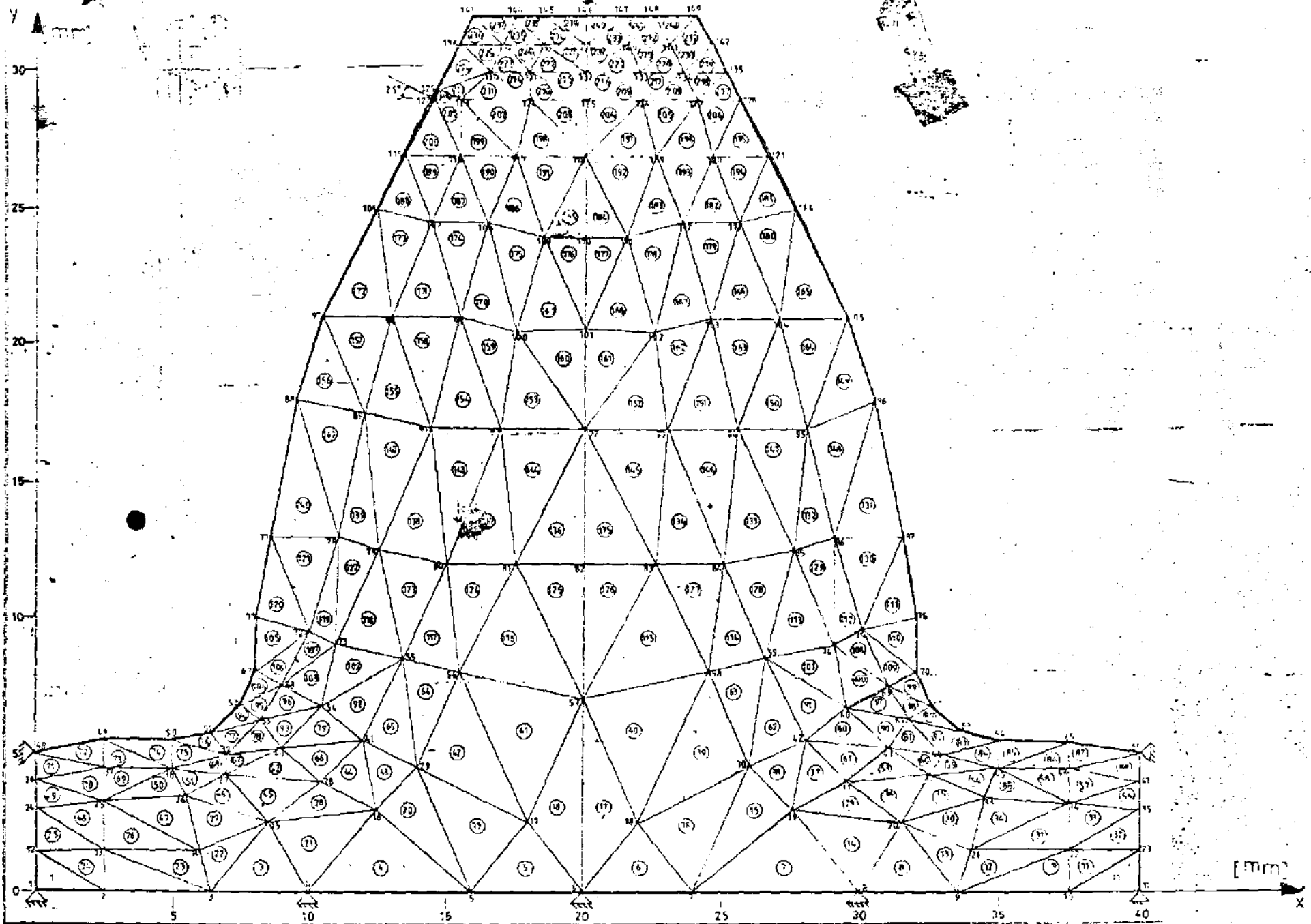


FIG. 6.2 242 constant strain triangle [CST]

element data (elastic properties, coordinates and connectivity of each element and the associated load components).

Care was taken to refine the mesh at expected regions of stress concentrations, that is at the root of the tooth and the point of load application.

Regularly, as in FEM procedure, the tooth was now fixed by means of several supports (at nodes 48, 1, 4, 6, 8, 11 and 66). The load was applied at a pressure angle of 25° at nodal point 122. It is well known that two values of pressure angle are used for spur gears. According to standards, these angles are 14.5° and 20° , the latter being the choice in most modern constructions. This pressure angle of 20° , however, could increase due to tooth correction, centre distance shifting, etc. [refs. 5 and 13]. It was noticed, when taking the photo-elastic measurements that the working pressure angle was 25° and such working pressure angle was assumed. The technique applied, however, is suitable for any standard or working pressure angle.

The face width (thickness of gear blank) of the tooth (5 mm) compared to the thickness of the tooth, measured along the pitch line (20 mm) and its height (26 mm) justifies the assumption of the plane state of stress and therefore the use of an in-plane FEM analysis here.

The accuracy of FEM calculation depends on the number of elements used. It was checked that discretization into 242 elements is sufficient for the analysis having used

coarser meshes.

Stress components σ_x , σ_y , τ_{xy} , principal stresses σ_1 and σ_2 and even $\sigma_1 - \sigma_2$ were calculated. The results are shown in the computer print-out attached (Fig. 6.1r and Fig. 6.1v). The nature of CST elements implies that these stresses are constant throughout each single triangular element (normally represented at the centroid of the element).

The analysis of the stresses print-out showed three regions of concentration with locally maximum stresses as follows:

at point of load application:

$$\sigma_2 = -52.59 \text{ MPa (element 212)}$$

at the left fillet:

$$\sigma_1 = +23.37 \text{ MPa (element 104)}$$

at the right fillet:

$$\sigma_2 = -20.24 \text{ MPa (element 89)}.$$

CHAPTER SEVEN

7.0. COMPARISON OF RESULTS OBTAINED BY DIFFERENT METHODS

7.1. Calculating The Fillet Stresses With The Use Of Lewis Formula:

In Chapter Two, it was said that the Lewis formula is highly deficient because of over-simplifying assumptions enumerated in the same chapter. The following calculation, when compared with others goes further to prove this.

The modified Lewis formula takes the effect of compressive load into account.

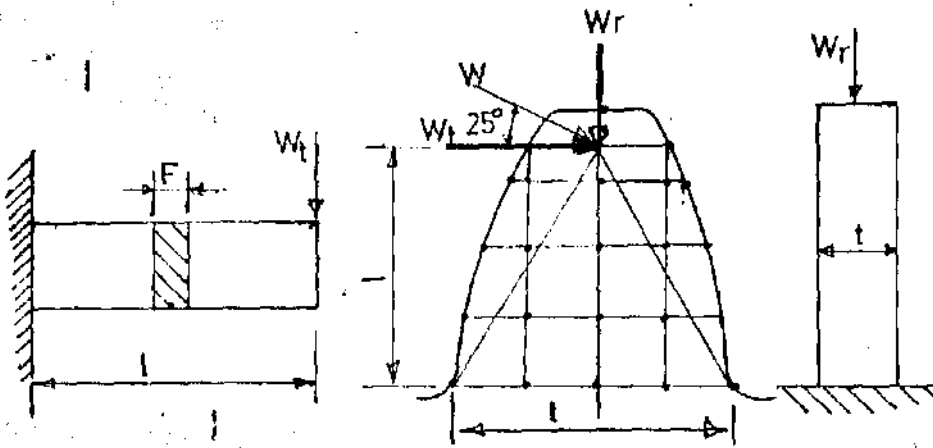


Fig. 7.1: Lewis Approach for Calculating Stresses.

Tensile stress, $\sigma_t = M / (Z_t)$ ----- (7.1)

where $M = \text{moment} = W_t \cdot l$ ----- (7.2)

and $Z_t = \text{Section Modulus} = \frac{Ft^2}{6}$ ----- (7.3)

Substituting equations (7.2) and (7.3) into (7.1), we have:

$\sigma_t = \frac{6W_t l}{Ft^2}$ ----- (7.4)

Taking effect of compressive load into account we have

$$\text{Compressive stress } \sigma_c = -M/(Z_c) \text{ ----- (7.5)}$$

$$\text{where } M = W_r \cdot \frac{t}{2} \text{ ----- (7.6)}$$

$$\text{and } Z_c = \frac{tl^2}{6} \text{ ----- (7.7)}$$

Substituting equations (7.6) and (7.7) into (7.5) we have:

$$\sigma_c = \frac{-3W_r}{l^2} \text{ ----- (7.8)}$$

$$\text{Total fillet stress, } \sigma = \pm \frac{6W_t l}{Ft^2} - \frac{3W_r}{l^2} \text{ ----- (7.9)}$$

where

$$W = \text{applied load} = 282.705 \text{ N}$$

$$W_t = W \cos 25^\circ$$

$$W_r = W \sin 25^\circ$$

$$t = \text{Width of tooth} = 26.4 \text{ mm}$$

$$l = 20.5 \text{ mm}$$

$$F = \text{Model thickness} = 5 \text{ mm.}$$

Substituting these values into equation (7.9) gives:

$$\begin{aligned} \sigma &= \pm \frac{6 \times 282.705 \cos 25^\circ \times 20.5 \times 10^{-3}}{5 \times 10^{-3} \times (26.4 \times 10^{-3})^2} - \frac{3 \times 282.705 \sin 25^\circ}{(20.5 \times 10^{-3})^2} \\ &= + 9043498.2 - 852894.44 \end{aligned}$$

Lewis Formula (Original):

$$\sigma = \underline{\underline{+9043498.2 \text{ N/m}^2}} \text{ (left fillet)}$$

$$\sigma = \underline{\underline{-9043498.2 \text{ N/m}^2}} \text{ (right fillet)}$$

Modified Lewis Formula:

$$\sigma = +9043498.2 - 852894.44 = \underline{\underline{+8190603.8 \text{ N/m}^2}} \text{ (left fillet)}$$

$$\sigma = -9043498.2 - 852894.44 = \underline{\underline{-9896392.6 \text{ N/m}^2}} \text{ (right fillet)}$$

7.2. Calculating The Fillet Stresses With The Use Of Sopwith Equation:

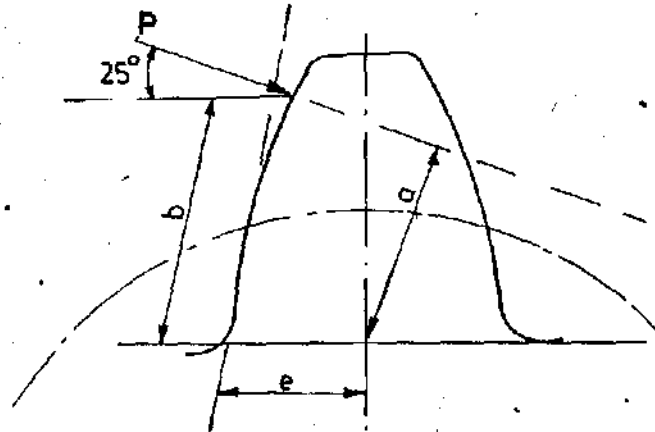


Fig. 7.2: Equivalent Flat-Sided Projection Constructed from Gear Tooth for the Calculation of Fillet Stress.

In Chapter Two also, it was said that Sopwith Equation is better than Lewis formula. This statement is proved by comparing the results obtained using the two equations with the results obtained using either finite difference method or finite element method.

Now referring to the above Fig. 7.2, and using the data therein, the fillet stresses according to Sopwith are (equation (2.7)):

$$\sigma = \pm K \left[\frac{1.5a}{e^2} + \sqrt{\frac{0.36}{b \cdot c}} \left(1 + \frac{1}{4} \sin \gamma \right) \right] \frac{W}{F} \quad \text{---- (7.10)}$$

where K = stress concentration factor

$$K = 1 + 0.26 \left(\frac{e}{R} \right)^{0.7} \quad \text{----- (7.11)}$$

a, b, e, are as shown in Figure 7.2

R = fillet radius = 0.2e for double root radii fillet.

From the same figure, $a = 19 \text{ mm}$, $e = 13.2 \text{ mm}$, $b = 22.6 \text{ mm}$,
 $R = 0.2e = 2.64 \text{ mm}$, $W = 282.705 \text{ N}$, $F = \text{face width} = 5 \text{ mm}$,
 $\gamma = \text{pressure angle} = 25^\circ$.

Substituting these values into equations (7.10)
and (7.11), we have:

$$K = 1 + 0.26 \left(\frac{13.2}{2.64} \right)^{0.7} = 1.802$$

$$\sigma = \pm 1.8 \left[\frac{1.5 \times 19 \times 10^{-3}}{(13.2 \times 10^{-3})^2} + \sqrt{\frac{0.36}{22.6 \times 10^{-3} \times 13.2 \times 10^{-3}} \left(1 + \frac{1}{4} \sin 25^\circ \right)} \right] \frac{282.705}{5 \times 10^{-3}}$$

$$\sigma = \pm 20.56 \text{ MPa}$$

$$\sigma = \underline{\underline{+20.56 \text{ MPa}}} \quad (\text{Left fillet})$$

$$\sigma = \underline{\underline{-20.56 \text{ MPa}}} \quad (\text{Right fillet})$$

7.3. Comparison Of Fillet Stresses:

Location	Lewis Formula	Modified Lewis Formula	Sopwith Equation	FDM+Photo Elasticity	FEM
Left Fillet	+9.04MPa	+8.19MPa	+20.56MPa	+20.76MPa	+23.37MPa
Right Fillet	-9.04MPa	-9.89MPa	-20.56MPa	-20.99MPa	-20.24MPa

TABLE 7.1: FILLET STRESSES BY DIFFERENT METHODS

Table 7.1 shows clearly how the Lewis formula, modified Lewis formula, Sopwith equation, FDM + photoelastic analysis and finite element method agree or disagree with one another.

7.4. Calculating The Contact Stress At The Point Of Load

Application With The Use Of Hertz Equation:

To obtain an expression for surface contact stress, the Hertz theory is employed. Without going into detailed derivation of the equation, Hertzian contact stress between cylinders may be computed from the equation:

$$\sigma = \frac{b}{\Delta} \text{----- (7.12)}$$

where

$$\Delta = \frac{1}{\frac{1}{2r_1} + \frac{1}{2r_2}} \left\{ \frac{1 - \mu_1^2}{E_1} + \frac{1 - \mu_2^2}{E_2} \right\} \text{----- (7.13)}$$

$$b = \sqrt{\frac{2W\Delta}{F\pi}} \text{----- (7.14)}$$

Applying the above equation to a pair of gears; μ_1, μ_2, E_1 and E_2 , are the elastic constants of the gear material while r_1, r_2 , are the instantaneous values of the radii of curvature on the pinion-and gear-tooth profile, respectively, at the point of contact. By accounting for load sharing in the value of W used, equation (7.12) can be solved for the Hertzian stress for any or all points from the beginning to the end of tooth contact. Of course, pure rolling exists only at the pitch point. Elsewhere, the motion is a mixture of rolling and sliding. Equation (7.12) does not account for any sliding action in the evaluation of stresses.

Referring to Figures 7.3 and 7.4, and making use of the equations (7.12), (7.13) and (7.14), the contact stress is calculated as follows:

$$r_1 = r_2 = r = 45.3 \text{ mm}$$

$$\mu_1 = \mu_2 = \mu = 0.325$$

$$E_1 = E_2 = E = 4.444 \times 10^9 \text{ N/m}^2$$

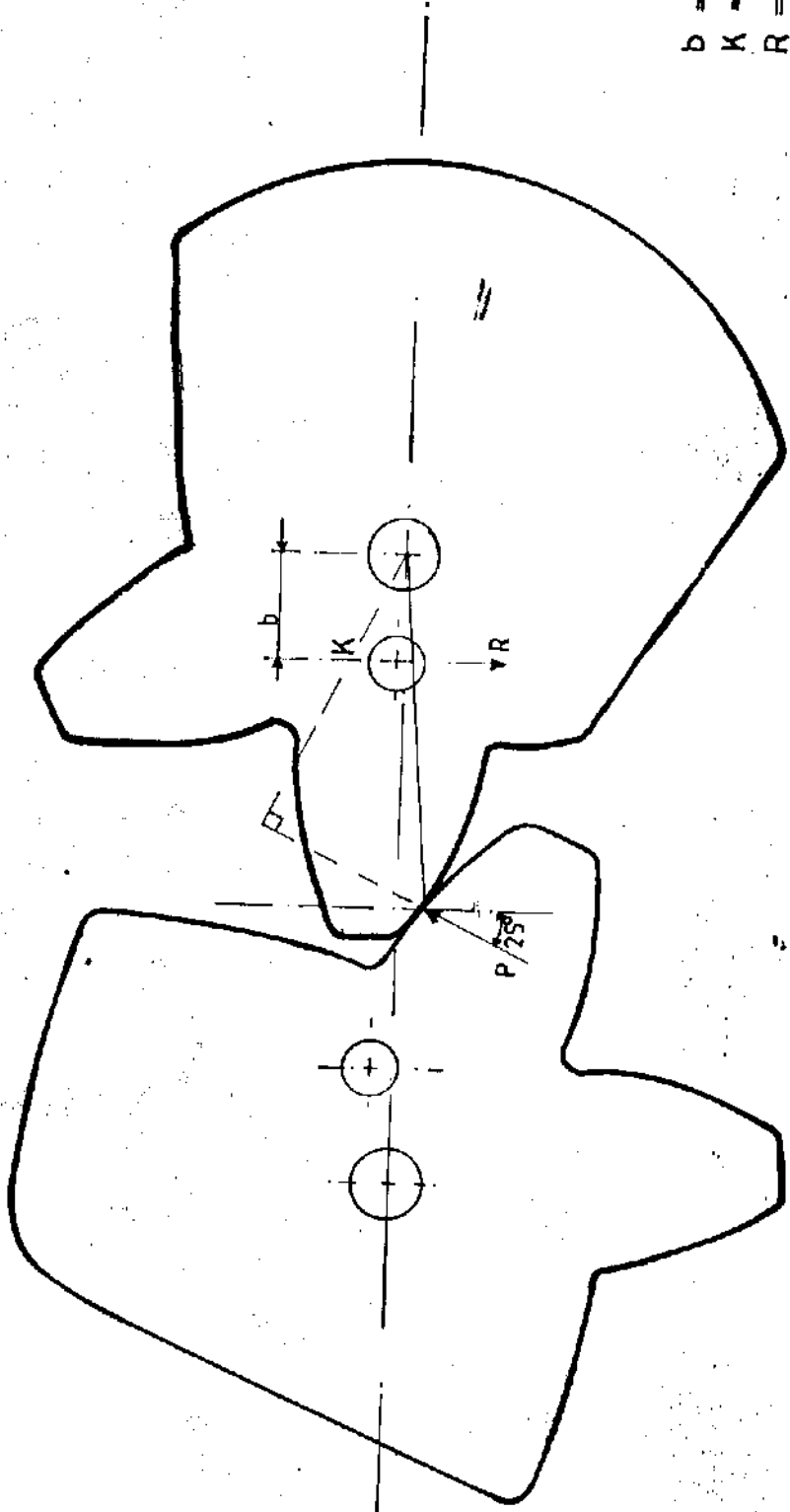
$$W = 282.7058 \text{ N}$$

$$F = 5 \text{ mm.}$$

Making use of equation (7.13):

$$\Delta = 2r \left(\frac{1 - \mu^2}{E} \right) = 2 \times 45.3 \times 10^{-3} \left(\frac{1 - (0.325)^2}{4.444 \times 10^9} \right)$$

$$= 1.8231853 \times 10^{-11} \text{ m}^3/\text{N}$$



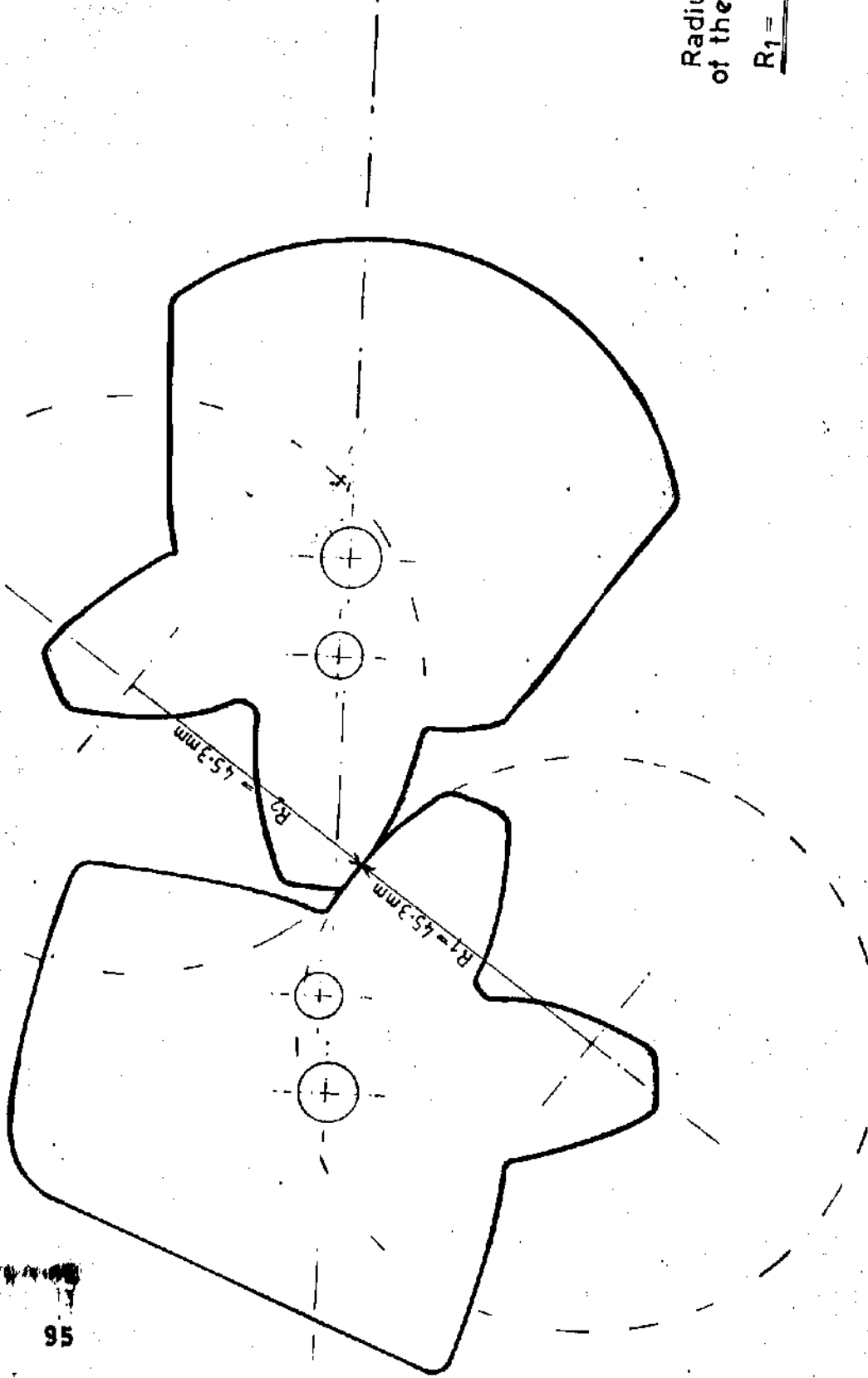
- $b = 144 \text{ mm}$
- $K = 40.8 \text{ mm}$
- $R = 801 \text{ N}$
- $r = 48 \text{ mm}$

$$R \cdot b = P \cdot K$$

$$\Rightarrow P = \frac{R \cdot b}{K} = \frac{801 \times 144}{40.8}$$

$$= 28270588 \text{ N}$$

G.73 Dimension required for the calculation of transmitted load P.



Radius of curvature
of the two cylinders

$$R_1 = R_2 = R = 45.3 \text{ m}$$

FIG. 7.4: Dimension required for the calculation of contact stress

From equation (7.14), we have:

$$b = \sqrt{\frac{2 \times 282.7058 \times 1.8231853 \times 10^{-11}}{5 \times 10^{-3} \times \pi}}$$

$$= \underline{\underline{8.1009849 \times 10^{-4} \text{ m}}}$$

Substituting the values of b and Δ into equation (7.12), we have:

$$\text{Contact Stress } \sigma = \frac{8.1009849 \times 10^{-4}}{1.8231853 \times 10^{-11}}$$

$$= \underline{\underline{44.43 \text{ MPa}}}$$

7.5. Comparison Of Contact Stresses:

Hertz Equation	Photoelasticity+ FDM (Node G)	FEM (Node 122)
-44.43 MPa	-44.43 MPa	-52.59 MPa

TABLE 7.2: CONTACT STRESSES BY DIFFERENT METHODS

Table 7.2 shows the extent the Hertz equation, the FDM+photoelasticity and FEM agree with one another when used to calculate the contact stresses.

7.6. Inferences:

Looking at the results obtained using Lewis formula, modified Lewis formula, Sopwith Equation, Hertz Equation, Photoelastic method plus FDM and FEM, the following inferences are made:

- (i) The Lewis formula has been proved deficient since the result obtained with it is almost 50% less than that obtained using either Sopwith Equation, Photoelastic method plus FDM or FEM.

- (ii) The results obtained using Sopwith equation agree very well with the photoelastic and finite element results.
- (iii) The photoelastic results agree with the finite element method results.
- (iv) Also the value of stress obtained using Hertz equation is in complete agreement with that given by photoelastic plus FDM analysis.
- (v) The contact stress value given by photoelastic plus FDM analysis does not agree well with that obtained using finite element method. The reason for the difference is that the finite element method always assumes a point load. As the load transmitted by the two gears increases, the point of contact enlarges to a line contact so that the pointload phenomenon does not hold anymore. As a result, less stress value is obtained by photoelastic plus FDM method than with the FEM analysis.

CHAPTER EIGHT

8.0. LIKELY SOURCES OF ERROR IN THIS WORK

Just like in all experimental work, there are in this work various sources of error of which some were guarded against while others were inevitable. In this work, the errors are likely to come from the use of strain gauges, the photoelastic and Numerical analyses.

8.1. Likely Sources of Error In Photoelastic Results:

The major sources of error and the ways some of them were guarded against in the photoelastic analysis part of this work are as follows:

Effect of Machining Stresses - When a photoelastic material is produced by machining processes, boundary stresses are induced in the model. The size of the machining stress depends primarily on the rigidity of the machine and sharpness of the cutting tools. In this work, the machining stresses were reduced to minimum by using a sharp, well-supported tool and rigid machine while turning the blank; and sharp hacksaw and smooth files while cutting the teeth. A non-load observation in the photoelastic bench showed hardly any residual stress.

Accuracy of Model - It can be said that the accuracy of a test is almost entirely dependent on the dimensional accuracy of the model. If a model is not produced to the accurate dimension and necessary tolerance included, there may be errors in the results obtained. Inaccurate models

result from hand-filing operations and even from milling and turning if the model is not clamped flat on the working table or face plate. In this work, there are bound to be some errors due to method of production of the models. This is because, although the model was rigidly clamped to the machine table, the teeth were cut with hacksaw and filed to shape. This is because, there was no milling cutter to use in producing the size of gear teeth needed. Although the gear teeth were produced by cutting and filing, I still believe that the error is minimal since extra care was taken in cutting and filling processes.

Time-Edge Effect - When some photoelastic materials are exposed to the air, fringes develop along the exposed edges. The time-edge effect is a function of time as the name reveals. It grows with time. As a result, one cannot finish preparing a model and put it away and expect to get accurate stress patterns at the edges some time after. In this project, this error is unavoidable since the model could not be finished one day and the readings taken the same day.

Faulty Loading Conditions - In addition to problems arising from machining stresses and time-edge effect, there are difficulties due to the loading conditions. If the loads are applied to the extreme fibres through pins, friction forces are developed which generally reduce the applied bending moment and shifts the position of neutral axis. In this work, the influence of friction forces was reduced by boring holes on the neutral axes of the models and loads applied through pins passing through these holes

(see Plate XX). The pins and the holes were lubricated to further reduce the effect of friction.

Creep - The problem of creep, in this work, was tackled by using an old, well-seasoned material which normally will show smaller rates of creep.

8.2. Likely Sources of Error in Strain Measurements:

As pointed out in Chapter Five, the strains at the nodal points 1, 2 and 3 were determined using strain gauges to enable us find the stresses at the points. There are bound to be errors in the measurement due to instability of gauge performance, though frantic effort was made to reduce the errors.

Instability of gauge performance is caused by the following:

- (i) Moisture
- (ii) Improper installation of gauges
- (iii) Insufficient drying of cement
- (iv) Damaged or imperfect connection
- (v) Ageing of bonding medium
- (vi) Use of frayed or wornout strained lead wire.

The following measures were taken to reduce the errors coming from the above mentioned sources.

On moisture prevention, since the weather under which the experiment was conducted was dry enough, there was no need of protecting the strain gauges from the influence of moisture by waxing it.

The bonding medium used was tested and proved to be efficient. So the issue of error coming in due to ageing of the bonding medium does not arise.

Frantic effort was made to see that the strain gauges were properly mounted on the test piece; and allowed one day before measurement was carried out to ensure complete drying of the cement.

The strain gauge connection was found to be perfect when it was tested for continuity using Avometer.

The strain gauges used were new ones, and the connecting wires were also new.

Although the precautions mentioned above were taken, one cannot still rule out the possibility of some errors being present, no matter how small.

8.3. Likely Sources Of Error In Numerical Analysis:

It has been said earlier that the finite difference method contains an essential approximation; consequently, solutions obtained by its use must be in some error, no matter how small. The error can be made less by taking the mesh sufficiently fine. In FDM plus photoelasticity applications, however, the refinement cannot go too far, as reading the fractional fringes becomes too difficult.

The error in FEM analysis results from:

- (i) the nature of the analysis and selected element;
- (ii) covering the real shape by the idealised one;
- (iii) insufficient idealization.

314007

The last factor, the most serious one in many cases, was almost eliminated by taking coarser meshes and refining them and comparing results (that was done as mentioned in

Chapter Six). The first two factors are inevitable. FEM is an approximate method but is accepted for this type of calculation. CST elements are widely used for in-plane analysis and they have the advantage of describing well all shapes (better than, for example, rectangular elements). The relatively thin model allowed two-dimensional analysis.

CHAPTER NINE

9.0. CONCLUSION

The stresses in a spur gear have been successfully determined with the use of photoelastic plus FDM and FEM analyses. The stresses were compared with the traditional Sopwith equation and Lewis formula.

Comparing the results obtained using different methods mentioned above, the following conclusions are drawn:

- (i) the Lewis formula is highly deficient. The deficiency is noticed in the results obtained using the formula and other methods. The value of fillet stress calculated using Lewis formula is about 50% less than that calculated using either Sopwith equation or numerical methods.
- (ii) The results obtained using Sopwith equation agree well with the photoelastic plus FDM and FEM results.
- (iii) The photoelastic plus FDM results agree with those of FEM.
- (iv) The result obtained using Hertz equation does not agree with that obtained using FEM but agrees well with the photoelastic plus FDM results, the reason being that FEM and analytical approaches assume point load which does not exist in the real sense. From this point of view, the photoelastic plus FDM method is highly recommended for contact stress measurement.

Carried out stress analysis revealed that when a pair of gears are meshing, stress concentration is noticed at the fillets and point of contact. Because of this stress concentration at the root, it is recommended that the gear designers should make the fillet radius as large as possible to reduce the stress concentration. The best results are obtained with the largest radius, that is, the semi-circular fillet.

On the photoelastic model, as revealed by the fringe photographs attached, it is possible for the designer to notice the areas of stress concentration. This helps him to modify the design as the case may be.

The results show that the in-plane, plane stress analysis is suitable for spur gears. In case of very thick gears, the photoelastic experiment would become difficult. The FEM in-plane analysis could easily be replaced, however, by a 3-D analysis. The advantage of using photoelastic plus FDM analysis is that the complete calculation (stress separation) is possible without using isoclinics. Isoclinics (loci of points along which the principal stresses have parallel directions) are less sharp and more difficult to determine compared with isochromatics (lines of constant maximum shear stress). In addition, Sopwith and Lewis equations can only analyse the stresses at the fillets but not at the nodal points on the tooth. Supposing a hole is drilled on the tooth for the purpose of weight reduction; FDM+photoelastic and FEM techniques can be used to find the effect of the hole on the strength of the tooth.

REFERENCES

1. BORESI, A.P., BOTTOM, O.M. et al. (1978): Advanced Mechanics of Materials (3rd Ed.), John Wiley and Sons, New York. PP. 581 - 627.
2. CHAPMAN, W.A.J. (1981): Workshop Technology (Part 3). The English Language Book Society and Edward Arnold (Publishers) Ltd., London. pp. 507 - 545.
3. CHEUNG, Y.K. and YEO, M.F. (1979): A Practical Introduction to Finite Element Analysis. Pitman Publishers Ltd., London. pp. 73 -79.
4. COKER, E.G. and FILON, L.N.G. (1957): A Treatise on Photoelasticity. Cambridge At the University Press. pp. 675 - 677.
5. DONALD, J. MYATT (1962): Machine Design - An Introductory Text. McGraw-Hill Book Company In., pp. 51 - 53 and 60 - 87.
6. DORN, W.S. and MCCRACKEN, D.D. (1972): Numerical Methods with Fortran IV Case Studies. John Wiley and Sons Inc. New York, pp. 155 - 218.
7. FROCHT, M.M. (1948): Photoelasticity Vol. 1. John Wiley and Sons, Inc. New York, pp. vii - xv, 64 - 215 and 323 - 398.
8. FROCHT, M.M. (1949): Photoelasticity Vol. II. John Wiley and Sons, Inc. New York, pp. 238 - 247.
9. HENDRY, A.W. (1964): Elements of Experimental Stress Analysis. Pergamon Press Ltd., Oxford, London, pp. 32 - 47 and 63 - 90

10. HENDRY, A.W.(1948): Introduction to Photoelastic Analysis. Blackie and Sons Ltd., Glasgow, Great Britain, pp. 1 - 138.
11. HETENYI, M.(Ed.) (1954): Handbook of Experimental Stress Analysis. John Wiley and Sons, Inc. New York, pp. 160 - 193 and 828 - 976.
12. HEYWOOD, R.B.(1952): Designing by Photoelasticity. Chapman and Hall Ltd., London, pp. 1 - 123 and 158 - 229.
13. HOUGHTON, P.S.(1901): Gears - Spur, Helical, Bevel and Worm. The Technical Press Ltd., London, pp. 1 - 55 and 174 - 251.
14. MCCRACKEN, D.D.(1972): A Guide to Fortran IV Programming. John Wiley and Sons, New York, pp. 1 - 268.
15. MITCHELL, D. and LANCASTER, P.R.(1980): Advanced Solid Mechanics - Theory, Worked Examples and Problems. The Macmillan Press Ltd., London, pp. 121-142
16. PAUL, H.BLACK (1955): Machine Design. McGraw-Hill Book Company, Inc. New York, pp. 251 - 277.
17. ROAK (1954): Formulas for Stress and Strain. McGraw-Hill Book Company, New York.
18. ROSSI, B.E.(Ed.) (1977): Society for Experimental Stress Analysis - Proceedings of the Society for Experimental Stress Analysis Vol. 34, U.S.A. pp. 392 - 397.
19. SHIGLEY, J.E.(1977): Mechanical Engineering Design. McGraw-Hill Kogakusha Ltd., Tokyo, pp. 26 - 93 and 398 - 455.

20. SINGH, S.(1982): Strength of Materials. Vikas Publishing House PVT Ltd., India. pp. 1 - 115 and 136 - 170.
21. SPOTTS, M.F.(1964): Mechanical Design Analysis. Prentice-Hall, Inc., Eaglewood Cliffs, New Jersey. pp. 172 - 242.
22. VAZIRAMI, V.N. and CHANDOLA, S.P.(1978): Experimental Stress Analysis. Khama Publishers, Delhi, India. pp. 12 - 60 and 78 - 132.
23. YAKOVLEV, V.F. and INYUTTIN, I.S.(1964): Measurement for Stresses in Machine Components. Pergamon Press, Oxford. pp. 1 - 5 and 14 - 26.
24. ZIENKIEWICZ, O.C. and HOLISTER, G.S.(1965): Stress Analysis - Recent Development in Numerical and Experimental Methods. John Wiley and Sons Ltd., London. pp. 1 - 40 and 85 - 119.

KASHIM IERANIM LIBRARY
AHMADU BELLO UNIVERSITY
ZARIA, NIGERIA.

FLOW CHART FOR COMPUTER PROGRAM FINELMT

